DOE/ET-53088-295 IFSR #295

Theoretical Microtearing Turbulence and Related Computational Studies of Constrained Turbulent Relaxation

Gerald G. Craddock, Jr.

Institute for Fusion Studies
The University of Texas at Austin
Austin, Texas 78712

August 1987

Theoretical Microtearing Turbulence and Related Computational Studies of Constrained Turbulent Relaxation

Gerald G. Craddock

The eventual goal of controlled nuclear fusion rests on the understanding of the underlying dynamical processes of the confined plasma. Magnetic fluctuations in magnetically confined plasmas have long been considered as a key to the understanding of anomalous heat losses in toroidal confinement devices, such as tokamaks. These fluctuations connect the confinement flux surfaces (relaxing the confining magnetic field) in tokamaks, thus leading to radial heat losses. Paradigms of magnetic turbulence are complicated, involving many free energy sources (current gradients, temperature gradients, etc.) and an inherently nonlinear nature. Statistical approaches to turbulence theory have the standard method of analysis of these paradigms. Unfortunately, the assumption of statistical homogeneity (gaussianity) breaks down in intermittent (nongaussian) flows, thus questioning the validity of these statistical approaches.

THEORETICAL MICROTEARING TURBULENCE AND RELATED COMPUTATIONAL STUDIES OF CONSTRAINED TURBULENT RELAXATION

APPROVED BY SUPERVISORY COMMITTEE:

Wendell Horton Jr.

P. H. Diamond

Marshall N. Rosenbluth

Robert L. Bert

Paul Terry

D E D I C A T I O N

To my parents, grandparents, and brothers

THEORETICAL MICROTEARING TURBULENCE AND RELATED COMPUTATIONAL STUDIES OF CONSTRAINED TURBULENT RELAXATION

by

GERALD G. CRADDOCK, JR., B.S.

DISSERTATION

Presented to the Faculty of the Graduate School of

The University of Texas at Austin

in Partial Fulfillment

of the Requirements

for the Degree of

DOCTOR OF PHILOSOPHY

THE UNIVERSITY OF TEXAS AT AUSTIN

August 1987

A C K N O W L E D G M E N T S

I wish to express my gratitude to the many people at the Institute for Fusion Studies (IFS) and Fusion Research Center (FRC) for their support, friendship, and sharing of knowledge.

First, I would thank my advisors and friends Dr. Patrick Diamond and Dr. Paul Terry. Their guidance, patience, advice and knowledge is deeply appreciated.

Second, I wish to thank the rest of my supervising committee, Professor Wendell Horton, Jr., Professor Herbert Berk, and Professor Marshall Rosenbluth, for careful reading of my dissertation and their helpful suggestions. I am especially indebted to Professor Rosenbluth for agreeing to read this work from afar.

Third, I am grateful to Ahmet Aydemir and David Thayer for their contributions to this dissertation. Dr. Aydemir provided the basic computer code for Chapter III and Dr. Thayer contributed the computational closure code results.

I appreciate the advice and knowledge of Dr. Richard Hazeltine and Dr. Swadesh Mahajan from my early years with the FRC.

Helpful discussions are also noted with Dr. David Ross, Dr. Jean-Noel Leboeuf, Dr. Bruce Scott, Dr. Hamid Biglari, Dr. Ron Bravenec, Dr. Cristoph Ritz, Dr. Burton Richards, and P. T. Katt. I especially treasure the friendship and interaction with Dr. T. S. Hahm.

From the administrative staff, I also appreciated the help of Rhandon Hurst, Carolyn Valentine, Dawn East, and Saralyn Stewart.

It has been said, that one can learn more from one's office mates and fellow students than from one's advisors. I greatly benefitted from many stimulating late-night discussions with Dr. Y. M. Li, Dr. Richard Sydora, Dr. G. S. Lee, and Dr. Tzihong Chiueh. I also enjoyed discussions with Dr. Todd Evans, Dr. David Brown, Dr. Kerry Coffman, Dr. Kathy Holcomb, Jung Hoon Han, Isidoros Doxas, Taina Kurki-Suonio, Nathan Mattor, Oh Jin Kwon, and Dr. Bruce Jensen.

In the Physics Department, I am grateful for the assistance of Carole Rutledge in the Graduate Student Office and Professor Austin Gleeson for his role in my start in the Graduate school.

The typing was done by the Martha Ann Zivley Typing Service and I especially thank Mrs. Zivley herself, whose experience helped me finish my dissertation.

Outside of Physics, I thank the Austin Kendo Dojo and Komizu Sensei for showing me the way of life that enabled me to find the strength to finish my dissertation.

I also cherish the support and friendship of Gere White, Nancy Bunch and Hilary Miller. I especially treasure the recent friendship and support of Catherine Burnell.

Most of all, I acknowledge the belief in my abilities, support and love of my parents, grandparents, and brothers which made this dissertation possible.

G. G. C., Jr.

The University of Texas at Austin
Austin, Texas
July 13, 1987

TABLE OF CONTENTS

L I S T O F F I G U R E S

C H A P T E R I

INTRODUCTION

The eventual goal of controlled nuclear fusion rests on the understanding of the underlying dynamical processes of the confined plasma. Magnetic fluctuations in magnetically confined plasmas have long been considered as key to the understanding of anomalous heat loses in torroidal confinement devices, such as tokamaks. These fluctuations connect the confining flux surfaces (relaxing the confining magnetic field) in tokamaks, thus leading to radial heat loses. Paradigms of magnetic turbulence are complicated, involving many free energy sources (current gradients, temperature gradients, etc.) and an inherently nonlinear nature. Statistical approaches to turbulence theory have been the standard method of analysis of these paradigms. Unfortunately, the assumption of statistical homogeneity (gaussianity) breaks down in intermittent (non-gaussian) flows, thus questioning the validity of these statistical approaches.

This dissertation is devoted to two specific studies of magnetic turbulence. The first is an analytic theory of semicollisional drift microtearing

turbulence driven by the gradient of the electron temperature. The second study involves constrained relaxation of a two-dimensional (2-D), two-field, undriven limit of a semicollisional microtearing model via computational simulation. The primary differences between the first and second study are that the first study is a 3-D, driven (unstable) problem, while the second is a 2-D undriven (stable) problem. A common link between the studies is found in the nonlinearities, with the computational study revealing nonlinear intermittent phenomena not predicted by the statistical turbulence theory used in the first study. The computational study can then be viewed as an extension of the analytic study. Thus, the first topic (analytic microtearing turbulence) is self-contained, while the second uses results from the first.

The study of microtearing turbulence (the first study) is motivated by recent experimental discussions[44,48] of the role of microtearing turbulence in the edge region of tokamaks. Edge magnetic fluctuations have been linked with the transition from low (L) to high (H) confinement[71] in neutral beam heated tokamaks.[10,44,48] Further, the electron temperature

gradient free energy source provides a mechanism for rigidity of the electron temperature profile (so called "profile consistency"[10,53,58]).

In Chapter II, a set of fluid equations (Ohm's Law and electron continuity) are introduced to describe semicollisional drift microtearing. A discussion of statistical equilibrium mechanics of these equations suggests the directions of energy transfer (to small scales) in a stationary state. Quantitative estimates of the saturated level of magnetic turbulence in a uniform and sheared equilibrium magnetic field are obtained from renormalized (using a statistical quasi-gaussian closure scheme) one point (Ohm's Law and continuity) and two point energy spectrum equations. The resulting electron thermal diffusivity is applied to heat transport in Ohmically and neutral beam heated tokamaks.

In the second study, we consider computationally the viscous relaxation of the 2-D microtearing equations (Ohm's Law and electron continuity) with a uniform electron temperature profile. The lack of resistivity constrains the problem such that mean square flux is conserved. This problem is motivated by a

similar problem suggested by H. K. Moffatt[46] in which 3-D MHD is relaxed viscously (with magnetic helicity conserved) to study the analyticity of 3-D Navier-Stokes flows. He suggests that an analogy exists between current in MHD and vorticity in Navier-Stokes fluids. Further, recent computational studies[45] of 2-D Navier-Stokes fluids indicate that a special kind of spatial intermittency (isolated vortices) appears in the final state from an initial random state. This intermittent behavior is characterized by the large higher order moment kurtosis, indicating statistically nongaussian flow. The ideas of constrained relaxation and intermittent behavior are combined into a study of the intermittent behavior of the constrained relaxation of 2-D microtearing.

In Chapter III, 2-D microtearing equations are relaxed computationally with mean square flux conserved. The resulting current flow is spatially intermittent characterized by large values of kurtosis and long-lived, isolated (interacting) current filaments. Thus current in 2-D microtearing plays the role of vorticity in 2-D Navier-Stokes. The implications of this intermittent (nongaussian) behavior are discussed

in light of the quasi-gaussian analytic theory used in Chapter II.

C H A P T E R I I

SEMICOLLISIONAL DRIFT MICROTEARING TURBULENCE

2.1 Introduction

One major problem in present fusion theory is the explanation of the physical mechanisms which underlie anomalous electron energy loses near the tokamak edge. Observations of improved energy confinement in the ASDEX and Doublet III[32,47,48,71] tokamaks suggest that edge confinement plays an important role in global energy confinement. Correlation variation in edge magnetic turbulence with the so called High (H) confinement and Low (L) confinement type diverter discharges lends support to a magnetic fluctuation turbulence model. Consideration of "profile consistency"[10,53,58] (rigidity of electron temperature profile) requires that the electron thermal diffusivity be dependent on the gradient of the electron temperature ($\chi_e \sim (\nabla T_e)^b$, $b > 0$). The increasing of χ_e as one goes radially outward supports the premise that edge turbulence is temperature gradient driven. Further, the edge fluctuations are broadband, low frequency ($\omega/2\pi \sim 5 - 50$ kHz, $\omega_*^T \sim (2\pi)13$ kHz, $m \sim 8$) and incoherent.[48] Low frequency implies the possible importance of diamagnetic drifts, while broadband and incoherent fluctuations indicate the turbulent character of the fluctuations.

Microtearing modes have been suggested as a candidate for edge magnetic fluctuations.[14,22,48,58] Such modes are driven by electron temperature gradients, are electromagnetic in character, and are collisional (i.e., electron ion collision frequency greater that diamagnetic drift frequency) near the edge. Microtearing modes rotate at the thermal diamagnetic frequency, which is smaller than the electron ion collision frequency ($\omega_*^T = k_y v_e \rho_e / L_T < \nu_e$, where k_y is the poloidal wave number, ρ_e is the electron gyroradius, L_T is the electron temperature gradient scale length and v_e is the electron thermal velocity). Tearing modes also connect magnetic flux surfaces through radial magnetic field perturbations (δB_r), thereby giving rise to increased thermal energy transport,[14,58] i.e., a net outward flux of electron thermal energy.

In order to examine a simple prototypical model in depth, we consider a fluid theory of semicollisional drift microtearing (high k_y) mode turbulence. Only the simplified model with electron density and magnetic fluctuations is considered. Magnetic field and density are the minimum number of perturbed fields required for a drift semicollisional microtearing mode.

The equations which govern these two fields are a generalized Ohm's Law[23,26] and electron continuity (Eqs. 2-1 and 2-2). Consideration of the effects of electron temperature fluctuations and electrostatic fluctuations is left to future study. These two evolution equations constitute a basic paradigm for magnetic microturbulence and are similar to a shear Alfven models.[12,19] This system has a linear energy source (i.e., the time dependent thermal force due to expansion free thermal energy along magnetic fluctuations) and a sink (resistive dissipation in Ohm's Law). The nonlinearities (similar, respectively, to E × B convection and the J × B force of reduced MHD,[19] are the electron pressure gradient along a fluctuating magnetic field .

$$\left(\frac{\delta B}{B} \cdot \underset{\sim}{\nabla} p_e\right) \quad \text{occurring}$$

in Ohm's Law and the fluctuating parallel compression

$$\left(\frac{\delta B}{B} \cdot \underset{\sim}{\nabla} v_{\parallel}\right) \quad \text{occurring}$$

in the continuity.

As in fluid turbulence, we define the Reynold's number as the inverse of the ratio of a nonlinear interaction time to the dissipation time or

$$R_l \sim \frac{\frac{\delta B}{B} \cdot \nabla p_e}{\eta J} ,$$

where η is the collisional Spitzer resistivity,[25] p_e is the electron pressure and J is the electron current (along the toroidal magnetic field). Later, it will be shown that, nonlocally,

$$R_l \sim \frac{v_D \pi}{\eta k_x |\Delta'|} ,$$

where k_x^{-1} is the radial scale (mode width), Δ' is a measure of the discontinuity of poloidal magnetic field across the mode rational surface,[19] and $v_D \sim \nabla p_e \times \hat{z}$ ($\hat{z}$ points in the torroidal direction), a diamagnetic "eddy velocity." Equivalently, the nonlinear interaction time is the perturbed "Alfven" time [35,57] $(\rho_s v_A \delta B/B_T)^{-1}$, where v_A is the Alfven velocity, B_T is the torroidal magnetic field and ρ_s is the ratio of ion thermal velocity at electron temperature ($c_s^2 = T_e/m_i$) to the ion gyrofrequency. In this work, $R_l > 1$, always,

indicating that nonlinear dissipation dominates Ohmic dissipation at most scales of interest.

Unlike fluid turbulence, we define another "Reynold's number" which represents the ratio of gradients along a fluctuating magnetic field to gradients along the sheared equilibrium magnetic field, i.e.,

$$R_s \sim \frac{\frac{\delta \underset{\sim}{B}}{B} \cdot \underset{\sim}{\nabla}}{(\nabla_\parallel)_0} \sim \frac{\frac{\delta B_r}{B_T} \frac{\partial}{\partial r}}{\frac{k_y}{L_s} r}$$

where r is the radial coordinate, L_s is the shear length ($L_s = q^2R/(r\,\partial q/\partial r)$), R is the major radius and q is the safety factor. R_s is essentially w_I^2/w_m^2 where w_I is the island width,

$$\left(\frac{\delta B}{B} \frac{L_s}{k_y}\right)^{1/2}$$

and w_m is the natural radial scale length which is the microtearing mode width. This second Reynold's number is a consequence of the inhomogeneity (radial scale structure) of microtearing and the stabilizing influence of shear. In this work, we will consider cases of $R_s \gg 1$ (strong turbulence) and $R_s \sim 1$ (moderate turbulence). For present experiments,[48] $R_s \sim 1$

(corresponding to island and mode widths of 1 - 2 cm and $\delta B/B \sim 2 \times 10^{-4}$) is most relevant.

Our goal is to characterize the physics of the saturated state of a long wavelength ($m \sim 10$) microtearing mode in a broadband bath of both magnetic and density fluctuations. Coherent and incoherent mode coupling is considered by an iterative closure of the energy spectrum equations[12] (as well as closure of one-point renormalized eigenmode equations). Unlike previous theories,[14] our inclusion of incoherent mode coupling plays an important role in the saturated state via energy equipartitioning (between internal and magnetic energies) at small scales.

Considerations of magnetic field shear in the nonlinear theory play an additional role. The only previous multihelicity nonlinear theory[14] ignores shear. Shear introduces linear stabilization, as well as giving microtearing mode radial eigenmode structure (nonlocally). This radial structure enters nonlinearly via the island width ($R_s \gtrsim 1$).

For comparison, the case of a uniform equilibrium magnetic field (2D) is treated first. The linear 2-D equivalent of the microtearing mode is the

self-filamentation mode.[26] The 2-D results provide a simple clarification of the sheared field results and are easily checked numerically.

The principal results are summarized as follows:

(i) One point and two point equations are derived for the microtearing mode in a multihelicity environment for uniform and sheared magnetic field using an iterative closure scheme.

(ii) The dominant anomalous effect in the renormalized Ohm's Law is a "hyper-resistivity" due to the back reaction of current compression on diamagnetic convection in Ohm's Law.

(iii) At small scales, a nonlinear "Alfven effect"[35] equipartition process (of magnetic and internal energy) occurs.

(iv) At large scales, the energies are, in general, not equipartitioned.

(v) Considerations of equilibrium statistical mechanics[22,36,40] provides evidence for the cascade of energy to small scales, while mean square flux is transferred to large scales.

(vi) High m stable equipartitioned background turbulence saturates the lower m (~10) unstable microtearing, while energy is driven to small scales.

(vii) The anomalous damping which saturates the unstable mode is the back-reaction of $\nabla_{\parallel} J$ compression on diamagnetic flows in Ohm's Law. In one point theory, this term takes the form of a hyper-resistivity.

(viii) By requiring that total energy be time independent, the saturation level of the magnetic field, in the case of a uniform equilibrium magnetic field (B_0) is:

$$\frac{\delta B}{B_0} \sim (1+\alpha)\alpha\alpha' \left(\frac{\beta_e}{2}\right)^{1/2} \frac{\Omega_e}{\nu_e} \left(\frac{\rho_e}{L_T}\right)^2 ,$$

where β_e is the ratio of thermal pressure to magnetic pressure, Ω_e is the electron gyrofrequency, and α, α' are constants (of order unity).

(ix) In the moderate or strong turbulence regime (island width comparable or larger than mode width), a mixing length theory is found.

the "force free conditions"

$$(\nabla_{\parallel}^{(0)} + (\delta\underset{\sim}{B}/B_T) \cdot \underset{\sim}{\nabla})J = 0$$

and

$$(\nabla_{\parallel}^{(0)} + (\delta\underset{\sim}{B}/B_T) \cdot \underset{\sim}{\nabla})n = 0$$

(where n is the density fluctuation and J is the current fluctuation) determine the mixing length and the stationarity of total (spectral) energy determines the saturation level. The mixing length analysis is discussed through a renormalized eigenmode solution of the one point equations.

(x) For present tokamaks, $R_s \sim 1$ and the saturation level is

$$\frac{\delta B_r}{B_T} \sim \frac{L_s}{L_T} \frac{\nu_e}{\Omega_e} \quad .$$

The corresponding thermal diffusivity (appropriate for the plasma edge) is $\chi_e \sim \chi_{\parallel}(\delta B/B_T)^2 = (v_e^2/\nu_e)(\delta B/B_T)^2$. χ_e scales as

$$\hat{S}^{-2} L_T^{-2} \; n_0 I_p^{-2} T_e^{-1/2},$$

where

$$\hat{S} = (r\partial q/\partial r)/q,$$

n_0 is the electron density and I_p is the plasma current. The corresponding temperature profile is "consistent"[10,58,58] as $\chi_e \sim T_e^{-1/2} L_T^{-2}$ and $L_R \sim q^{1/2}/P_{Heat}^{-1/4} T_e^{-1/8}$, where P_{Heat} is the power transferred to the electrons by Ohmic heating or neutral beams.

(xi) If the temperature scale length is maintained Ohmically, then the energy confinement time is (a is the minor radius)

$$\tau_e \sim \chi_e^{-1} a^2 \sim a^2 \hat{S} T_e^{3/2} \quad (\hat{S} \sim 1\text{-}2),$$

independent of magnetic field.

(xii) If we consider the microtearing mode as a model for edge turbulence during the L phase of beam heated discharges, then electron energy confinement time scales as

$$\tau_E \sim a^2 T_e^{3/4} \hat{s} P_{Heat}^{-1/2} I_p.$$

This result is independent of torroidal magnetic field and density and partially agrees with the scaling of Ohyabu[48] for Doublet III in the L mode (P_{Heat} goes as beam power).

(xiii) Strong shear and higher electron temperatures stabilize the microtearing mode, indicating possible mechanisms for transition from L to H mode confinement.

The remainder of this chapter is organized as follows. The second section is devoted to the basic model and to a review of linear theory (2.2). The third section discusses equilibrium statistical mechanics (2.3), while the fourth outlines the nonlinear theory for a uniform magnetic field. In the fifth section (2.5), the renormalized one and two point equations are derived for the case of a sheared field. Saturation mechanisms are discussed in Section 2.6. Section 2.7 reviews and critiques theoretical as well as experimental results and discusses the implications of Section 2.6 for tokamak heat transport. Finally, Section 2.8 is the conclusion.

2.2 Basic Equations and Linear Behavior

In this section, model equations which constitute a simple characterization of microtearing turbulence are introduced and discussed. Conservation laws associated with this model are also described. Finally, the linear stability analysis of this system is briefly reviewed.

The geometry is a sheared slab: the equilibrium magnetic field points principally in the z (toroidal) direction, with a y (poloidal) component which varies as a function of x (radial direction), and is given by

$$\underset{\sim}{B} = B_0(\hat{z} + (x/L_s)\hat{y}).$$

L_s is the shear length, defined by:

$$L_s = rq^2/rq'$$

where q is the safety factor. The electron temperature, $T_0(x)$, varies with radius on a scale L_T, but for simplicity, the average electron density $n_0(x)$ is uniform. Effectively, we assume $L_T \ll L_n$, where L_n is the density scale length.

Fluctuations in the magnetic field arise as field lines reconnect across the resistive layer, near the rational surface. Driven by the time dependent thermal force[25] (TDTF), these fluctuations couple to the density through Ohm's Law. The density fluctuations are governed by the continuity equation. The nonlinear equations describing these coupled density and magnetic field fluctuations are:[25]

$$\frac{\partial \psi}{\partial t} - \left(\frac{\rho_s}{a}\right)^2 \left(\nabla_\parallel n + (1+\alpha)\nabla_\parallel T_0 - \frac{\alpha\alpha'}{\nu_e}\frac{\partial}{\partial t}\nabla_\parallel T_0 \right) - \eta J = 0 , \qquad (2\text{-}1)$$

$$\frac{\partial n}{\partial t} = -\nabla_\parallel J, \qquad (2\text{-}2)$$

and

$$J = \nabla_\perp^2 \psi , \qquad (2\text{-}3)$$

where ψ is the parallel component of the magnetic vector potential,

$$\rho_s = c_s/\Omega_i = (T_e/m_i)^{1/2} m_i c/eB_0,$$

and a is the minor radius. α and α' are constants derived from the Chapman-Enskog solution of the underlying kinetic equations. η and ν_e are dimensionless resistivity and electron collisionality, respectively. $\underset{\sim}{B}$ is given by:

$$\underset{\sim}{B} = \underset{\sim}{B}_0 + \underset{\sim}{\nabla}\psi \times \hat{z},$$

where

$$\nabla_{\parallel} = (\nabla_{\parallel})_0 + \underset{\sim}{\nabla}\psi \times \hat{z} \cdot \underset{\sim}{\nabla}$$

with $(\nabla_{\parallel})_0$ being the derivative along the equilibrium magnetic field. The normalizations follow those of Hazeltine with time normalized to the Alfven time $\tau_A = a/v_A$ ($v_A^2 = B_0^2/4\pi n_0 m_i$), and length normalized to the minor radius, vector potential normalized to $1/aB_0$, and electron density to $n = n_e/n_0$.

Equation 2-1 is Ohm's law in the semicollisional regime.[14,27] This regime is characterized by finite electron collisionality $\nu_e > \omega$ and by the condition on parallel diffusion of electrons[27] such that

$$\omega \cong (\nabla_{\parallel})_0^2 v_e^2/\nu_e \qquad (2\text{-}4)$$

where v_e is the electron thermal velocity and ω is the mode frequency. The perturbed linear parallel current J is localized around the mode rational surface (mrs) by the spacial extent of the conductivity,[13,14,23] determined when $(\nabla_{\parallel})_0 = k'_{\parallel}\Delta_\sigma$, subject to the restriction given by Eq. 2-4. Here, $k'_{\parallel} = k_y/L_s$, where k_y is the poloidal wavenumber. The electrostatic potential (ϕ) is small when Eq. 2-4 holds, since

$$\Delta_\sigma << \Delta_E, \qquad (2\text{-}5)$$

where Δ_E is the spacial extent[13,23] of the parallel electric field

$$E_{\parallel} = \frac{-\partial\psi}{\partial t} - (\nabla_{\parallel})_0\phi \ .$$

Δ_E is the point where the electrostatic piece "shorts out" the inductive piece of $E_{\parallel}$, i.e., when

$$\Delta_E \cong \left(\frac{\omega}{v_A^2 (k'_{\parallel})^2 \eta}\right)^{1/4} . \qquad (2\text{-}6)$$

Hence, the electrostatic potential can be ignored if the restrictions in Eqs. (2-1), (2-4) and (2-5) are satisfied. Temperature fluctuations are also ignored for simplicity, since they do not alter the linear theory significantly. Nonlinearly, it has been shown that temperature fluctuations are responsible for quasi-linear stabilization of the tearing mode.[63] However, a calculation of multihelcity turbulence, although involved, indicates that temperature fluctuations do not play a new significant role in the physics of the saturated state. Careful consideration of this third field is left for future work.

The terms present in Eq. (2-1) correspond to the inductive piece of the electric field, the parallel pressure gradient, the thermal force, resistive dissipation and the TDTF.[25] A discussion of the physics underlying the time dependent thermal force is given in Ref. 25. Note that the TDTF permits tearing instabilities to access the free energy available in the electron temperature gradient, even when Δ' is negative (no free energy available in the current gradient). The pressure gradient and thermal force act only to cause a diamagnetic rotation in the system, since they are

90° out of phase with the destabilizing time dependent thermal force.

The second equation, Eq. (2-2) describes electron density fluctuations, which couple to magnetic fluctuations through parallel compression, analogous to the J × B force. Appropriate to the assumption of negligible electrostatic fluctuations convective drifts due to perpendicular flows (diamagnetic and E × B drifts) do not enter the density evolution equation. The third equation, Eq. (2-3) is Ampere's law and relates the current to the vector potential.

In the absence of dissipation, this system of equations has three conservation laws.[27] The first of these expresses the conservation total energy E_{TOT}, consisting of magnetic energy $(\nabla_\perp \psi)^2/2$ and internal energy $(\rho_s/a)^2 n^2/2 \sim (T_0/n_0)n^2/2$. Multiplying Eq. (2-1) by $-J$ and Eq. (2-2) by $(\rho_s/a)^2 n$, adding and integrating over volume, one obtains the evolution equation for E_{TOT},

$$\frac{\partial E_{TOT}}{\partial t} = \frac{\partial}{\partial t} \int d\underset{\sim}{x}[(\nabla_\perp \psi)^2/2 + (\rho_s/a)^2 n^2/2] = -\int d\underset{\sim}{x} \eta J^2$$

$$- (\rho_s/a)^2 \int d\underset{\sim}{x} (\alpha\alpha'/\nu_e) J \frac{\partial}{\partial t} \nabla_\parallel T_0 + \int d\underset{\sim}{x}\, \Delta_E \qquad (2\text{-}7),$$

where

$$\Delta_E = -J(\rho_s/a)^2 \underset{\sim}{\nabla}\psi \times \hat{z} \cdot \underset{\sim}{\nabla} n$$

$$- (\rho_s/a)^2 n \underset{\sim}{\nabla}\psi \times \hat{z} \cdot \underset{\sim}{\nabla} J. \qquad (2\text{-}8)$$

The evolution of total energy is driven by resistive dissipation and "inverse dissipation" from the temperature gradient free energy source tapped via the TDTF. Energy is conserved up to dissipation and drive because the contribution from the nonlinearities,

$$\int d\underset{\sim}{x}\ \Delta_E,$$

vanishes identically. This result follows from substitution of Eq. (2-7) into Eq. (2-9), partial integration of one of the two terms of Eq. (2-6) and the fact that $\nabla \cdot B = 0$.

The second conservation law is for mean square flux $\int d\underset{\sim}{x}(\psi)^2/2$. Multiplying Ohm's Law, Eq. (2-1), by ψ and integrating over space,

$$\frac{\partial}{\partial t}\int d\underset{\sim}{x}(\psi)^2/2 = -\eta\int d\underset{\sim}{x}(\nabla_\perp\psi)^2$$

$$+(\rho_s/a)^2\alpha\alpha'/\nu_e\int d\underset{\sim}{x}\psi\frac{\partial}{\partial t}\nabla_\parallel T_0 + \int d\underset{\sim}{x}\Delta_\psi, \qquad (2\text{-}9)$$

where

$$\Delta_\psi = (\rho_s/a)^2\psi\nabla_\parallel n = \underset{\sim}{v}_D\cdot\underset{\sim}{\nabla}(\psi^2/2), \qquad (2\text{-}10)$$

and

$$\underset{\sim}{v}_D = (\rho_s/a)^2\underset{\sim}{\nabla}n\times\hat{z}\ .$$

The right hand side of this equation contains Ohmic dissipation, the TDTF term and the nonlinearity Δ_ψ. Mean square flux is conserved up to dissipation and TDTF because

$$\int d\underset{\sim}{x}\ \Delta_\psi = 0.$$

The convection of mean square flux by diamagnetic drift v_D is conservative because incompressibility of the diamagnetic flow allows Δ_ψ to be written as a total derivative, so that $\int d\underset{\sim}{x}\ \Delta_\psi = 0$.

The structure of the nonlinearities admits a third conservative law, that of "cross helicity" $H = \int d\underset{\sim}{x}\, n\psi$. We set H equal to zero for convenience. In general, though, conservation of cross helicity is an important physical consideration and is presented here for completeness. Multiplying Eq. (2-1) by n and integrating yields

$$\frac{\partial}{\partial t}\int d\underset{\sim}{x}\, n\psi = -\eta \int d\underset{\sim}{x}(\nabla_\perp n)(\nabla_\perp \psi)$$

$$- (\rho_s/a)^2 \alpha\alpha'/\nu_e \int d\underset{\sim}{x}\, n \frac{\partial}{\partial t} \nabla_\parallel T_0 + \int d\underset{\sim}{x}\Delta_H \qquad (2\text{-}11)$$

where

$$\Delta_H = (\rho_s/a)^2(n\nabla_\parallel n - \psi\nabla_\parallel J). \qquad (2\text{-}12)$$

Cross helicity is conserved up to resistive dissipation and the TDTF because $\int d\underset{\sim}{x}\, \Delta_H = 0$. This is readily verified by writing

$$\nabla_\parallel nn = n\underset{\sim}{\nabla} n \times \hat{z} \cdot \underset{\sim}{\nabla}\psi$$

and integrating by parts. In the case of the first

nonlinearity, and simple partial integration in the second case. Note that unlike energy conservation, where two nonlinearities cancel, cross helicity is conserved because each vanishes individually. As with mean square flux, (anticipating later discussion of mean square flux cascades) the individual conservation could be connected to a cascade to large or small scales.

The first two conservation laws play an important role in regulating saturation and the transfer among spectral components of energy and mean square flux in the turbulent steady state. They will be discussed in greater detail in later sections, 2.3, 2.4 and 2.5.

The linear theory of microtearing modes has been presented elsewhere.[13,23,27] Here it is briefly reviewed, mainly to stress concepts which will prove to be of importance in the renormalized turbulence theory. The linear eigenmode equation is obtained by Fourier transforming the linearized basic equations, Eqs. (2-1), (2-2), and (2-3). The Fourier transform is given by

$$\begin{Bmatrix} \psi(x,y,z,t) \\ n(x,y,z,t) \end{Bmatrix} = \int d\omega \int dy \int dz \, \exp[ik_z z + ik_y y - i\omega t] \begin{Bmatrix} \psi_k(x) \\ n_k(x) \end{Bmatrix}_{\omega} ,$$

where

$$L_s = rq^2/rq'$$

and x is the distance to the mode rational surface. The eigenmode equation is

$$\nabla_\perp^2 \psi_{\underset{\sim}{k}} = -i\omega\sigma(x)\psi_{\underset{\sim}{k}}, \tag{2-14}$$

where

$$\sigma(x) = \frac{\left[1 - \frac{\omega_*^T}{\omega}\left(1 + \alpha + \frac{i\alpha\alpha'\omega}{\nu_e}\right)\right]}{\eta\left(1 + \frac{x^2}{\bar{w}^2}\right)}, \tag{2-15}$$

$$\omega_*^T = k_y T_e / L_T B_0,$$

and

$$w^2 = L_s^2 \eta\omega(a/\rho_s)^2/k_y^2. \tag{2-16}$$

The dispersion relation is obtained by integrating over x according to the usual constant ψ[19] prescription. Hence, ψ is taken as constant over width w of the resistive layer and the jump in ψ',

$$\psi^{-1} d\psi/dx \Big|_{-w}^{w} = \Delta' = -2|k_y|$$

is given by the solution of the external problem. For

$$\eta\Delta'/4\pi < w(1 + \alpha)\omega_*^T,$$

the complex frequency is

$$\omega = (1 + \alpha)\omega_*^T + i\alpha\alpha'(1 + \alpha)\frac{\omega_*^{T2}}{\nu_e} - \eta 2^{1/2} k_y i^{3/2}/w\pi \qquad (2\text{-}17)$$

where to good approximation w is determined from Eq. (2-16) by substituting the drift part of the eigenfrequency for ω:

$$w^2 = \frac{L_s^2}{k_y^2}(1 + \alpha)\omega_*^T \eta \ (a^2/\rho_s^2) \ .$$

Eq. (2-17) is valid only for $\omega_*^T < \nu_e$. In the opposite limit, the Chapman-Enskog solution breaks down[25] and $(\omega_*^T)^2/\nu_e$ in Eq. (2-17) is effectively replaced by ν_e.[28] In the semicollisional regime, ν_e is insignificant due

to the restriction in Eq. (2-4), especially near the mode rational surface. This feature implies the existence of growth and dissipation ranges in the k_y spectrum. For k_y small, $\omega_*^T < \nu_e$ and the TDTF is able to overcome resistive dissipation, producing a growing mode. As k_y becomes large, $\omega_*^T > \nu_e$ and the linear source turns off. Furthermore, the mode width w tends to decrease with increasing k_y, ($w \sim k_y^{-1}$ for $\omega k_y > 1$) thus increasing the resistive damping. Therefore energy is effectively injected at small k_y and dissipated at large k_y.

The shearless analogue (uniform equilibrium magnetic field) of the dispersion relation, Eq. (2-17) is

$$\omega = (1 + \alpha)\omega_*^T + i\alpha\alpha'(1 + \alpha)\frac{\omega_*^{T2}}{\nu_e} - \eta(k_x^2 + k_y^2), \tag{2-18}$$

sometimes called the "self filamentation mode."[26] The dissipation is now weakened (by $k_y w < 1$) over the sheared case, portraying shear as a dissipation mechanism.

Physically, shear provides a sink of energy through field line bending. We see from the dispersion relation, Eq. (2-17), that the microtearing mode indicates a competition between temperature gradient drive and resistive dissipation, enhanced by shear. Increasing temperature and poloidal mode number and decreasing temperature gradient, magnetic field and density also stabilize the mode. Given current interest in the concept of profile consistency, it is an amusing exercise to express the temperature gradient stability boundary such that

$$\left|\frac{dT_e}{dr}\right| > C(T_e^{-7/10} B_0 n_0^{2/5} L_s^{-2/5} k_y^{-3/5}) \qquad (2\text{-}19)$$

is required for instability, where C is a constant. Note that the restriction $\omega_*^T < \nu_e$ [13,23] does not constitute a stability "boundary," but indicates the onset of a gradual transition of growth rate from $\gamma \sim (\omega_*^T)^2/\nu_e$ (moderate) to $\gamma \sim \nu_e$ (small), as found by a full kinetic theory.[13,23]

Two additional key assumptions and constraints on the linear theory are (1) $k_y w < 1$ and (2) constant

ψ.[19] The former constraint is a measure of the extent of line bending or spatial nonlocality and allows one to let

$$\nabla_{\perp}^2\psi = \frac{\partial^2}{\partial x^2} - k_y^2\,\psi \cong \frac{\partial^2\psi}{\partial x^2} .$$

The latter restriction is a constraint on plasma beta. Constant ψ requires (see Appendix)

$$|\omega\sigma(x)|w^2 \ll 1 \qquad (2\text{-}19)$$

which reduces to (noting that $k_{\parallel}^2 v_e^2/\nu_e \cong \omega_*^T$)

$$\frac{\beta_e}{2} < \left(\frac{L_T}{L_s}\right)^2 \qquad (2\text{-}20)$$

where

$$\beta_e \equiv 8\pi n_0 T_0/B^2 .$$

The restrictions discussed above limit the validity of Eqs. (2-1), (2-2), and (2-3) to the tokamak edge. Edge plasmas have sufficiently low densities and temperatures to insure that the collisionality condition

$\omega_*^T < \nu_e$ is satisfied. Also the plasma betas are sufficiently low to guarantee that the constant ψ approximation ($\beta_e < (L_T/L_s)^2$) is satisfied. Further, the semi-collisional condition

$$k_\parallel^2 v_e^2/\nu_e \cong \omega_*^T$$

restricts ν_e such that electrons are not hydrodynamic

$$(\omega_*^T > k_\parallel^2 v_e^2/\nu_e)$$

(and requires strong shear near the edge). To neglect electrostatic effects, the condition $\Delta_\sigma << \Delta_E$ requires

$$\nu_e/\omega_*^T < (m_i/m_e)(L_T/L_s)^2$$

and also restricts collisionality. Hence, plasma edge conditions which are too cold eliminate microtearing as a possible explanation of edge fluctuations.

Edge fluctuations are broadband and hence the "nonlocality" condition $k_y w < 1$ is satisfied for a variety of poloidal mode numbers (typically $m \sim 7$-10). Finally, evidence of strong electron temperature

gradients near the edge provides the free energy source for instability. We conclude that the model presented in this section provides a simple set of equations to study the physics of microtearing turbulence near the edge.

2.3 Equilibrium Statistical Mechanics

Our exposition of the theory of microtearing turbulence begins with a discussion of the equilibrium statistical mechanics of the nonlinear system, Eqs. (2-1), (2-2) and (2-3). The goal of this section is to determine the cascade directions of mean square flux, magnetic energy, and total energy.

We begin by noting that turbulence resembles equilibrium statistical mechanics[69] because both systems have an infinite number of degrees of freedom and both involve phase mixing of individual degrees of freedom. In classical systems,[69] equilibrium is based upon a Liouville theorem such that:

$$\frac{\partial}{\partial \underset{\sim}{q}} \cdot \frac{\partial}{\partial t} \underset{\sim}{q} + \frac{\partial}{\partial \underset{\sim}{p}} \cdot \frac{\partial}{\partial t} \underset{\sim}{p} = 0 \qquad (2\text{-}21)$$

where $\underset{\sim}{q}$ and $\underset{\sim}{p}$ are the canonical coordinates and momenta, respectively. For turbulent systems, similar Liouville theorems exist,[22,40,42] but these systems can not be put into Hamiltonian forms (i.e., not derivable from a Hamiltonian). Typically, these "Liouville theorems" for nonlinear systems are a result of conserved quantities (such as energy) and constraints such as incompressibility.[40]

Let us consider a conservative turbulent system (one with a Liouville theorem) such that initially it is perturbed about an equilibrium. Then (in the final state), the equilibrium probability distribution, P, must be a function of the conserved quantities. This probability distribution gives the equilibrium average of the quantity f as:

$$\langle f \rangle = \frac{\int d\underset{\sim}{p} d\underset{\sim}{q} P f}{\int d\underset{\sim}{p} d\underset{\sim}{q} P} \qquad (2\text{-}22)$$

where $d\underset{\sim}{p}d\underset{\sim}{q}$ are the canonical (or noncanonical) variables used in Liouville's theorem. Two important distributions corresponding to the microcanonical and canonical ensembles of Gibb's[69] are:

$$P = \prod_i \delta(\epsilon_i - \langle \epsilon \rangle_i) \qquad (2\text{-}23)$$

and

$$P = \exp(-\sum_i \alpha_i \epsilon_i)$$

where ϵ_i are the conserved quantities and α_i are constants (Lagrange multipliers). The former distribution is applicable to an isolated system, and the latter corresponds to system in contact with a "heat" bath. Turbulent systems[40] are frequently in contact with outside sources, and the canonical distribution seems appropriate. Further, for two systems in contact, the canonical distribution preserves the constancy of the ϵ_i[40] (i.e., this distribution is stable under arbitrary perturbations of the equations of motion which preserve ϵ_i).

In general, statistical closures are perturbations about some equilibrium. In this sense, Liouville theorems could exist for DIA-like closures. Further, one can show that equivalent to Liouville's theorem, is the existence of an H theorem such that

$$\frac{\partial S}{\partial t} > 0 \qquad (2\text{-}24)$$

where

$$S = \int d\underset{\sim}{p} d\underset{\sim}{q} \log P \ . \qquad (2\text{-}25)$$

In a recent paper,[9] an H theorem is shown to be generic to systems equivalent to truncated second order Markovian closure models (such as EDQM). The restrictions that govern the applicability of this result to the present case (microtearing) are that the eddy turnover time S (nonlinear interaction rates) must not be field dependent (i.e., different for Ohm's Law and continuity equations), the system must be homogeneous, and no forcing (instability) or dissipation exist in the system.

Consider the application of the above framework to 2-D Navier-Stokes fluids.[40] The inviscid constants of motion are energy and enstrophy. The basic inviscid equation for vorticity is

$$\frac{d\omega}{dt} = 0$$

where $\underset{\sim}{\omega} = \underset{\sim}{\nabla} \times \underset{\sim}{v}$,

$$\frac{d}{dt} = \frac{\partial}{\partial t} + \underset{\sim}{v} \cdot \underset{\sim}{\nabla} ,$$

and $\underset{\sim}{v}$ can be written as $v = \underset{\sim}{\nabla}\phi \times \hat{z}$ (ϕ is the stream function). Energy and enstrophy can be defined, respectively, as:

$$E = \int d\underset{\sim}{x} \frac{(v \cdot v)^2}{2}$$

and

$$\Omega = \int d\underset{\sim}{x} \frac{\omega^2}{2} \quad .$$

Using the canonical distribution, equilibrium statistical mechanics predicts that:

$$E = \sum_k E_k \sim \sum_k \frac{1}{\alpha + \beta k^2}$$

and

$$\Omega = \sum_k \Omega_k \sim \sum_k \frac{k^2}{\alpha + \beta k^2} ,$$

where α and β are constants (representing effective inverse "temperatures") and $E_{\underset{\sim}{k}}$ and $\Omega_{\underset{\sim}{k}}$ are fourier amplitudes. The Liouville theorem is based on the incompressibility of the flow. Writing the fourier amplitude of velocity as $\underset{\sim}{v}_{\underset{\sim}{k}} = \underset{\sim}{g}_{\underset{\sim}{k}} + i\underset{\sim}{b}_{\underset{\sim}{k}}$, then

$$\frac{\partial}{\partial \underset{\sim}{a}_{\underset{\sim}{k}}} \cdot \frac{\partial}{\partial t} \left(\underset{\sim}{a}_{\underset{\sim}{k}}\right) + \frac{\partial}{\partial \underset{\sim}{b}_{\underset{\sim}{k}}} \cdot \frac{\partial}{\partial t} \left(\underset{\sim}{b}_{\underset{\sim}{k}}\right) = 0. \qquad (2\text{-}26)$$

As k approaches infinity (k_{max}), the spectral component of enstrophy grows indicating that $\Omega_{\underset{\sim}{k}}$ is dominated by the largest wavenumbers. Similarly, $E_{\underset{\sim}{k}}$ is dominated by the smallest wavenumbers. This behavior indicates an accumulation of enstrophy at small scales while energy tends to accumulate at large scales.

With the addition of magnetic field dynamics, the system of interest is 2-D MHD.[22] The dissipationless equations are

$$\frac{\partial \psi}{\partial t} + \underset{\sim}{v}_E \cdot \underset{\sim}{\nabla} \psi = 0$$

and

$$\frac{\partial \omega}{\partial t} + \underset{\sim}{v} \cdot \underset{\sim}{\nabla} \omega = \underset{\sim}{B} \cdot \underset{\sim}{\nabla} J$$

where $\underset{\sim}{v}_E = \underset{\sim}{\nabla}\phi \times \hat{z}$ ($\underset{\sim}{E} \times \underset{\sim}{B}$ drift), $\omega = \nabla_\perp^2\phi$, ψ is the vector potential, $B = \underset{\sim}{\nabla}\psi \times \hat{z}$ and $J = \nabla_\perp^2\psi$. Total energy and mean square flux are conserved, so that:

$$\frac{\partial}{\partial t} E_T = \frac{\partial}{\partial t} \frac{1}{2} \int d\underset{\sim}{x}((\underset{\sim}{v} \cdot \underset{\sim}{v}) + (\underset{\sim}{B} \cdot \underset{\sim}{B}) = 0$$

and

$$\frac{\partial \mathcal{A}}{\partial t} = \frac{\partial}{\partial t} \frac{1}{2} \int d\underset{\sim}{x}\ \psi^2 = 0.$$

In contrast to Navier-Stokes intuition, the total energy goes to small scales and mean square flux accumulates at large scales. This follows from equilibrium statistical mechanics, where a Liouville theorem (similar to Eq. (2-26) results from fluid incompressibility and $\underset{\sim}{\nabla} \cdot \underset{\sim}{B} = 0$. Analogous to 2-D fluids, a canonical distribution yields

$$E_k^m = \frac{1}{2} \int d\underset{\sim}{x}(\underset{\sim}{B} \cdot \underset{\sim}{B})\exp(-i\underset{\sim}{k} \cdot \underset{\sim}{x}) \sim \frac{k^2}{\beta + \alpha k^2}$$

and

$$E_k^K = \int dx \, \frac{(\underset{\sim}{v} \cdot \underset{\sim}{v})}{2} \exp(-i\underset{\sim}{k} \cdot \underset{\sim}{x}) \sim \alpha^{-1}$$

$$a_k = \int dx \, \frac{\psi^2}{2} \exp(-i\underset{\sim}{k} \cdot \underset{\sim}{x}) \sim \frac{1}{\beta + \alpha k^2} \, .$$

From large and small limits of wavenumber, we see that $a_{\underset{\sim}{k}}$ is dominated by large scales and $E_{\underset{\sim}{k}}^m$ is dominated by small scales. Thus, magnetic energy has a tendency to accumulate at small scales while mean square flux goes to large scales. In addition, we see that kinetic energy (fluid energy) is equipartitioned with magnetic energy at small scales. However, one might expect that the straining of flux ψ by $\underset{\sim}{v}_E$ would make ψ go to small scales. The reason straining does not dominate mean square flux dynamics, is that:

(1) the J × B back-reaction in Ohm's Law determines the straining of mean square flux (ψ is not a passive scaler)

(2) the J × B force ($\underset{\sim}{B} \cdot \underset{\sim}{\nabla} J$) breaks conservation of enstrophy.

The microtearing equations (Eqs. (2-1), (2-2), (2-3)) in the limit of negligible dissipation ($\eta = 0$), rotation ($\omega_*^T = 0$), and shear ($k_\parallel = 0$) are similar to those of 2-D MHD. Notice, however, the important

differences:

(1) the E × B (electrostatic) convective drift (v_E) is replaced by the diamagnetic convective drift ($\underset{\sim}{v}_D = \underset{\sim}{\nabla} n \times \hat{z}$)

(2) inertia ($\frac{\partial}{\partial t} \nabla_\perp^2 \phi$) is replaced by electron density

(3) convection ($\underset{\sim}{v}_E \cdot \underset{\sim}{\nabla}\nabla^2\phi$) does not enter because $\underset{\sim}{v}_D \cdot \underset{\sim}{\nabla} n = 0$.

Because of the incompressibility of the diamagnetic flow ($\underset{\sim}{\nabla} \cdot \underset{\sim}{v}_D = 0$) and $\underset{\sim}{\nabla} \cdot \underset{\sim}{B} = 0$, a Liouville theorem exists, such that

$$\sum_{\underset{\sim}{k}} \frac{\partial \dot{y}_{\underset{\sim}{k}}}{\partial y_{\underset{\sim}{k}}} = 0$$

where the $y_{\underset{\sim}{k}}$ are the real imaginary parts of the spectral components of current and "diamagnetic vorticity" ($\underset{\sim}{\nabla} \times \underset{\sim}{v}_D$) (such that the reality condition of spectral components is assumed). A probability density follows, corresponding to the canonical distribution function, whereby

$$P = \exp[-(\alpha E_T + \beta \mathcal{Q})].$$

E_T and $\mathcal{A}$ are the total energy and mean square flux, respectively. These quadratic quantities have been shown to be conserved in the previous section such that:

$$\frac{\partial E_T}{\partial t} = \frac{\partial}{\partial t} \int dx \left(\frac{B^2}{2} + (\rho_s/a)^2 \frac{n^2}{2} \right) = 0$$

and

$$\frac{\partial \mathcal{A}}{\partial t} = \frac{\partial}{\partial t} \int dx \frac{\psi^2}{2} = 0.$$

Average quantities in this "statistical equilibrium" are, for any f,

$$\langle f \rangle = \frac{\int \Pi_i dy_i f P}{\int \Pi_i dy_i P} .$$

Hence, the fourier amplitudes of magnetic energy, internal energy and mean square flux are:

$$E^m_{\underset{\sim}{k}} \sim \frac{k^2}{\beta + \alpha k^2} \qquad (2\text{-}27)$$

$$E^I_{\underset{\sim}{k}} \sim \alpha^{-1} \qquad (2\text{-}28)$$

$$\mathcal{A}_{\underset{\sim}{k}} \sim \frac{1}{\beta + \alpha k^2} \qquad (2\text{-}29)$$

Here, α and β are inverse "temperatures," with $\alpha > 0$ and $\alpha > -\beta/k_m^2$ (normalizability of P). k_m is the minimum wavenumber in this system. A further constraint is found by matching the spectral amplitudes to their conserved quantities, such that:

$$E^T = \sum_{\underset{\sim}{k}} \frac{1}{\alpha} + \frac{k^2}{\beta + \alpha k^2} \tag{2-30}$$

and

$$\mathcal{A} = \sum_{\underset{\sim}{k}} \frac{1}{\beta + \alpha k^2} \quad . \tag{2-31}$$

From Eqs. (2-27), (2-28) and (2-29) we see that, as in 2-D MHD,[22] magnetic energy is dominated by large wavenumbers, while mean square flux is dominated by small wavenumbers, indicating a cascade of magnetic energy to small scales and an accumulation of mean square flux at large scales. Internal and magnetic energy tend to be equipartitioned at small scales. Using Eqs. (2-28) through (2-31) we see that in general,

$$\sum_{\underset{\sim}{k}} (E^m_{\underset{\sim}{k}} - E^I_{\underset{\sim}{k}}) = \frac{-2\mathcal{A}\beta}{\alpha} \tag{2-32}$$

indicating that total magnetic energy and total internal energy are not equal.

The above exercise has a number of limitations.[9,22,40] First, we are limited to a truncated system ($k_{min} < k < k_{max}$). Second, inhomogeneity (such as temperature gradients), and dissipation break the conservation laws and thus must be absent. The same holds for any forcing, such as instability. Third, these results hold for two dimensions, such that shear can not be treated.

Unfortunately, real microtearing turbulence is 3-D, inhomogeneous, forced, and dissipative. Nevertheless, in a strongly nonlinear turbulent system, statistical mechanics does give an indication of the preferred final states reached by cascading. This is especially true because in 3-D microtearing turbulence, magnetic energy is more sensitive to small scales than mean square flux (since the energy involves small radial scales through:

$$E_k^m = -J_k\psi_k \sim -\psi_k \frac{\partial^2 \psi_k}{\partial x^2} \quad .$$

Further, eddy turnover times dominate the linear

dissipative and forcing times (growth time) in a strongly turbulent system.

2.4 Renormalized Theory in a Uniform Equilibrium Magnetic Field

We now discuss the derivation of the renormalized one point and two point (energy and mean square flux) equations for the simple case of semicollisional microtearing turbulence in a spatially homogeneous plasma immersed in a uniform magnetic field $B_0\hat{z}$. Special attention is paid to physical origin, content and interpretation of the one point and two point renormalized equations.

In the shearless limit, the exact equations resemble two-dimensional MHD[56,41] (see Section 2.2), but with a TDTF[25] source. The source term is not modified if shear is added. On the other hand, the sink (or dissipation), although qualitatively the same, reflects the radial eigenmode structure introduced by finite shear via the mode width $w \ll k_y^{-1}$.

The dispersion relation for the "self filamentation" mode[26] is given by Eq. (2-18), with instability for

$$v_D^2/\nu_e > (\nu_e c^2/\omega_{pe}^2)(k_\perp^2/k_y^2)$$

($\omega_*^T = k_y v_D$, c^2/ω_{pe}^2 is the collisionless skin depth). Physically, this corresponds to spontaneous current filamentation, even though the initial magnetic field is uniform.

A two dimensional model, although not representative of the strong radial dependence in tokamaks, can be relevant because the linear source does not change with shear. Further, a two dimensional problem is easily simulated numerically, allowing comparisons of analytic theory with the simulation.

2.4.1 One-Point Theory

We begin with a derivation of the one point renormalized equations following the analysis of Diamond, et al.[12] Some results are omitted.

Fourier decomposing Eqs. (2-1), (2-2), and (2-3) such that

$$\begin{Bmatrix}\psi(x,y,t)\\ n(x,y,t)\end{Bmatrix} = \int dx \int dy \int d\omega \exp[-i\omega t + ik_x x + ik_y y] \begin{Bmatrix}\psi_{\underline{k}}\\ n_{\underline{k}}\end{Bmatrix},$$

where

$$\underset{\sim}{k} = (k_x, k_y, \omega),$$

then the eigenmode equations are

$$-i\omega\psi_{\underset{\sim}{k}} - i\omega_*^T(1 + \dot{\alpha} + \alpha\alpha'\omega/\nu_e)\psi_{\underset{\sim}{k}} + \eta k_\perp^2 \psi_{\underset{\sim}{k}} = N_{\perp R} \tag{2-33}$$

$$-i\omega n_{\underset{\sim}{k}} = N_{\perp U} \tag{2-34}$$

where

$$N_{\perp R} = (\rho_s/a)^2[\underset{\sim}{\nabla}\psi \times \hat{z} \cdot \underset{\sim}{\nabla} n]_{\underset{\sim}{k}},$$

$$N_{\perp U} = -[\underset{\sim}{\nabla}\psi \times \hat{z} \cdot \underset{\sim}{\nabla} J]_k,$$

and

$$J_{\underset{\sim}{k}} = (\nabla_\perp^2 \psi)_{\underset{\sim}{k}} = -k_\perp^2 \psi_{\underset{\sim}{k}} \cdot \tag{2-35}$$

For any f, the convolution is

$$[\underset{\sim}{\nabla}\psi \times \hat{z} \cdot \underset{\sim}{\nabla} f]_{\underset{\sim}{k}}$$

$$= \frac{1}{2} \sum_{\underset{\sim}{k}'} (\underset{\sim}{k} \times \hat{z} \cdot k')(\psi_{-\underset{\sim}{k}'} f_{k+k'} - \psi_{\underset{\sim}{k}+\underset{\sim}{k}'} f_{-\underset{\sim}{k}'}) \quad (2\text{-}36)$$

(note that in cross products $\underset{\sim}{k} = (k_x, k_y)$).

Some initial considerations are addressed before detailing the renormalization. First, a broad spectrum ("bath") of modes is assumed. Consistent with the linear growth rate, we assume this "bath" consists of linearly stable small scale modes and unstable large scale modes. Second, cross helicity terms ($\langle n\psi \rangle$ and $\langle nJ \rangle$) are set to zero for simplicity (although, in general, parity mixing does occur in nonlinear systems). The important symmetry[12] (analogous to 2-D MHD),

$$\psi_{-\underset{\sim}{k}} = \psi_{\underset{\sim}{k}} \quad (2\text{-}37)$$

$$n_{-\underset{\sim}{k}} = -n_{\underset{\sim}{k}} ,$$

is broken in k_y due to diamagnetic rotation. The symmetry still remains in k_x.

Under these considerations, the beat interaction fields ($\psi_{\underset{\sim}{k}+\underset{\sim}{k}'}, n_{\underset{\sim}{k}+\underset{\sim}{k}'}$) appearing in Eqs. (2-33) and (2-34) are obtained and iteratively substituted back into Eqs. (2-33) and (2-34). Consistent with quasi-gaussian statistics, the beat interaction fields are derived by retaining solely the lowest order piece of the nonlinearity (the piece phase coherent with the test mode $\underset{\sim}{k}$) thus closing the equations.[16,24] The phase incoherent pieces are negligible due to the sum over modes with random phases. Hence, for any field f

$$(\nabla_{\parallel} f)_{\underset{\sim}{k}+\underset{\sim}{k}'} = \frac{1}{2}(\psi_{\underset{\sim}{k}} f_{\underset{\sim}{k}'} - f_{\underset{\sim}{k}} \psi_{\underset{\sim}{k}'})(\underset{\sim}{k}' \times \hat{z} \cdot \underset{\sim}{k}). \qquad (2\text{-}38)$$

Using Eqs. (2-33) and (2-34) the driven beat fields are

$$\psi_{\underset{\sim}{k}''} = R \mathcal{L}^{(1)}_{\underset{\sim}{k},\underset{\sim}{k}',\underset{\sim}{k}''} \qquad (2\text{-}39)$$

$$n_{\underset{\sim}{k}''} = U \mathcal{L}^{(2)}_{\underset{\sim}{k},\underset{\sim}{k}',\underset{\sim}{k}''} \qquad (2\text{-}40)$$

where $\underset{\sim}{k}'' = \underset{\sim}{k} + \underset{\sim}{k}'$,

$$R = (\rho_s/a)^2 (\nabla_{\parallel} n)_{k''},$$

$$U = -(\nabla_{\parallel} J)_{\underset{\sim}{k}''},$$

and $\mathcal{L}^{(1)}_{\underset{\sim}{k},\underset{\sim}{k}',\underset{\sim}{k}''}$ and $\mathcal{L}^{(2)}_{\underset{\sim}{k},\underset{\sim}{k}',\underset{\sim}{k}''}$ represent the propagators for the driven Ohm's Law and continuity, respectively. These propagators are derived from a EDQM[24,50,56] closure and are

$$\mathcal{L}^{(1)}_{\underset{\sim}{k},\underset{\sim}{k}',\underset{\sim}{k}''} = \frac{1}{-i\Delta\omega + \delta\gamma_{\underset{\sim}{k}} + \delta\gamma_{\underset{\sim}{k}'} + \delta\gamma_{\underset{\sim}{k}''}} \tag{2-41}$$

and

$$\mathcal{L}^{(2)}_{\underset{\sim}{k},\underset{\sim}{k}',\underset{\sim}{k}''} = \frac{1}{\delta\gamma_{\underset{\sim}{k}} + \delta\gamma_{\underset{\sim}{k}'} + \delta\gamma_{\underset{\sim}{k}''}} \quad , \tag{2-42}$$

where

$$\Delta\omega = \omega_{\underset{\sim}{k}} - \omega_{\underset{\sim}{k}''} + \omega_{\underset{\sim}{k}'}$$

and

$$\omega_{\underset{\sim}{k}} = \omega_*^T(1 + \alpha)$$

$$+ i((\omega_*^T)^2(1 + \alpha)\alpha\alpha'/\nu_e - \eta k_\perp^2).$$

$\Delta\omega$ represents the three-wave frequency mismatch[24] and $\delta\gamma$ is the nonlinear interaction time (or "eddy turnover time"). Although $\psi^{(2)}_{\underset{\sim}{k}''}$ precesses at ω^T_*, the rotation rate is nondispersive and hence $Re(\Delta\omega) = 0$. $Im(\Delta\omega)$ is negligible in a high Reynold's number plasma, where $\delta\gamma >> \eta k_\perp^2$. As we will find in the next subsection, $\delta\gamma$ is a "diamagnetic eddy turnover time"

$$k_\perp \delta v_D \sim k_\perp^2 \rho_e v_e (n/n_0)_{rms}$$

when the magnetic and internal energies are equipartitioned such that

$$\rho_e v_e (n/n_0)_{rms}$$

$$= \rho_s v_A (\delta B/B_0)_{rms}$$

($\delta\gamma$ is an equipartitioning time).

Substituting Eqs. (2-39) and (2-40) into Eqs. (2-33) and (2-34), the renormalized one point equations are

$$-i\omega\psi_{\underset{\sim}{k}} + i\omega_*^T(1 + \alpha + i\alpha\alpha'\omega/\nu_e)\psi_{\underset{\sim}{k}}$$

$$+ \eta k_\perp^2\psi_{\underset{\sim}{k}} = -(c_{\underset{\sim}{k}} + d_{\underset{\sim}{k}})\psi_{\underset{\sim}{k}} \tag{2-43}$$

and

$$-i\omega n_{\underset{\sim}{k}} = -a_{\underset{\sim}{k}} n_{\underset{\sim}{k}} , \tag{2-44}$$

where the phase independent coefficients are

$$d_{\underset{\sim}{k}} = (\rho_s/a)^2 \sum_{k'} (\underset{\sim}{k} \cdot \underset{\sim}{k}' \times \hat{z})^2 \mathcal{L}^{(1)}_{\underset{\sim}{k},\underset{\sim}{k}',\underset{\sim}{k}''} \left|n_{\underset{\sim}{k}'}\right|^2 \tag{2-45}$$

$$c_{\underset{\sim}{k}} = (\rho_s/a)^2 \sum_{k'} (\underset{\sim}{k} \cdot \underset{\sim}{k}' \times \hat{z})^2 \mathcal{L}^{(2)}_{\underset{\sim}{k},\underset{\sim}{k}',\underset{\sim}{k}''} (k_\perp^2 - k_\perp'^2) \left|\psi_{k'}\right|^2 \tag{2-46}$$

$$a_{\underset{\sim}{k}} = (\rho_s/a)^2 \sum_{k'} (k \cdot k' \times \hat{z})^2 \mathcal{L}^{(1)}_{\underset{\sim}{k},\underset{\sim}{k}',\underset{\sim}{k}''}$$

$$(k_\perp''^2 - k_\perp^2)(\psi_{\underset{\sim}{k}'})^2$$

$$\cong (\rho_s/a)^2 \sum_{\underset{\sim}{k}'} (\underset{\sim}{k} \cdot \underset{\sim}{k}' \times z)^2 \mathcal{L}^{(1)}_{\underset{\sim}{k},\underset{\sim}{k}',\underset{\sim}{k}''} k_\perp^2 \left|\psi_{\underset{\sim}{k}'}\right|^2 \tag{2-47}$$

We now discuss the renormalized equations and focus on the physical meaning of the various terms. The nonlinear pressure gradient in Ohm's Law ($\nabla_\parallel n$) yields

two effects. First, $d_{\underset{\sim}{k}}$ (Eq. 2-45) represents convection of flux (ψ) by random diamagnetic drifts and is analogous to the diffusion arising from convection due to E × B drift in 2-D MHD turbulence (compare to Diamond, et al.[12]). This term is derived from the interaction of background density fluctuations with nonlinearly driven flux ($\psi^{(2)}_{\underset{\sim}{k}''}$). Its contribution to Ohm's Law is that of an anomalous resistivity, which dissipates magnetic energy.

The second contribution to Ohm's Law is $c_{\underset{\sim}{k}}$ and is interpreted as the back-reaction of parallel compression ($\nabla_{\parallel} J$), analogous to the J × B force, on Ohm's Law. $c_{\underset{\sim}{k}}$ is derived from the interaction of magnetic turbulence with the nonlinearly driven density ($n^{(2)}_{k''}$) (an analogous term, but modified, exists in a shearless theory). It is related to the inverse transfer of mean square flux, where for $k \ll k'$, $c_{\underset{\sim}{k}}$ is a negative resistivity and drives the growth of magnetic flux, while for large scale background ($k \gg k'$), $c_{\underset{\sim}{k}}$ is a hyper-resistivity and damps magnetic flux. By multiplying Ohm's Law by $\psi_{\underset{\sim}{k}}$ and summing over k, $c_{\underset{\sim}{k}}$ vanishes under k,k' interchange and hence conserves mean square flux. The transfer process, implied by $c_{\underset{\sim}{k}}$, of

magnetic flux to large scales is a conservative process (in the sense of mean square flux). The hyperresistivity can be related to a result of Boozer.[6] He has shown, in 3-D, that if helicity ($\underset{\sim}{B} \cdot \underset{\sim}{A}$, where $\underset{\sim}{A}$ is the vector potential) is conserved and magnetic energy is always damped in a turbulent system, then Ohm's Law is

$$\underset{\sim}{E} + \underset{\sim}{v} \times \underset{\sim}{B} = - \frac{\underset{\sim}{B}}{B_0} \underset{\sim}{\nabla} \cdot \lambda \underset{\sim}{\nabla} \frac{J_{\parallel}}{B_0} ,$$

where λ is a positive constant, E is the electric field, $J_{\parallel}$ is the current along the magnetic field, and $\underset{\sim}{B}$ is the magnetic field. In two dimensions, let Ohm's Law be:

$$E_{\parallel} = R,$$

where R is the nonlinearity. Assume that $\int d\underset{\sim}{x} R = 0$ and that magnetic energy is damped by R. Then, in general $R = \underset{\sim}{\nabla} \cdot \underset{\sim}{h}$ and the magnetic energy evolution is

$$\int d\underset{\sim}{x} \underset{\sim}{J} \cdot \underset{\sim}{E} = \int dx J \underset{\sim}{\nabla} \cdot \underset{\sim}{h} = \int d\underset{\sim}{x} \underset{\sim}{\nabla} J \cdot \underset{\sim}{h}$$

$$= - \int d\underset{\sim}{x} \lambda (\underset{\sim}{\nabla} J)^2$$

where λ is a positive constant, and $\underset{\sim}{h} = -\lambda\underset{\sim}{\nabla}J$ for dissipation of magnetic energy. Thus,

$$E_{\parallel} = \underset{\sim}{\nabla} \cdot \lambda\underset{\sim}{\nabla}J$$

where λ is a hyper-resistivity. In our case, $R = -\nabla_{\parallel}p$ (p is electron pressure). $\nabla_{\parallel}p$ does not contribute to the spacial average of the parallel electric field because $\underset{\sim}{\nabla} \cdot \underset{\sim}{B} = 0$ (or because diamagnetic flows are incompressible, where $\nabla_{\parallel}p = -\underset{\sim}{v}_D \cdot \underset{\sim}{\nabla}\psi$). Any nonlinearity in Ohm's Law which is of the form $\underset{\sim}{b} \cdot \underset{\sim}{\nabla}f$ and is constrained such that $\underset{\sim}{\nabla} \cdot \underset{\sim}{b} = 0$ will not contribute to $\int d\underset{\sim}{x}E_{\parallel}$. Hence, we see that our hyper-resistivity is a result of the conservative form of the fluctuating parallel pressure (due to incompressibility constraints). In the case of a sheared system, the hyper-resistivity is the dominant piece of $c_{\underset{\sim}{k}}$ (especially when internal and magnetic energy equipartition) and is the key to the saturation of the microtearing instability.

The nonlinear parallel compression of the current ($\nabla_{\parallel}J$) admits one anomalous term, $a_{\underset{\sim}{k}}$. This term is the stress of background magnetic turbulence on density fluctuations and is analogous to the Alfven effect.[35] Derived from the interaction of magnetic

turbulence with the nonlinearly driven flux and current ($\psi_{\underset{\sim}{k}''}^{(2)}$ and $J_{\underset{\sim}{k}''}^{(2)}$), $a_{\underset{\sim}{k}}$ is a diffusive term which tends to damp density fluctuations. $a_{\underset{\sim}{k}}$ is similar to the anomalous coefficient in the vorticity equation of reduced MHD which acts to damp the vorticity. Physically, diamagnetic eddies ($\underset{\sim}{v}_D \sim \underset{\sim}{\nabla} n \times \hat{z}$) interact with large scale magnetic fields and induce Alfvenic fluctuations along the field. These fluctuations then carry internal energy away from the eddies.

At this point, a set of shearless renormalized equations have been found and the various anomalous coefficients have been identified and described. It is worthwhile pointing out that while most of the anomalous coefficients discussed in this section act to damp either density or flux, the conservation constraints discussed in the previous Section 2.2., effectively reveal that these coefficients, when appropriately paired, are conservative and represent cascades. The conservation constraints include incoherent terms which are not retained in one point closures. Thus a complete description of turbulence ultimately requires considerations of a "two point" renormalization in which such terms are retained. While

it is possible to infer a saturation level from these equations, we also desire to address questions concerning the partitioning of energy (between magnetic and internal components), the transfer of energy and flux between scales (discussed in Section 2.3) and the spectral distribution of energy. For these questions, two point energy and mean square flux spectrum equations, which contain the incoherent mode coupling terms, are constructed in the next section.

2.4.2 Two-Point Theory in a Uniform Equilibrium Magnetic Field

Renormalized spectrum equations for mean square flux and energy are obtained by closure of the evolution equations of the spectral components of mean square flux, magnetic energy, and internal energy for the case of a shearless equilibrium magnetic field. These three quadratic quantities were defined in Section 2.2 as

$$\mathcal{A} = \frac{1}{2}\int dx(\psi)^2 = \frac{1}{2}\sum_{\underset{\sim}{k}} \psi^*_{\underset{\sim}{k}}\psi_{\underset{\sim}{k}},$$

$$E_m = \frac{1}{2} \int dx (\nabla_\perp \psi)^2 = \frac{1}{2} \sum_{\underset{\sim}{k}} k_\perp^2 \psi_{\underset{\sim}{k}}^* \psi_{\underset{\sim}{k}}$$

and

$$E_I = \frac{(\rho_s/a)^2}{2} \int dx (n)^2$$

$$= \frac{(\rho_s/a)^2}{2} \sum_{\underset{\sim}{k}} n_{\underset{\sim}{k}}^* n_{\underset{\sim}{k}} ,$$

where

$$\mathcal{A}_{\underset{\sim}{k}} = \frac{1}{2} \psi_{\underset{\sim}{k}}^* \psi_{\underset{\sim}{k}},$$

$$E_{\underset{\sim}{k}}^m = \frac{1}{2} k_\perp^2 \psi_{\underset{\sim}{k}}^* \psi_{\underset{\sim}{k}},$$

and

$$E_{\underset{\sim}{k}}^I = \frac{1}{2} (\rho_s/a)^2 n_{\underset{\sim}{k}}^* n_{\underset{\sim}{k}}$$

are the k-th spectral components of mean square flux, magnetic energy, and internal energy, respectively. By multiplying Ohm's Law by $\frac{1}{2} \psi_k^*$ and adding the complex conjugate equation, we obtain the spectrum evolution equation for mean square flux. Similarly, by

multiplying Ohm's Law by $\frac{1}{2} J_k^*$ and continuity by $\frac{1}{2}(\rho_s/a)^2 n_k$ (and adding complex conjugate equations) we obtain the spectrum evolution equations for magnetic and internal energies. The resulting equations are:

$$\frac{\partial \mathcal{A}_{\underset{\sim}{k}}}{\partial t} - \frac{2\alpha\alpha'}{\nu_e}\,\omega_*^T\, R_e(\omega_{\underset{\sim}{k}})\,\mathcal{A}_{\underset{\sim}{k}}$$

$$+ 2\eta(J_{\underset{\sim}{k}})^2 = \sum_{\underset{\sim}{p}+\underset{\sim}{q}=-\underset{\sim}{k}} S^a(\underset{\sim}{p},\underset{\sim}{q},\underset{\sim}{k}), \qquad (2\text{-}48)$$

$$\frac{\partial E^m_{\underset{\sim}{k}}}{\partial t} - 2\,\frac{\omega_*^T}{\nu_e}\,\alpha\alpha' R_e(\omega_{\underset{\sim}{k}})\,E^m_{\underset{\sim}{k}}$$

$$+ 2\eta(J_{\underset{\sim}{k}})^2 = \sum_{\underset{\sim}{p}+\underset{\sim}{q}=-\underset{\sim}{k}} S^m(\underset{\sim}{k},\underset{\sim}{p},\underset{\sim}{q}), \qquad (2\text{-}49)$$

and

$$\frac{\partial E^I_{\underset{\sim}{k}}}{\partial t} = \sum_{\underset{\sim}{p}+\underset{\sim}{q}=-\underset{\sim}{k}} S^I(\underset{\sim}{k},\underset{\sim}{p},\underset{\sim}{q}) \qquad (2\text{-}50)$$

where

$$R_e(\omega_{\underset{\sim}{k}}) = (1+\alpha)\omega_*^T,$$

$$S^a(\underset{\sim}{k},\underset{\sim}{p},\underset{\sim}{q}) = \frac{1}{2}(\rho_s/a)^2(\underset{\sim}{p}\cdot\underset{\sim}{q}\times\hat{z})(\psi_{-\underset{\sim}{k}}\psi_{-\underset{\sim}{q}}\psi_{-\underset{\sim}{p}}$$

$$+ \text{c.c.}),$$

$$S^m(\underset{\sim}{k},\underset{\sim}{p},\underset{\sim}{q}) = \frac{1}{2}(\rho_s/a)^2(\underset{\sim}{p}\cdot\underset{\sim}{q}\times\hat{z})(J_{-\underset{\sim}{k}}n_{-\underset{\sim}{q}}\psi_{-\underset{\sim}{p}}$$

$$+ \text{c.c.}),$$

and

$$S^I(\underset{\sim}{k},\underset{\sim}{p},\underset{\sim}{q}) = \frac{1}{2}(\rho_s/a)^2(\underset{\sim}{p}\cdot\underset{\sim}{q}\times\hat{z})(n_{-\underset{\sim}{k}}\psi_{-\underset{\sim}{q}}J_{-\underset{\sim}{p}}$$

$$+ \text{c.c.}).$$

$\sum_{\underset{\sim}{p}+\underset{\sim}{q}=-\underset{\sim}{k}}$ indicates the sum over p and q where the vectors p and q form a triangle such that $\underset{\sim}{p} + \underset{\sim}{q} = \underset{\sim}{k}$ (see Figure 2.1).

We begin with the spectrum equation for mean square flux. The renormalization procedure is outlined in Part A of this section. The triplet nonlinearity is written perturbatively:

$$S^a(\underset{\sim}{k},\underset{\sim}{p},\underset{\sim}{q}) = -\frac{1}{2}(\rho_s/a)^2(\psi_{-\underset{\sim}{k}}n_{-\underset{\sim}{q}}\psi^{(2)}_{\underset{\sim}{k}+\underset{\sim}{q}}$$

$$+ \psi_{-\underset{\sim}{k}}n^{(2)}_{\underset{\sim}{k}+\underset{\sim}{q}}\psi_{-\underset{\sim}{q}} + \psi^{(2)}_{\underset{\sim}{p}+\underset{\sim}{q}}n_{-\underset{\sim}{p}}\psi_{-\underset{\sim}{q}}). \qquad (2\text{-}51)$$

where $\psi^{(2)}_{\underset{\sim}{k}}$ and $n^{(2)}_{\underset{\sim}{k}}$ are the driven fields given by

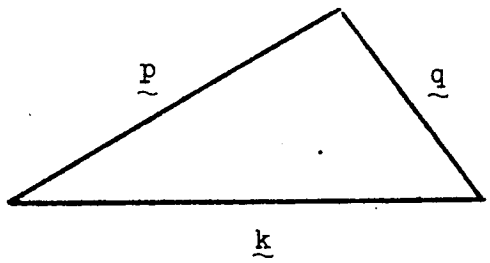

FIGURE 2.1. The triangle formed by $\underset{\sim}{p} + \underset{\sim}{q} = -\underset{\sim}{k}$, representing a triad interaction.

Eqs. (2-39) and (2-40). Comparing Eq. (2-51) with the one point Eqs. (2-43) and (2-44) we see that the first two terms of S^a correspond to those in one point theory--$d_{\underset{\sim}{k}}$ and $c_{\underset{\sim}{k}}$, respectively. The third term incorporates the nonlinear iteration of the conjugate fields used to form mean square flux, and is thus not included in one point theory. Substitution of the driven fields, Eqs. (2-39) and (2-40) into this term yields products of the quadratic quantities, neither of whose wavenumbers are $\underset{\sim}{k}$, the test mode wavenumber. This term thus gives phase-incoherent contributions to the evolution of mean square flux, i.e., incoherent mode coupling contributions.

Multiplying the one point equation (2-43) by $\psi^*_{\underset{\sim}{k}}$ and adding the complex conjugate, we find that, in this case, the triplet nonlinearity is:

$$\sum_{\underset{\sim}{p}+\underset{\sim}{q}=-\underset{\sim}{k}} S^a_1(\underset{\sim}{k},\underset{\sim}{p},\underset{\sim}{q})$$

$$= \sum_{\underset{\sim}{p}+\underset{\sim}{q}=-\underset{\sim}{k}} \frac{1}{2}(\rho_s/a)^2(\underset{\sim}{p}\cdot\underset{\sim}{q}\times\hat{z})(\psi_{-\underset{\sim}{k}}{}^{n}{}_{-\underset{\sim}{q}}\psi^{(2)}_{\underset{\sim}{k}+\underset{\sim}{q}}$$

$$+ \psi_{-\underset{\sim}{k}}{}^{n}{}^{(2)}_{\underset{\sim}{k}+\underset{\sim}{q}}\psi_{-\underset{\sim}{q}}) = -R_e(d_{\underset{\sim}{k}} + c_{\underset{\sim}{k}})\, a_{\underset{\sim}{k}}$$

Mean square flux is conserved when

$$\sum_{\underset{\sim}{k}} \sum_{\underset{\sim}{p}+\underset{\sim}{q}=-\underset{\sim}{k}} S^a(\underset{\sim}{k},\underset{\sim}{p},\underset{\sim}{q}) = 0.$$

Thus, using one point theory, mean square flux is not conserved, since

$$\sum_{\underset{\sim}{k}} \sum_{\underset{\sim}{p}+\underset{\sim}{q}=-\underset{\sim}{k}} S_1^a(\underset{\sim}{k},\underset{\sim}{p},\underset{\sim}{q}) = -\sum_{\underset{\sim}{k}} R_e(d_{\underset{\sim}{k}})\, \mathcal{A}_{\underset{\sim}{k}} \neq 0.$$

In this case, total mean square flux is damped by spurious random diamagnetic convection. The back reaction ($c_{\underset{\sim}{k}}$), however, does conserve mean square flux. When we sum over $\underset{\sim}{k}$ in the two point triplet nonlinearity, we find that incoherent mode coupling ($\psi^{(2)}_{\underset{\sim}{p}+\underset{\sim}{q}}$) exactly balances the coherent mode coupling ($\psi^{(2)}_{\underset{\sim}{k}+\underset{\sim}{q}}$ or the $d_{\underset{\sim}{k}}'$ term). It is readily apparent that one-point theory, which only contains coherent mode coupling, cannot conserve mean square flux. Also, because mean square flux conservation in two point theories is a direct consequence of the symmetry of second order driven fields to interchange of wavenumber, any renormalization scheme which maintains this symmetry conserves energy.

From conservation of mean square flux, we see that two physical processes are involved. The

pairing of incoherent mode coupling ($\psi^{(2)}_{\underset{\sim}{p}+\underset{\sim}{q}}$) and coherent damping ($\psi^{(2)}_{\underset{\sim}{k}+\underset{\sim}{q}}$) corresponds to stretching of constant flux contours. From Eq. (2-1) the gradient of flux is written as:

$$\frac{\partial}{\partial t}\,(\underset{\sim}{\nabla}\psi) = -\underset{\sim}{\nabla}\underset{\sim}{v}_D \cdot \underset{\sim}{\nabla}\psi \qquad (2\text{-}52)$$

where $\underset{\sim}{\nabla}\underset{\sim}{v}_D$ is the diamagnetic velocity strain. From Eq. (2-52) the mean square flux gradient or magnetic energy evolves as:

$$\frac{\partial}{\partial t}\,(\underset{\sim}{\nabla}\psi)^2 = -\underset{\sim}{\nabla}\underset{\sim}{v}_D : (\underset{\sim}{\nabla}\psi\underset{\sim}{\nabla}\psi). \qquad (2\text{-}53)$$

Thus, analogous to vortex straining in 2-D Navier Stokes fluids, diamagnetic velocity strain increases the flux gradient (see Figure 2.2) and hence small scale magnetic energy is increased. Using this argument, mean square flux cascades to small scales, as vorticity cascades in 2-D Navier Stokes fluids. Unfortunately, the basis of this argument is flux being treated as a passive scaler --valid when internal energy is much greater than magnetic energy. The other physical process is related to the breakdown of the passive scaler assumption and

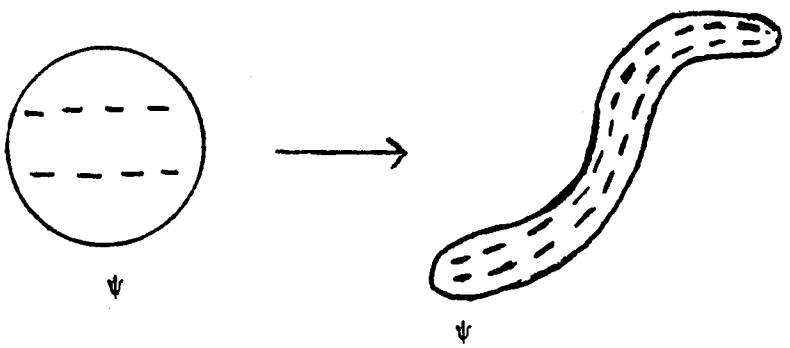

FIGURE 2.2. Representation of flux ψ as a passive scaler in a diamagnetically drifting flow. Gradient of flux is increased by straining (dotted line is contour of constant flux).

corresponds to the vanishing of the $n^{(2)}_{\underset{\sim}{k}+\underset{\sim}{q}}$ or c_k term of S^a in mean square flux conservation. This effect is the back reaction of $\underset{\sim}{B} \cdot \underset{\sim}{\nabla} J$ (analogous to Lorentz force) on the diamagnetic strain field. From Part 2.4.1 of this section we have seen that the back reaction has a tendency to transfer mean square flux to large scales. This transfer is consistent with equilibrium statistical mechanics, discussed in Section 2.3, where an accumulation of mean square flux at large scales was predicted. Thus, two competing nonlinear processes result from mean square flux conservation.

After substituting the driven fields (Eqs. (2-39), (2-40) into Eq. (2-51), we find

$$\frac{\partial a_{\underset{\sim}{k}}}{\partial t} - \frac{2\alpha\alpha'}{\nu_e} (\omega_*^T)^2 (1 + \alpha)\, a_{\underset{\sim}{k}} + 2\eta E^m_{\underset{\sim}{k}}$$

$$= (\rho_s/a)^2 \sum_{\underset{\sim}{p}+\underset{\sim}{q}=-\underset{\sim}{k}} (\underset{\sim}{p} \cdot \underset{\sim}{q} \times \hat{z})^2 \qquad (2\text{-}54)$$

$$\left\{ R_e(\mathcal{L}^{(2)}_{\underset{\sim}{k},\underset{\sim}{p},\underset{\sim}{q}}) \frac{(q_\perp^2 - k_\perp^2)}{q^2} E^m_{\underset{\sim}{q}} a_{\underset{\sim}{k}} \right.$$

$$\left. - R_e(\mathcal{L}^{(1)}_{\underset{\sim}{k},\underset{\sim}{p},\underset{\sim}{q}}) E^I_{\underset{\sim}{q}} a_{\underset{\sim}{k}} + R_e(\mathcal{L}^{(1)}_{\underset{\sim}{k},\underset{\sim}{p},\underset{\sim}{q}}) E^I_{\underset{\sim}{p}} a_{\underset{\sim}{q}} \right\}$$

where the propagators ($\mathcal{L}^{(1)}$ and $\mathcal{L}^{(2)}$) are given by Eqs. (2-41) and (2-42). Physically, the propagator is the nonlinear interaction time,

$$\tau_{eq}^{-1} \sim k^2 \rho_s v_A \left(\frac{\delta B}{B_0}\right)_{rms} ,$$

which is the Alfven-like time resulting from a diamagnetic eddy interacting with magnetic field lines. This interaction excites Alfven waves which tend to damp the eddy.

By summing over $\underset{\sim}{k}$, we see that the first and third term on the right hand side of Eq. (2-54) conserve mean square flux while the second term independently vanishes. The closure reveals that the incoherent mode coupling is a source of mean square flux. The first and second terms correspond to $d_{\underset{\sim}{k}}$ and $c_{\underset{\sim}{k}}$, respectively, of one point theory (random diamagnetic convection and back reaction).

To quantitatively discuss the closure equation and the onlinear process, we concentrate on nonlocal effects, as discussed by Pouquet, et al. They found that these effects are key to energy equipartition and the "Alfven effect."[35,56,57] Further, these

nonlocal effects (interactions between widely separated scales) are the basis for the back reaction transferring mean square flux to large scales. The $-\underset{\sim}{k} = \underset{\sim}{p} + \underset{\sim}{q}$, or bipolar interaction is represented pictorally in Figure 2.1. Local interactions occur when $|k| \sim |p| \sim |q|$ or the triangle is approximately equilateral. These interactions tend to be more pronounced in few mode systems such as three wave or chaotic systems. Nonlocal interactions are typical in many mode systems which support fully developed turbulence. These interactions are represented by oblique triangles. Two subgroups[34,56,57] arise and are shown in Figures 2.3 and 2.4.

The first subgroup, $|p| \cong |k| >> -|q|$ or $|q| \cong |k| >> |p|$ (Figure 2.3), represents the interaction of test mode k with large scale fluctuations. The second group, $|p| \cong |q| >> |k|$ (Figure 2.4), represents the interaction of the test mode with small scale fluctuations. Due to the nature of the microtearing instability, the large scale fluctuations comprising the background in the first subgroup are unstable whereas the small scale fluctuations are stable (or marginally damped). For test modes in the upper range

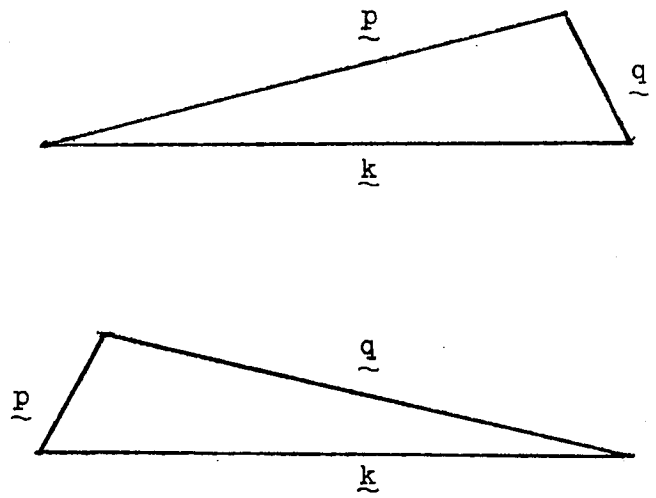

FIGURE 2.3. Triangles representing small scale test modes interacting with large scale background modes or $|\underset{\sim}{k}|\sim|\underset{\sim}{p}|>>|\underset{\sim}{q}|$ and $|k|\sim|q|>>|p|$ interactions.

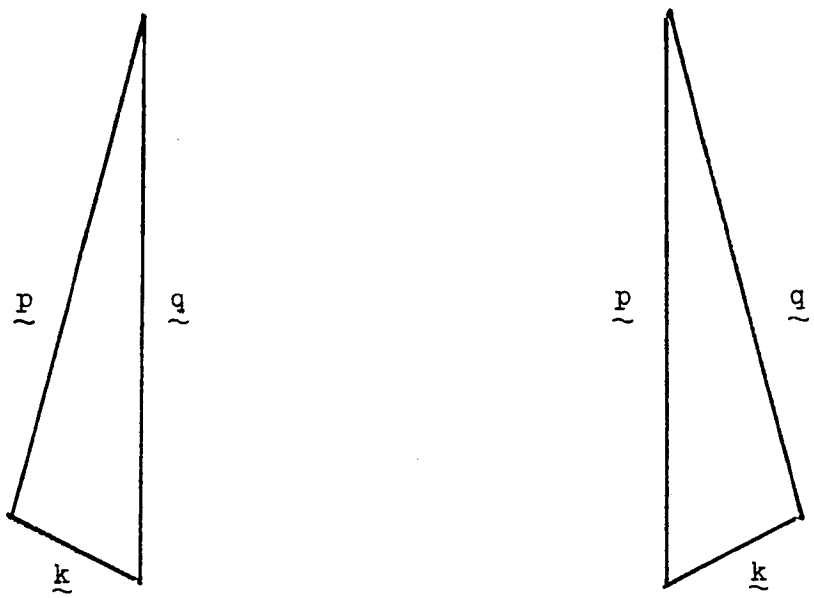

FIGURE 2.4. Triangles representing large scale test modes interacting with small scale background modes or $|\underset{\sim}{p}| \sim |\underset{\sim}{q}| >> |\underset{\sim}{k}|$ interactions.

of the k spectrum, the nonlinear interactions predominantly fall into the first subgroup. In this limit

$$\frac{\partial \mathcal{A}_{\underset{\sim}{k}}}{\partial t} - 2\eta E^m_{\underset{\sim}{k}}$$

$$= -(\rho_s/a)^2 \sum_{k'} (\underset{\sim}{k} \cdot \underset{\sim}{k}' \times \hat{z})^2 \mathcal{A}_{\underset{\sim}{k}'} \left[\mathrm{Re}(\mathcal{L}^{(2)}_{\underset{\sim}{k},\underset{\sim}{k}',\underset{\sim}{k}''}) E^m_{\underset{\sim}{k}} \right.$$

$$\left. - R_e(\mathcal{L}_{\underset{\sim}{k},\underset{\sim}{k}',\underset{\sim}{k}''}) E^I_{\underset{\sim}{k}} \right]. \qquad (2\text{-}55)$$

Note that $\mathcal{L}^{(1)} = \mathcal{L}^{(2)}$ (nonlinear interaction time for Ohm's Law and continuity are the same) because ω^T_* is nondispersive.[24] We see that the first term on the right hand side of Eq. (2-55) is the damping of small scale mean square flux by back reaction, while the second term is incoherent emission (to large k, due to straining). We see that when $E^m_{\underset{\sim}{k}} > E^I_{\underset{\sim}{k}}$, back reaction effects dominate, while when $E^m_{\underset{\sim}{k}} < E^I_{\underset{\sim}{k}}$, fluid straining dominates. Thus a transfer of mean square flux to large scales occurs in a magnetically dominated system, while a cascade to small scales occurs in a diamagnetic fluid dominated system.

The second subgroup of nonlocal interactions corresponds to the evolution of low k unstable

microtearing modes in a broad spectrum of stable high k fluctuations. This is the case relevance to the problem of determining microtearing saturation and is discussed in detail in Section 2.5. Ignoring linear growth and dissipation, mean square flux evolution in this limit is

$$\frac{\partial \mathcal{A}_{\underset{\sim}{k}}}{\partial t} = (\rho_s/a)^2 \sum_{\underset{\sim}{k}'} (\underset{\sim}{k} \cdot \underset{\sim}{k}' \times \hat{\underset{\sim}{z}})^2 \Big\{ R_e(\mathcal{L}^{(2)}_{\underset{\sim}{k},\underset{\sim}{k}',\underset{\sim}{k}'}) E^m_{\underset{\sim}{k}'} - R_e(\mathcal{L}^{(1)}_{\underset{\sim}{k},\underset{\sim}{k}',\underset{\sim}{k}'}) E^I_{\underset{\sim}{k}'} \Big\} \mathcal{A}_{\underset{\sim}{k}} + S^a \qquad (2\text{-}56)$$

where S^a is incoherent emission to high k, given by

$$S^a = (\rho_s/a)^2 \sum_{\underset{\sim}{p}+\underset{\sim}{q}=-\underset{\sim}{k}} (\underset{\sim}{p} \cdot \underset{\sim}{q} \times \hat{\underset{\sim}{z}}) R_e(\mathcal{L}^{(1)}_{\underset{\sim}{p},\underset{\sim}{q},\underset{\sim}{k}}) E^I_{\underset{\sim}{p}} \mathcal{A}_{\underset{\sim}{q}}. \qquad (2\text{-}57)$$

Again, the relative magnitude of magnetic and internal energy determines whether back reaction dominates straining or vice versa. The first term on the right hand side of Eq. (2-56) is the negative anomalous resistivity due to back reaction, while the second term is the anomalous damping due to diamagnetic straining. Comparing Eqs. (2-56) and (2-57) we conclude that the closure reflects quantitatively the tendency to transfer mean square flux to large scales via back reaction of

$\underset{\sim}{B} \cdot \underset{\sim}{\nabla} J$ and to cascade to small scales due to straining of flux contours.

We now consider the spectral evolution of magnetic and internal energies. Writing the triplet nonlinearities perturbatively, the triplet of magnetic energy is

$$S^m(\underset{\sim}{k},\underset{\sim}{p},\underset{\sim}{q})$$

$$= \frac{1}{2}(\rho_s/a)^2(\underset{\sim}{p} \cdot \underset{\sim}{q} \times \hat{z})(-J_{-\underset{\sim}{k}} n_{-\underset{\sim}{q}} \psi_{\underset{\sim}{k}+\underset{\sim}{q}} \tag{2-58}$$

$$+ J_{-\underset{\sim}{k}} n_{\underset{\sim}{k}+\underset{\sim}{q}} \psi_{-\underset{\sim}{q}} + J_{\underset{\sim}{p}+\underset{\sim}{q}} n_{-\underset{\sim}{p}} \psi_{-\underset{\sim}{q}})$$

and the triplet for internal energy is:

$$S^I(\underset{\sim}{k},\underset{\sim}{p},\underset{\sim}{q})$$

$$= \frac{1}{2}(\rho_s/a)^2(\underset{\sim}{p} \cdot \underset{\sim}{q} \times \hat{z})(n_{-\underset{\sim}{k}} \psi_{-\underset{\sim}{q}} J_{\underset{\sim}{k}+\underset{\sim}{q}} \tag{2-59}$$

$$-n_{-\underset{\sim}{k}} \psi_{\underset{\sim}{k}+\underset{\sim}{q}} J_{-\underset{\sim}{q}} + n_{\underset{\sim}{p}+\underset{\sim}{q}} \psi_{-\underset{\sim}{p}} J_{-\underset{\sim}{q}}).$$

The first two terms of S^m and S^I correspond to one point (coherent) nonlinearities. In S^m, the first term

is the random diamagnetic convection ($d_{\underset{\sim}{k}}$ in Eq. (2-43)) and the second is the back reaction of $\underset{\sim}{B} \cdot \underset{\sim}{\nabla} J$ ($c_{\underset{\sim}{k}}$ in Eq. (2-43)). The first two terms of S^I correspond to the effect of magnetic fluctuations on continuity ($a_{\underset{\sim}{k}}$ in Eq. (2-44)) or an effect similar to the "Alfven Effect."[56,57] (As noted previously, a diamagnetic eddy interacts with a large scale magnetic field line and excites Alfvenic fluctuations which carry off energy, "damping" the eddy, i.e., internal energy.) The last term of S^m and S^I are not included in one point theories, and are incoherent mode coupling effects which are necessary for energy conservation (the one point Eqs. (2-43) and (2-44) cannot conserve energy). Looking at Eqs. (2-58) and (2-59) energy is conserved when

$$\sum_{\underset{\sim}{k}} \sum_{\underset{\sim}{p}+\underset{\sim}{q}=-\underset{\sim}{k}} (S^m(\underset{\sim}{k},\underset{\sim}{p},\underset{\sim}{q}) + S^I(\underset{\sim}{k},\underset{\sim}{p},\underset{\sim}{q})) = 0 .$$

When we expand S^m and S^I,

$$S^m(\underset{\sim}{k},\underset{\sim}{p},\underset{\sim}{q}) + S^I(\underset{\sim}{k},\underset{\sim}{p},\underset{\sim}{q}) = \frac{1}{2} (\rho_s/a)^2 (\underset{\sim}{p} \cdot \underset{\sim}{q}$$

$$\times \hat{z})(-J_{-\underset{\sim}{k}} n_{-\underset{\sim}{q}} \psi^{(2)}_{\underset{\sim}{k}+\underset{\sim}{q}} + J_{-\underset{\sim}{k}} n^{(2)}_{\underset{\sim}{k}+\underset{\sim}{q}} \psi_{-\underset{\sim}{q}} + J^{(2)}_{\underset{\sim}{p}+\underset{\sim}{q}} n_{-\underset{\sim}{p}} \psi_{-\underset{\sim}{q}}$$

$$+ n_{-\underset{\sim}{k}} \psi_{-\underset{\sim}{q}} J^{(2)}_{\underset{\sim}{k}+\underset{\sim}{q}} - n_{-\underset{\sim}{k}} \psi^{(2)}_{\underset{\sim}{k}+\underset{\sim}{q}} J_{-\underset{\sim}{q}} + n^{(2)}_{\underset{\sim}{p}+\underset{\sim}{q}} \psi_{-\underset{\sim}{p}} J_{-\underset{\sim}{q}}) .$$

Under

$$\sum_{\underset{\sim}{k}} \sum_{\underset{\sim}{p}+\underset{\sim}{q}=-\underset{\sim}{k}} ,$$

the first and fifth terms and the third and fourth terms cancel pairwise under a single index interchange. The second term cancels the sixth term after a double index interchange. Note that two pairs of cancelling terms involve coherent-incoherent pairings, whereas one is a pairing of two coherent terms. The coherent-coherent $(\psi^{(2)}_{\underset{\sim}{k}+\underset{\sim}{q}})$ cancellation is significant in that one point theory predicts this result, unlike the other two pairings.

Physically, the $\psi^{(2)}$ and $J^{(2)}$ pairings correspond to the diamagnetic velocity straining of magnetic field lines, similar to the effect on mean square flux. These effects can be represented by diamagnetic eddies interacting with large scale magnetic fields. Kinetic energy is damped by Alfvenic excitations along the field lines, while magnetic energy is driven to smaller scales by passively being stretched by these eddies. On the other hand, the $n^{(2)}$ pairing is the back reaction effect of $\underset{\sim}{B} \cdot \underset{\sim}{\nabla} J$ (current compression or

parallel electron flux). Here, magnetic eddies, or current filaments interact with diamagnetic velocity lines, distorting density contours.

The closed set of spectrum energy equations, obtained by substituting driven fields $\psi^{(2)}$, $J^{(2)}$, and $n^{(2)}$ (Eqs. (2-39) and (2-40) into Eqs. (2-58) and (2-59) are:

$$\frac{\partial E_{\underset{\sim}{k}}^{m}}{\partial t} - \frac{2\alpha\alpha'}{\nu_e} R_e(\omega_{\underset{\sim}{k}})\omega_*^T E_{\underset{\sim}{k}}^{m} + 2\eta(J_{\underset{\sim}{k}})^2$$

$$= \sum_{\underset{\sim}{p}+\underset{\sim}{q}=-\underset{\sim}{k}} S^m(\underset{\sim}{k},\underset{\sim}{p},\underset{\sim}{q}) = (\rho_s/a)^2 \sum_{\underset{\sim}{p}+\underset{\sim}{q}=-\underset{\sim}{k}} (\underset{\sim}{p}\cdot\underset{\sim}{q}\times\hat{z})^2$$

$$\left\{\frac{(q_\perp^2 - k_\perp^2)}{q_\perp^2} R_e(\mathcal{L}^{(2)}_{\underset{\sim}{k},\underset{\sim}{p},\underset{\sim}{q}}) E_{\underset{\sim}{q}}^{m} E_{\underset{\sim}{k}}^{m}\right. \qquad (2\text{-}60)$$

$$- R_e(\mathcal{L}^{(1)}_{\underset{\sim}{k},\underset{\sim}{p},\underset{\sim}{q}}) E_q^I E_{\underset{\sim}{k}}^{m}$$

$$\left. + (k_\perp^2/q_\perp^2) R_e(\mathcal{L}^{(1)}_{\underset{\sim}{k},\underset{\sim}{p},\underset{\sim}{q}}) E_{\underset{\sim}{p}}^I E_{\underset{\sim}{q}}^{m}\right\}.$$

and

$$\frac{\partial E_{\underset{\sim}{k}}^{I}}{\partial t} = \sum_{p+q=-k} S^I(\underset{\sim}{k},\underset{\sim}{p},\underset{\sim}{q}) = -(\rho_s/a)^2 \sum_{\underset{\sim}{p}+\underset{\sim}{q}=-\underset{\sim}{k}} (\underset{\sim}{p}\cdot\underset{\sim}{q}$$

$$\times \hat{z})^2 \frac{(p_\perp^2 - q_\perp^2)}{q_\perp^2}\left\{ R_e(\mathcal{L}^{(1)}_{\underset{\sim}{k},\underset{\sim}{p},\underset{\sim}{q}}) E_{\underset{\sim}{q}}^{m} E_{\underset{\sim}{k}}^{I}\right. \qquad (2\text{-}61)$$

$$\left. + R_e(\mathcal{L}^{(2)}_{\underset{\sim}{k},\underset{\sim}{p},\underset{\sim}{q}}) E_{\underset{\sim}{p}}^{m} E_{\underset{\sim}{q}}^{m}\right\}.$$

The first two terms on the right hand side of Eq. (2-60) (spectral evolution of magnetic energy) correspond to back reaction ($c_{\underset{\sim}{k}}$) and diamagnetic convection ($d_{\underset{\sim}{k}}$). The last term is incoherent emission to higher k due to magnetic field line stretching. When a diamagnetic eddy interacts with a magnetic field line, energy is lost from the eddy to Alfvenic fluctuations. This energy is incoherently emitted to magnetic energy.

Internal energy is damped due to the "Alfven effect"[56,57] already discussed (first term on right hand side of Eq. (2-61)). The second term is the incoherent mode coupling which conserves energy with back-reaction ($n^{(2)}$). Physically, this term corresponds to current filaments (magnetic eddies) distorting density contours, and thus internal energy. When a small scale filament interacts with a diamagnetic eddy (of larger scale, or weaker energy), the filament is damped, incoherently emitting its energy to the eddy. Large scale filaments, on the other hand, absorb energy from diamagnetic eddies. This scale dependent absorbtion or emission of energy of an interacting filament reflects the scale dependence in $c_{\underset{\sim}{k}}$ (back reaction). Further, the incoherent mode coupling in internal energy

evolution is both a source and sink, depending on the scale of the interacting current filament.

When we consider the effects of large scale background modes on small scale test modes (the nonlocal triad interaction given by Figure 2.8), the spectrum energy equations are:

$$\frac{\partial E^m_{\underset{\sim}{k}}}{\partial t} - 2\eta J^2_{\underset{\sim}{k}} = -(\rho_s/a)^2 \sum_{\underset{\sim}{k}'} (\underset{\sim}{k} \cdot \underset{\sim}{k}' \times \hat{z})^2 E^m_{\underset{\sim}{k}'}$$

$$\left\{ \mathrm{Re}(\mathcal{L}^{(2)}_{\underset{\sim}{k},\underset{\sim}{k}',\underset{\sim}{k}''}) E^m_{\underset{\sim}{k}} - \mathrm{Re}(\mathcal{L}^{(1)}_{\underset{\sim}{k},\underset{\sim}{k}',\underset{\sim}{k}''}) E^I_{\underset{\sim}{k}} \right\} \qquad (2\text{-}62)$$

$$= - \frac{\partial E^I_{\underset{\sim}{k}}}{\partial t} ,$$

where $\mathcal{L}^{(1)} \sim \mathcal{L}^{(2)} \sim 1/\delta\gamma$. Hence, the energies equipartition at small scales (using the fact that the propagators are equal). The time scale on which equipartitioning occurs is obtained from Eq. (2-62) and is given by

$$\delta\gamma \cong \tau_{eq}^{-1} = k_\perp^2 \rho_s V_A \left(\frac{\delta B}{B_0} \right)_{rms} .$$

Physically, this represents the time for an Alfven excitation to travel down a fluctuating magnetic field

in a finite electron temperature plasma. At equipartition, this is the nonlinear time

$$\tau_{ep}^{-1} = k_{\perp} v_D,$$

where

$$\underset{\sim}{v}_D = \frac{\rho_e v_e}{n_0} \underset{\sim}{\nabla} n \times \hat{z} ,$$

which is the eddy turnover time for a diamagnetic eddy. Because the second term of Eq. (2-62) is an incoherent term, it is clear that incoherent mode coupling plays an important role in equipartition of magnetic and internal energies. Equipartition of energy at small scales has been reported for 2-D MHD, which is similar to the shearless case presented here.[56] In both cases, the equipartitioned state at small scales corresponds to a force free state where $\nabla_{\parallel} n$ and $\nabla_{\parallel} J$ are zero. Special note should be made of the fact that both field stretching terms and back reaction terms contribute to the equipartitioning. Physically, small scale diamagnetic eddys scatter energy to large scale magnetic fields while small scale current filaments scatter energy to

large scale diamagnetic eddies. The scattered energy is in turn emitted at small scales through incoherent mode coupling. Thus, this circular energy exchange forces magnetic and internal energy to equipartition.

Finally, we compare the nonlinear processes derived from the closure equations with those of equilibrium statistical mechanics.[22] From Section 2.3 (Eqs. (2-27), (2-28) and (2-29),

$$E_k^m \sim \frac{k^2}{\alpha k^2 + \beta}$$

$$E_k^I \sim \alpha^{-1}$$

$$a_k \sim \frac{1}{\alpha k^2 + \beta}$$

where α and β are constants representing effective temperatures for total energy and mean square flux, respectively. We see that the differing k dependence of the conserved quantities indicates that magnetic energy accumulates at small scales while mean square flux goes to large scales. Apparently, stretching of magnetic field lines prefers the stronger small scale dependence of magnetic energy, while back reaction

of $\underset{\sim}{B} \cdot \underset{\sim}{\nabla} J$ transfers mean square flux to large scales. In both cases, the competing effe should retard or impede the cascade or transfer. The third nonlinear process is revealed by these equations as k goes to infinity, i.e.,

$$E^m_{\underset{\sim}{k}} = E^I_{\underset{\sim}{k}} = \alpha^{-1} \ .$$

Equipartition of magnetic and internal energy at small scales is consistent with equilibrium statistical mechanics.

2.5 Renormalized Theory in a Sheared Equilibrium Magnetic Field

2.5.1 One-Point Theory

We now consider the renormalized one point equations for multihelicity drift semicollisional microtearing modes in a sheared field. Special attention is paid to physical origin, content and interpretation of the renormalized equations.

The derivation follows that of Diamond et al. For a sheared field, the Fourier transformation of Eqs. (2-1), (2-2), and (2-3) yields

$$\frac{\partial}{\partial t}\psi_{\underset{\sim}{k}} + i\omega_*^T(1 + \alpha + i\alpha\alpha'\omega/\nu_e)\psi_{\underset{\sim}{k}}$$

$$- \eta J_{\underset{\sim}{k}} - ik_\parallel(\rho_s/a)^2 n_{\underset{\sim}{k}} = N_{\perp R}, \tag{2-63}$$

$$\frac{\partial n_{\underset{\sim}{k}}}{\partial t} = -ik_\parallel J_{\underset{\sim}{k}} + N_{\perp U} - ik_y \frac{\partial J_0}{\partial x}\psi_{\underset{\sim}{k}}, \tag{2-64}$$

and

$$\nabla_\perp^2 \psi_{\underset{\sim}{k}} = \frac{\partial^2}{\partial x^2} - k_y^2 \psi_{\underset{\sim}{k}} = J_{\underset{\sim}{k}},$$

where

$$N_{\perp R} = (\rho_s/a)^2[\underset{\sim}{\nabla}\psi \times \hat{z} \cdot \underset{\sim}{\nabla} n]_k,$$

$$N_{\perp U} = -[\underset{\sim}{\nabla}\psi \times \hat{z} \cdot \underset{\sim}{\nabla} J]_k,$$

and J_0 is the equilibrium current due to the sheared field. For any fields f, g

$$[\underset{\sim}{\nabla} f \times \hat{z} \cdot \underset{\sim}{\nabla} g]_k = \frac{\partial}{\partial x}\left(\sum_{\underset{\sim}{k}'}(-ik_y')f_{-\underset{\sim}{k}} g_{\underset{\sim}{k}+\underset{\sim}{k}'}\right.$$

$$-ik_y \sum_{\underset{\sim}{k}'} \frac{\partial f_{-\underset{\sim}{k}'}}{\partial x} g_{\underset{\sim}{k}+\underset{\sim}{k}'} - \frac{\partial}{\partial x}\left(\sum_{\underset{\sim}{k}'}(-ik_y')g_{-\underset{\sim}{k}'} f_{\underset{\sim}{k}+\underset{\sim}{k}'}\right) \tag{2-65}$$

$$\left. -ik_y \sum_{\underset{\sim}{k}'} \frac{\partial g_{-\underset{\sim}{k}'}}{\partial x} f_{\underset{\sim}{k}+\underset{\sim}{k}'}\right)$$

where $\underset{\sim}{k}$ (k_y,k_z), $k_\parallel = xk_y/L_s$, and x is the distance to the singular surface where $\underset{\sim}{k} \cdot \underset{\sim}{B}_0 = 0$.

Some initial considerations are addressed before detailing the renormalization. First, as in the case of a uniform magnetic field, a broad bath of $k_y(m)$ modes is assumed, with stable small scale modes and unstable large scale modes. Cross helicity, $\langle \psi n \rangle$, is set to zero for convenience. Although no k_y symmetry exists, we maintain an even tearing parity in x. Finally, all modes are considered to be semicollisional microtearing modes with $k_y w < 1$.

With these considerations, beat interaction fields $(J_{\underset{\sim}{k}+\underset{\sim}{k}'}, \psi_{\underset{\sim}{k}+\underset{\sim}{k}'}, n_{\underset{\sim}{k}+\underset{\sim}{k}'})$ appearing in Eqs. (2-63), (2-64), and (2-65) are obtained and interactively substituted into Equations (2-63)-(2-65). As in Section 2.4, the beat interaction fields are solved by retaining solely the nonlinearity (the phase coherent piece with test mode k), thus closing the equations. Hence, for any field f

$$(\nabla_\parallel f)_{\underset{\sim}{k}+\underset{\sim}{k}'} \cong -\frac{1}{2}\left[ik_y' f_{\underset{\sim}{k}'} \frac{\partial \psi_{\underset{\sim}{k}}}{\partial x} - \frac{\partial f_{\underset{\sim}{k}'}}{\partial x} ik_y \psi_{\underset{\sim}{k}}\right.$$

$$\left. + ik_y f_{\underset{\sim}{k}} \frac{\partial \psi_{\underset{\sim}{k}'}}{\partial x} - ik_y' \frac{\partial f_{\underset{\sim}{k}}}{\partial x} \psi_{\underset{\sim}{k}'}\right].$$

Using the above equation to express the nonlinearities of the driven equations, the driven fields $\psi^{(2)}_{\underset{\sim}{k}+\underset{\sim}{k}'}$, $J^{(2)}_{\underset{\sim}{k}+\underset{\sim}{k}'}$, and $n^{(2)}_{\underset{\sim}{k}+\underset{\sim}{k}'}$ satisfy

$$-i\omega'' \psi^{(2)}_{\underset{\sim}{k}+\underset{\sim}{k}'} - ik_{\parallel}''(\rho_s/a)^2 n^{(2)}_{\underset{\sim}{k}+\underset{\sim}{k}'} - \eta J^{(2)}_{\underset{\sim}{k}+\underset{\sim}{k}'} + i\omega^{T}_{*k}''(1 + \alpha + \alpha\alpha'\omega/\nu_e)\psi_{\underset{\sim}{k}+\underset{\sim}{k}'} = R \,, \tag{2-66}$$

$$-i\omega'' n^{(2)}_{\underset{\sim}{k}+\underset{\sim}{k}'} + ik_{\parallel}'' J^{(2)}_{\underset{\sim}{k}+\underset{\sim}{k}'} = U - ik_y'' \frac{\partial J_0}{\partial x} \psi^{(2)}_{\underset{\sim}{k}+\underset{\sim}{k}'} \,, \tag{2-67}$$

and

$$J^{(2)}_{\underset{\sim}{k}+\underset{\sim}{k}'} = \frac{\partial^2}{\partial x''^2} - (k_y + k_y')^2 \psi^{(2)}_{\underset{\sim}{k}+\underset{\sim}{k}'} \,, \tag{2-68}$$

where

$$R = (\rho_s/a)^2 \left[\psi_{\underset{\sim}{k}'} ik_y' \frac{\partial n_{\underset{\sim}{k}}}{\partial x} - ik_y \frac{\partial \psi_{\underset{\sim}{k}'}}{\partial x} n_{\underset{\sim}{k}} + ik_y \psi_{\underset{\sim}{k}} \frac{\partial n_{\underset{\sim}{k}'}}{\partial x} - ik_y' \frac{\partial \psi_{\underset{\sim}{k}}}{\partial x} n_{\underset{\sim}{k}'} \right], \tag{2-69}$$

$$U = \Big[- \psi_{\underset{\sim}{k}'} ik_y' \frac{\partial J_{\underset{\sim}{k}}}{\partial x} - ik_y \frac{\partial \psi_{\underset{\sim}{k}'}}{\partial x} J_{\underset{\sim}{k}} + ik_y \psi_{\underset{\sim}{k}} \frac{\partial J_{\underset{\sim}{k}'}}{\partial x} - ik_y' \frac{\partial \psi_{\underset{\sim}{k}}}{\partial x} J_{k'} \Big] , \tag{2-70}$$

$\omega = \omega + \omega'$, and $k_{\|}'' = k_{\|} + k_{\|}' = k_y'' x''/L_s$. Note that x'' is the distance to the $k'' \cdot B_0 = 0$ singular surface.

As in Ref. 12, the relative orientation of the $\underset{\sim}{k}$ (test mode), $\underset{\sim}{k}'$ (background mode), and $\underset{\sim}{k}''$ (driven mode) singular surfaces is important, as this affects the degree of overlap of the spacial structures. Two cases have been defined.[12] The first is that of sparsely packed turbulence, where in the $\underset{\sim}{k} \cdot \underset{\sim}{B}_0 = 0$ surface falls in the exterior magnetohydrodynamic region of the driven $\underset{\sim}{k} \cdot \underset{\sim}{B}_0 = 0$ mode. The second case is that of densely packed turbulence and is distinguished by the fact that the $\underset{\sim}{k} \cdot \underset{\sim}{B}_0 = 0$ surface falls in or near the k'' interior region. The later case corresponds to the fully developed, multihelicity turbulence characteristic of edge tearing fluctuations and is the case addressed in this work. The former corresponds to a system of a few, large amplitude overlapping kink-tearing modes and is detailed in Ref.12. As the present treatment is limited to densely packed turbulence, it

is noted that the last term on the right hand side of Eq. (2-64), the current gradient drive term, is unimportant and may be dropped.

Assuming densely packed turbulence, constant ψ (mode width << the resistive skin depth, see Appendix), and tearing symmetry, the driven solutions are derived in the Appendix and are

$$\psi^{(2)}_{\underset{\sim}{k}+\underset{\sim}{k}'} = \psi_{\underset{\sim}{k}+\underset{\sim}{k}'}(x = 0)$$

$$- k_{\parallel}'' L^{(1)}_{\underset{\sim}{k},\underset{\sim}{k}',\underset{\sim}{k}''}(\rho_s/a)^2 U/\omega'' = L^{(1)}_{\underset{\sim}{k},\underset{\sim}{k}',\underset{\sim}{k}''} R \qquad (2\text{-}71)$$

$$- k_{\parallel}'' L^{(1)}_{\underset{\sim}{k},\underset{\sim}{k}',\underset{\sim}{k}''}(\rho_s/a)^2 U/\omega'' ,$$

$$J^{(2)}_{\underset{\sim}{k}+\underset{\sim}{k}'} = \frac{\Delta'_{\underset{\sim}{k}+\underset{\sim}{k}'} L^{(1)}_{\underset{\sim}{k},\underset{\sim}{k}',\underset{\sim}{k}''} R}{(1 + x''^2/w^2_{\underset{\sim}{k}''})} , \qquad (2\text{-}72)$$

and

$$n^{(2)}_{\underset{\sim}{k}+\underset{\sim}{k}'} = L^{(2)}_{\underset{\sim}{k},\underset{\sim}{k}',\underset{\sim}{k}''} U$$

$$- ik_{\parallel}'' L^{(2)}_{\underset{\sim}{k},\underset{\sim}{k}',\underset{\sim}{k}''} J_{\underset{\sim}{k}+\underset{\sim}{k}'} , \qquad (2\text{-}73)$$

where

$$L^{(1)}_{\underset{\sim}{k},\underset{\sim}{k}',\underset{\sim}{k}''} = \frac{1}{-i(\Delta\omega) + \delta\gamma_{\underset{\sim}{k}} + \delta\gamma_{\underset{\sim}{k}'} + \delta\gamma_{\underset{\sim}{k}''}} \quad , \tag{2-74}$$

and

$$L^{(2)}_{\underset{\sim}{k},\underset{\sim}{k}',\underset{\sim}{k}''} = \frac{1}{\delta\gamma_{\underset{\sim}{k}} + \delta\gamma_{\underset{\sim}{k}'} + \delta\gamma_{\underset{\sim}{k}''}} \quad , \tag{2-75}$$

$$\Delta\omega = \omega_{\underset{\sim}{k}} - \omega_{\underset{\sim}{k}''} + \omega_{\underset{\sim}{k}'} ,$$

$$\omega_{\underset{\sim}{k}} = \omega^T_*(1 + \alpha) + i\left(\frac{\omega^T_*}{\nu_e}(1 + \alpha) + \frac{\eta\Delta'_{\underset{\sim}{k}'}}{\pi w_{\underset{\sim}{k}'}}\right) \quad ,$$

and

$$w^2_{\underset{\sim}{k}+\underset{\sim}{k}'} = \frac{L_s^2(1 + \alpha)\omega^T_*\eta a^2}{k''^2_y\rho_s^2} \quad .$$

$\Delta\omega$ is the three wave frequency mismatch and $\delta\gamma$ is the EDQM[50,56] nonlinear interaction time. $R_e(\Delta\omega)$ is zero since ω^T_* is nondispersive and $Im(\Delta\omega)$ is negligible in a high Reynold's number plasma where

$$\delta\gamma >> \frac{\eta|\Delta'|}{\pi w} \quad .$$

In 2.5.2 of this section, we will find

$$\delta\gamma \sim \frac{\rho_s v_A}{w}\left(\frac{|\Delta'|}{w}\right)^{1/2}\left(\frac{\delta B}{B_0}\right)_{rms}$$

analogous to the "Alfven Effect."[35]

Note that the limit of x" going to infinity corresponds to sparsely packed turbulence and will not be considered here. For x" ~ w, we are in the semi-collisional regime, and substituting Eqs. (2-71), (2-72), and (2-73) into Eqs. (2-63) and (2-64) we obtain

$$-i\omega\psi_{\underset{\sim}{k}} + i\omega_*^T(1 + \dot{\alpha} + \alpha\alpha'\omega/\nu_e)\psi_{\underset{\sim}{k}}$$

$$-ik_\parallel(\rho_s/a)^2 n_{\underset{\sim}{k}} - (\eta + d_{\underset{\sim}{k}} - c_{\underset{\sim}{k}}^{(2)})J_{\underset{\sim}{k}} \qquad (2\text{-}76)$$

$$+ c_{\underset{\sim}{k}}^{(1)}\frac{\partial^2 J_{\underset{\sim}{k}}}{\partial x^2} = 0,$$

and

$$-i\omega n_{\underset{\sim}{k}} + ik_\parallel J_{\underset{\sim}{k}} = a_{\underset{\sim}{k}}\frac{\partial^2 n_{\underset{\sim}{k}}}{\partial x^2}, \qquad (2\text{-}77)$$

$$c_k^{(1)} = (\rho_s/a)^2 \sum_{\underset{\sim}{k}'} k_y'^2 L^{(2)}_{\underset{\sim}{k},\underset{\sim}{k}',\underset{\sim}{k}''}\left|\psi_{\underset{\sim}{k}'}\right|^2 \qquad (2\text{-}78)$$

$$c_k^{(2)} = -(\rho_s/a)^2 \sum_{\underset{\sim}{k}'} k_y'^2 L_{\underset{\sim}{k},\underset{\sim}{k}',\underset{\sim}{k}''}(\psi^*_{\underset{\sim}{k}'}, J_{\underset{\sim}{k}'}), \tag{2-79}$$

$$d_k = (\rho_s/a)^4 \sum_{\underset{\sim}{k}'} k_y'^2 L^{(1)}_{\underset{\sim}{k},\underset{\sim}{k}',\underset{\sim}{k}''} |n_{\underset{\sim}{k}'}|^2 \tag{2-80}$$

and

$$a_k = -(\rho_s/a)^2 \sum_{\underset{\sim}{k}'} \frac{\Delta'_{\underset{\sim}{k}+\underset{\sim}{k}'} k_y'^2}{\pi w_{\underset{\sim}{k}+\underset{\sim}{k}'} \left[1 + \frac{x''}{w_{\underset{\sim}{k}''}}\right]^2} L^{(1)}_{\underset{\sim}{k},\underset{\sim}{k}',\underset{\sim}{k}''} \left[1 - \left(\frac{m'}{m''}\right)^2\right] |\psi_{\underset{\sim}{k}'}|^2. \tag{2-81}$$

We now discuss the additional (compared to shearless theory) shear-related effects in the renormalized coefficients. $d_{\underset{\sim}{k}}$ remains basically the same as in the shearless theory, with a similar physical explanation. $a_{\underset{\sim}{k}}$ acts to damp density fluctuations (when $\Delta'_{\underset{\sim}{k}+\underset{\sim}{k}'} < 0$). Again, $a_{\underset{\sim}{k}}$ is analogous to the "Alfven Effect,"[35,56] where density fluctuations are damped by interaction with large scale magnetic field lines. Internal energy is lost to Alfvenic fluctuations propagating along the magnetic field. Also note that $a_{\underset{\sim}{k}}$ is proportional to $\Delta'_{\underset{\sim}{k}+\underset{\sim}{k}'} < 0$, indicating a coupling to stable modes by a driven current sheet at $\underset{\sim}{k}'' \cdot \underset{\sim}{B} = 0$, thus damping total energy. The second anomalous

contribution to Ohm's Law is $c_{\underset{\sim}{k}}$ and is interpreted as the back reaction of parallel compression ($\nabla_{\parallel} J$) on Ohm's Law and results from the interaction of magnetic turbulence with nonlinearly driven density $n_{k+k'}$ (for classical tearing, the analogous term is negligible). Unlike the shearless case, eigenmode structure ($k_y w \ll 1$) forces

$$| c_{\underset{\sim}{k}}^{(1)} \, \partial^2/\partial x^2 | \gg c_{\underset{\sim}{k}}^{(2)},$$

thereby reducing the effect of $k_y \gg k_y'$ and $k_y \ll k_y'$ limits (although it will be shown in the next section a weak inverse cascade exists in mean square flux).

Note that $c_{\underset{\sim}{k}}^{(1)}$ is a hyper-resistivity and is similar to the hyper-resistivity recently discussed by Strauss.[64] Whereas his result is the back reaction of the $J \times B$ force on Ohm's Law, our result is the back reaction of parallel current compression on Ohm's Law. Further,

$$c_{\underset{\sim}{k}}^{(1)} \frac{\partial^2 J_{\underset{\sim}{k}}}{\partial x^2},$$

resembles Boozer's result.[6] This resemblance can be

traced, as in the shearless theory, to the incompressibility of diamagnetic drift and, consequently, the nonlinear parallel pressure gradient does not contribute to the parallel electric field (as seen in Section 2.4).

2.5.2 Spectrum Equations for a Sheared Magnetic Field

Renormalized spectrum energy and mean square flux equations are obtained using the closure method discussed in Section 2.4.2 for the case of a sheared equilibrium magnetic field.[12] The procedure is very similar to that used in the shearless case.

Beginning with mean square flux, the unrenormalized equation is:

$$\frac{\partial}{\partial t}\int dx\, a_{\underset{\sim}{k}} + 2\eta \int dx\, E^{m}_{\underset{\sim}{k}} - 2\frac{\omega^{T}_{*}}{\nu_e}\alpha\alpha'(\rho_s/a)^2 R_e(\omega_{\underset{\sim}{k}})\int dx\, a_{\underset{\sim}{k}} + (\rho_s/a)^2 \int dx\, ik\,(n^{*}_{\underset{\sim}{k}}\psi_{\underset{\sim}{k}} - n_{\underset{\sim}{k}}\psi^{*}_{\underset{\sim}{k}}) = \sum_{\underset{\sim}{p}+\underset{\sim}{q}=-\underset{\sim}{k}} \mathcal{J}^{a}(\underset{\sim}{k},\underset{\sim}{p},\underset{\sim}{q}) = \tag{2-82}$$

$$= \sum_{\underset{\sim}{p}+\underset{\sim}{q}=-\underset{\sim}{k}} -(\rho_s/a)^2 \int dx \Bigg\{ \Bigg(\psi^*_{\underset{\sim}{k}} i k_y \frac{\partial n_{-\underset{\sim}{q}}}{\partial x} - i q_y n_{-\underset{\sim}{q}} \frac{\partial \psi^*_{\underset{\sim}{k}}}{\partial x} \Bigg) \psi^{(2)}_{\underset{\sim}{k}+\underset{\sim}{q}} + \Bigg(\frac{\partial \psi^*_{\underset{\sim}{k}}}{\partial x} i q_y \psi_{-\underset{\sim}{q}} - \frac{\partial \psi_{-\underset{\sim}{q}}}{\partial x} i k_y \psi^*_{\underset{\sim}{k}} \Bigg) n^{(2)}_{\underset{\sim}{k}+\underset{\sim}{q}} + \Bigg(\frac{\partial \psi_{-\underset{\sim}{p}}}{\partial x} i q_y n_{-\underset{\sim}{q}} - \frac{\partial n_{-\underset{\sim}{q}}}{\partial x} i p_y \psi_{-\underset{\sim}{p}} \Bigg) \psi^{(2)}_{\underset{\sim}{p}+\underset{\sim}{q}} + \text{c.c.} \Bigg\}, \tag{2-83}$$

where

$$E^m_{\underset{\sim}{k}} = - \left(J^*_{\underset{\sim}{k}} \psi_{\underset{\sim}{k}} + J_{\underset{\sim}{k}} \psi^*_{\underset{\sim}{k}} \right).$$

Comparing Eq. (2-56) with Eq. (2-83), two important differences are found between the shearless and sheared equation. First, nonlocality (radial structure) can significantly alter the relative magnitudes of different terms.[35] Second, a linear line bending ($k_\parallel$) term appears in the sheared field case. This term does not conserve mean square flux and represents shear damping. Using Eq. (2-77) in Section 2.4.1,

$$\frac{\partial n_{\underset{\sim}{k}}}{\partial t} = -i k_\parallel J_{\underset{\sim}{k}} - \delta \gamma_{\underset{\sim}{k}} n_{\underset{\sim}{k}}, \tag{2-84}$$

we find that

$$\frac{\partial a_{\underset{\sim}{k}}}{\partial t} + \cdots = -2\int dx \frac{k^2 (w_{\underset{\sim}{k}}/|\Delta'_{\underset{\sim}{k}}|)}{|\omega_{\underset{\sim}{k}} + i\delta\gamma_{\underset{\sim}{k}}|^2} (J_{\underset{\sim}{k}})^2 (\delta\gamma_{\underset{\sim}{k}} + \mathrm{Im}(\omega_{\underset{\sim}{k}})), \tag{2-85}$$

where $\delta\gamma_{\underset{\sim}{k}}$ is the sheared version of the "Alfven Effect" damping, given by

$$\delta\gamma \sim \frac{1}{w_{\underset{\sim}{k}}} \left(\frac{|\Delta'_{\underset{\sim}{k}}|}{w_{\underset{\sim}{k}}}\right)^{1/2} \rho_s v_A \left(\frac{\delta B_r}{B_0}\right)_{rms}$$

Hence, in linear theory (for the case of unstable mode) mean square flux is damped by shear. For strong nonlinearity, when $\delta\gamma_{\underset{\sim}{k}} \gtrsim |I_m(\omega_{\underset{\sim}{k}})|$, mean square flux is again damped. Physically, magnetic fluctuations are damped by convection of pressure along the sheared field. Nonlinearly, this effect is further enhanced when sheared field lines cross fluctuating magnetic lines. Diamagnetic eddies (parcels of density) lose energy to Alfvenic[35] fluctuations along the intersecting field lines, thus enhancing the convection. Note that this loss of mean square flux (magnetic energy), is countered by a gain in internal energy (due to conservation of energy).

Mean square flux conservation follows from Eq. (2-83) by cancellations among the same terms that govern mean square flux conservation in the shearless equations. Using an analogy with 2-D mean square flux, the first and third terms of $\mathcal{J}^a$ correspond to fluid straining of flux while the second term is the back reaction of current compression.

We close mean square flux by iteratively substituting the driven fields (Eqs. (2-71), (2-72), (2-73)) into Eq. (2-83). This yields for the triplet nonlinearity:

$$\begin{aligned}
&\mathcal{J}^a(\underset{\sim}{k},\underset{\sim}{p},\underset{\sim}{q}) \\
&= -(\rho_s/a)^4 \int dx\ R_e(L^{(1)}_{\underset{\sim}{k},\underset{\sim}{p},\underset{\sim}{q}}) \left[k_y^2(\psi_{\underset{\sim}{k}})^2\left(\frac{\partial n_{\underset{\sim}{q}}}{\partial x}\right)^2\right. \\
&\left. + q_y^2(n_{\underset{\sim}{q}})^2\left(\frac{\partial \psi_{\underset{\sim}{k}}}{\partial x}\right)^2\right] \qquad (2\text{-}86) \\
&+ (\rho_s/a)^2 \int dx\ R_e(L^{(2)}_{\underset{\sim}{k},\underset{\sim}{p},\underset{\sim}{q}}) \left\{k_y^2\left[(\psi_{\underset{\sim}{k}})^2 \frac{\partial \psi^*_{\underset{\sim}{q}}}{\partial x}\frac{\partial J_{\underset{\sim}{q}}}{\partial x}\right.\right. \\
&\left. - J_{\underset{\sim}{k}}\psi^*_{\underset{\sim}{k}}\left(\frac{\partial \psi_{\underset{\sim}{q}}}{\partial x}\right)^2\right] + q_y^2\left[\left(\frac{\partial \psi_{\underset{\sim}{k}}}{\partial x}\right)^2 \psi^*_{\underset{\sim}{q}} J_{\underset{\sim}{q}}\right. \\
&\left.\left. - (\psi_{\underset{\sim}{q}})^2 \frac{\partial J_{\underset{\sim}{k}}}{\partial x}\frac{\partial \psi^*_{\underset{\sim}{k}}}{\partial x}\right]\right\} +
\end{aligned}$$

$$+ (\rho_s/a)^4 \int dx\ R_e(L^{(1)}_{\underset{\sim}{k},\underset{\sim}{p},\underset{\sim}{q}}) \left[p_y^2 (n_{\underset{\sim}{p}})^2 \left(\frac{\partial \psi_{\underset{\sim}{q}}}{\partial x}\right)^2 \right.$$

$$\left. + q_y^2 (\psi_{\underset{\sim}{q}})^2 \left(\frac{\partial n_{\underset{\sim}{p}}}{\partial x}\right)^2 \right]$$

where the propagators $L^{(1)}$ and $L^{(2)}$ are given in Part A of this section. We can simplify for $k_y w_k \ll 1$ (strong shear) to find:

$$\mathcal{J}^a(\underset{\sim}{k},\underset{\sim}{p},\underset{\sim}{q}) \cong$$

$$- (\rho_s/a)^4 \int dx\ R_e(L^{(1)}_{\underset{\sim}{k},\underset{\sim}{p},\underset{\sim}{q}}) k_y^2 (\psi_{\underset{\sim}{k}})^2 \left(\frac{\partial n_{\underset{\sim}{q}}}{\partial x}\right)^2 \qquad (2\text{-}87)$$

$$+ (\rho_s/a)^2 \int dx\ R_e(L^{(2)}_{\underset{\sim}{k},\underset{\sim}{p},\underset{\sim}{q}}) \left\{ k_y^2 (\psi_{\underset{\sim}{k}})^2 \frac{\partial \psi^*_{\underset{\sim}{q}}}{\partial x} \frac{\partial J_{\underset{\sim}{q}}}{\partial x} \right.$$

$$\left. - q_y^2 (\psi_{\underset{\sim}{q}})^2 \frac{\partial J_{\underset{\sim}{k}}}{\partial x} \frac{\partial \psi^*_{\underset{\sim}{k}}}{\partial x} \right\}$$

$$+ (\rho_s/a)^2 \int dx\ R_e(L^{(1)}_{\underset{\sim}{k},\underset{\sim}{p},\underset{\sim}{q}}) q_y^2 (\psi_{\underset{\sim}{q}})^2 \left(\frac{\partial n_{\underset{\sim}{p}}}{\partial x}\right)^2$$

The nonlinear structure of mean square flux evolution is qualitatively the same as the shearless case. The back reaction (second term of Eq. (2-87)) still transfers flux to large scales,[22] although nonlocality ($k_y w_k \ll 1$) introduces inhomogeneity.

Comparing the second term of Eq. (2-86) and of Eq. (2-56), we find that $(k_y^2 - q_y^2)$ in shearless theory is replaced by

$$\frac{1}{w_{\underset{\sim}{k}}^2} - \frac{1}{w_{\underset{\sim}{q}}^2}$$

with shear. Noting that $w_{\underset{\sim}{k}}^2 \sim k_y^{-1}$, we see that the transfer is weak (less dependence on the difference between background wavenumber (q) and test wavenumber (k)). The first and third terms only reflect the larger magnitude of poloidal diamagnetic drift compared with the radial drift, and thus differ little from shearless theory. Physically, fluid straining of flux seems less sensitive to the addition of shear. This reflects the fact that a sheared equilibrium magnetic field mainly affects magnetic fluctuations. (Back reaction is primarily magnetic, while straining treats flux as a passive scaler in a diamagnetically drifting fluid.)

The unrenormalized spectrum energy equations are:

$$\frac{\partial}{\partial t}\int dx\ E^m_{\underset{\sim}{k}} + 2\eta \int dx\ (J_{\underset{\sim}{k}})^2$$

$$-2\,\frac{\alpha\alpha'}{\nu_e}\,\omega_*^T \mathrm{Re}(\omega_{\underset{\sim}{k}})\int dx\ E^m_{\underset{\sim}{k}}$$

$$+ (\rho_s/a)^2 \int dx\ ik_\parallel (n_{\underset{\sim}{k}} J^*_{\underset{\sim}{k}} - n^*_{\underset{\sim}{k}} J_{\underset{\sim}{k}})$$

$$= \sum_{\underset{\sim}{p}+\underset{\sim}{q}=-\underset{\sim}{k}} \mathcal{J}^m(\underset{\sim}{k},\underset{\sim}{r},\underset{\sim}{q})$$

$$= (\rho_s/a)^2 \int dx \sum_{\underset{\sim}{p}+\underset{\sim}{q}=-\underset{\sim}{k}} \Bigg\{ \Bigg(J^*_{\underset{\sim}{k}} ik_y \frac{\partial n_{-\underset{\sim}{q}}}{\partial x} \tag{2-88}$$

$$-iq_y n_{-\underset{\sim}{q}} \frac{\partial J^*_{\underset{\sim}{k}}}{\partial x}\Bigg)\ \psi^{(2)}_{\underset{\sim}{k}+\underset{\sim}{q}}$$

$$+\left(\frac{\partial J^*_{\underset{\sim}{k}}}{\partial x}\, iq_y \psi_{-\underset{\sim}{q}} - \frac{\partial \psi_{-\underset{\sim}{q}}}{\partial x}\, ik_y J^*_{\underset{\sim}{k}}\right) n^{(2)}_{\underset{\sim}{k}+\underset{\sim}{q}}$$

$$+\left(\frac{\partial \psi_{-\underset{\sim}{p}}}{\partial x}\, iq_y n_{-\underset{\sim}{q}} - \frac{\partial n_{-\underset{\sim}{q}}}{\partial x}\, ip_y \psi_{-\underset{\sim}{p}}\right) J^{(2)}_{\underset{\sim}{p}+\underset{\sim}{q}} + \text{c.c.}\Bigg\}$$

and

$$\frac{\partial}{\partial t}\int dx\ E^I_{\underset{\sim}{k}}$$

$$+ (\rho_s/a)^2 \int dx\ ik\,(n^*_{\underset{\sim}{k}} J_{\underset{\sim}{k}} - n_{\underset{\sim}{k}} J^*_{\underset{\sim}{k}})$$

$$= (\rho_s/a)^2 \sum_{\underset{\sim}{p}+\underset{\sim}{q}=-\underset{\sim}{k}} \mathcal{J}^I(\underset{\sim}{k},\underset{\sim}{p},\underset{\sim}{q}) =$$

square flux, magnetic energy is damped by parallel convection of pressure $(v_{\parallel}(\nabla_{\parallel})_0 T_e n)$ along the sheared field, with nonlinear enhancement due to the "Alfven Effect." Energy conservation follows from Eqs. (2-88) and (2-89) by cancellations among the same pairings that govern energy conservation in the shearless equations.

Closing the nonlinearity by iteratively substituting the driven fields into Eqs. (2-88 and 2-89), and the triplet nonlinearities are:

$$\mathcal{S}_m(\underset{\sim}{k},\underset{\sim}{p},\underset{\sim}{q}) =$$

$$- (\rho_s/a)^4 \int dx \frac{|\Delta'_{\underset{\sim}{p}}|}{\pi w_{\underset{\sim}{p}}} \frac{k_y^2}{p_y^2} \frac{R_e L^{(1)}_{\underset{\sim}{k},\underset{\sim}{p},\underset{\sim}{q}}}{(1 + (x_{\underset{\sim}{p}}/w_{\underset{\sim}{p}})^2)}$$

$$\left[k_y^2(\psi_{\underset{\sim}{k}})^2\left(\frac{\partial n_{\underset{\sim}{q}}}{\partial x}\right)^2 + q_y^2\left(\frac{\partial \psi_{\underset{\sim}{k}}}{\partial x}\right)^2 (n_{\underset{\sim}{q}})^2\right] \qquad (2\text{-}90)$$

$$- (\rho_s/a)^2 \int dx\, R_e(L^{(2)}_{\underset{\sim}{k},\underset{\sim}{p},\underset{\sim}{q}}) \left\{q_y^2 \left[\left(\frac{\partial J_{\underset{\sim}{k}}}{\partial x}\right)^2 (\psi_{\underset{\sim}{q}})^2\right.\right.$$

$$\left. - \left(\frac{\partial J^*_{\underset{\sim}{k}}}{\partial x} \frac{\partial \psi_{\underset{\sim}{k}}}{\partial x}\right)(\psi^*_{\underset{\sim}{q}} J_{\underset{\sim}{q}})\right] + k_y^2 \left[(J_{\underset{\sim}{k}})^2 \left(\frac{\partial \psi_{\underset{\sim}{q}}}{\partial x}\right)^2\right.$$

$$\left.\left. - \left(\frac{\partial \psi^*_{\underset{\sim}{q}}}{\partial x} \frac{\partial J_{\underset{\sim}{q}}}{\partial x}\right)(J^*_{\underset{\sim}{k}} \psi_{\underset{\sim}{k}})\right] +\right.$$

$$+ (\rho_s/a)^4 \int dx \frac{R_e(L^{(1)}_{\underset{\sim}{k},\underset{\sim}{p},\underset{\sim}{q}})|\Delta'_{\underset{\sim}{k}}|}{(1 + (x/w_{\underset{\sim}{k}})^2)\pi w_{\underset{\sim}{k}}} \left[q_y^2(\psi_{\underset{\sim}{q}})^2 \left(\frac{\partial n_{\underset{\sim}{p}}}{\partial x}\right)^2 + p_y^2(n_{\underset{\sim}{p}})^2 \left(\frac{\partial \psi_{\underset{\sim}{q}}}{\partial x}\right)^2 \right] \tag{2-90}$$

$$\mathcal{J}^I(\underset{\sim}{k},\underset{\sim}{p},\underset{\sim}{q}) =$$

$$- (\rho_s/a)^4 \int dx \frac{|\Delta'_{\underset{\sim}{p}}|}{\pi w_{\underset{\sim}{p}}} \frac{R_e(L^{(1)}_{\underset{\sim}{k},\underset{\sim}{p},\underset{\sim}{q}})}{(1 + (x_{\underset{\sim}{p}}/w_{\underset{\sim}{p}})^2)} \left[q_y^2(\psi_{\underset{\sim}{q}})^2 \left(\frac{\partial n_{\underset{\sim}{k}}}{\partial x}\right)^2 + k_y^2 \left(\frac{\partial \psi_{\underset{\sim}{q}}}{\partial x}\right)^2 (n_{\underset{\sim}{k}})^2 \right]$$

$$+ (\rho_s/a)^4 \int dx \frac{|\Delta'_{\underset{\sim}{p}}|}{\pi w_{\underset{\sim}{p}}} \left(\frac{q_y}{p_y}\right)^2 \frac{R_e(L^{(1)}_{\underset{\sim}{k},\underset{\sim}{p},\underset{\sim}{q}})}{(1 + (x_{\underset{\sim}{p}}/w_{\underset{\sim}{p}})^2)} \tag{2-91}$$

$$\left[q_y^2(\psi_{\underset{\sim}{q}})^2 \left(\frac{\partial n_{\underset{\sim}{k}}}{\partial x}\right)^2 + k_y^2 \left(\frac{\partial \psi_{\underset{\sim}{q}}}{\partial x}\right)^2 (n_{\underset{\sim}{k}})^2 \right]$$

$$+ (\rho_s/a)^2 \int dx \, R_e(L^{(2)}_{\underset{\sim}{k},\underset{\sim}{p},\underset{\sim}{q}}) \left\{ q_y^2 (\psi_{\underset{\sim}{q}})^2 \left(\frac{\partial J_{\underset{\sim}{p}}}{\partial x}\right)^2 - \left(\frac{\partial J_{\underset{\sim}{p}}}{\partial x} \frac{\partial \psi^*_{\underset{\sim}{p}}}{\partial x}\right) (J^*_{\underset{\sim}{q}} \psi_{\underset{\sim}{q}}) \right] + p_y^2 \left[(J_{\underset{\sim}{p}})^2 \left(\frac{\partial \psi_{\underset{\sim}{q}}}{\partial x}\right)^2 - (\psi^*_{\underset{\sim}{p}} J_{\underset{\sim}{p}}) \left(\frac{\partial \psi_{\underset{\sim}{q}}}{\partial x} \frac{\partial J^*_{\underset{\sim}{q}}}{\partial x}\right) \right] \right\}$$

When the $k_y w_{\underset{\sim}{k}} \ll 1$ ordering is imposed (strong shear):

$$\mathcal{J}^{m}(\underset{\sim}{k},\underset{\sim}{p},\underset{\sim}{q}) \cong$$

$$- (\rho_s/a)^4 \int dx \, \frac{k_y^2 |\Delta'_{\underset{\sim}{p}}|}{\pi w_{\underset{\sim}{p}}} \left(\frac{k_y}{p_y}\right)^2 \frac{R_e(L^{(1)}_{\underset{\sim}{k},\underset{\sim}{p},\underset{\sim}{q}})}{(1 + (x_{\underset{\sim}{p}}/w_{\underset{\sim}{p}})^2)}$$

$$(\psi_{\underset{\sim}{k}})^2 \left(\frac{\partial n_{\underset{\sim}{q}}}{\partial x}\right)^2$$

$$- (\rho_s/a)^2 \int dx \, R_e(L^{(2)}_{\underset{\sim}{k},\underset{\sim}{p},\underset{\sim}{q}}) q_y^2 (\psi_{\underset{\sim}{q}})^2 \left(\frac{\partial J_{\underset{\sim}{k}}}{\partial x}\right)^2$$

$$+ (\rho_s/a)^4 \int dx \, \frac{q_y^2 |\Delta'_{\underset{\sim}{k}}|}{\pi w_{\underset{\sim}{k}}} \frac{R_e(L^{(1)}_{\underset{\sim}{k},\underset{\sim}{p},\underset{\sim}{q}})}{(1 + (x/w_{\underset{\sim}{k}})^2} (\psi_{\underset{\sim}{q}})^2 \left(\frac{\partial n_{\underset{\sim}{p}}}{\partial x}\right)^2 \tag{2-92}$$

and

$$I(\underset{\sim}{k},\underset{\sim}{p},\underset{\sim}{q}) =$$

$$- (\rho_s/a)^4 \int dx \, \frac{q_y^2 |\Delta'_{\underset{\sim}{p}}|}{\pi w_{\underset{\sim}{p}}} \frac{R_e(L_{\underset{\sim}{k},\underset{\sim}{p},\underset{\sim}{q}})}{(1 + (x_{\underset{\sim}{p}}/w_{\underset{\sim}{p}})^2)} (\psi_{\underset{\sim}{q}})^2 \left(\frac{\partial n_{\underset{\sim}{k}}}{\partial x}\right)^2$$

$$+ (\rho_s/a)^4 \int dx \, \frac{q_y^2 |\Delta'_{\underset{\sim}{p}}|}{\pi w_{\underset{\sim}{p}}} \frac{R_e(L^{(1)}_{\underset{\sim}{k},\underset{\sim}{p},\underset{\sim}{q}})}{(1 + (x_{\underset{\sim}{p}}/w_{\underset{\sim}{p}})^2)} \left(\frac{q_y}{p_y}\right)^2 (\psi_{\underset{\sim}{q}})^2 \left(\frac{\partial n_{\underset{\sim}{k}}}{\partial x}\right)^2$$

$$+ (\rho_s/a)^2 \int dx \, q_y^2 R_e(L_{\underset{\sim}{k},\underset{\sim}{p},\underset{\sim}{q}}) (\psi_{\underset{\sim}{q}})^2 \left(\frac{\partial J_{\underset{\sim}{p}}}{\partial x}\right)^2 . \tag{2-93}$$

Briefly, the coherent terms of $\mathcal{J}^{m}$ and $\mathcal{J}^{I}$ can be identified with those in one point theory. The first term of $\mathcal{J}^{m}$ is $d_{\underset{\sim}{k}}$, or random diamagnetic convection and acts as a sink of magnetic energy (straining

of magnetic field lines). The second term is the back reaction of parallel compression on Ohm's Law. In the case of strong shear, unlike the shearless theory, non-locality causes this term to be a sink of magnetic energy. Apparently, since magnetic energy prefers small scales (as compared to mean square flux), the negative resistivity piece in the absence of shear is negligible compared to the positive (small scale) resistivity piece of the back reaction in magnetic energy evolution. A corresponding effect is found on the incoherent term in internal energy, making the back reaction an incoherent source. Physically, current perturbations (filaments) (which are localized (small scale) near the mode rational surface) are damped by large scale diamagnetic eddies. This loss of magnetic energy is incoherently emitted to internal energy.

As in the 2-D shearless case, we consider the interaction of test mode $\underset{\sim}{k}$ with large poloidal scale fluctuations (see Figure 2.3) and find:

$$\mathcal{J}^m(\underset{\sim}{k},\underset{\sim}{p},\underset{\sim}{q}) \cong (\rho_s/a)^2 \int dx\, q_y^2 (\psi_{\underset{\sim}{q}})^2 \left[(\rho_s/a)^2 \frac{|\Delta'_{\underset{\sim}{k}}|}{\pi w_{\underset{\sim}{k}}} \frac{\Re_e(L^{(1)}_{\underset{\sim}{k},\underset{\sim}{p},\underset{\sim}{q}})}{(1+(x/w_{\underset{\sim}{k}})^2)} \left(\frac{\partial n_{\underset{\sim}{k}}}{\partial x} \right)^2 - \right. \qquad (2\text{-}94)$$

$$- R_e(L^{(2)}_{\underset{\sim}{k},\underset{\sim}{p},\underset{\sim}{q}}) \left(\frac{\partial J_{\underset{\sim}{k}}}{\partial x}\right)^2 \Bigg]$$

$$= - \mathcal{I}^I(\underset{\sim}{k},\underset{\sim}{p},\underset{\sim}{q}). \qquad (2\text{-}94)$$

The long time (or stationary) solution of the large scale background fluctuation problem is an equipartition between magnetic and internal energy such that

$$(\rho_s/a)^2 \frac{|\Delta'_{\underset{\sim}{k}}|}{\pi w_{\underset{\sim}{k}}} \left(1 + (x/w_{\underset{\sim}{k}})^2\right)^{-1} \left(\frac{\partial n_{\underset{\sim}{k}}}{\partial x}\right)^2$$

$$= \left(\frac{\partial J_{\underset{\sim}{k}}}{\partial x}\right)^2 , \qquad (2\text{-}95)$$

where $L^{(1)} = L^{(2)} \sim (\delta\gamma)^{-1}$. Using

$$J_{\underset{\sim}{k}} \sim \frac{-|\Delta'_{\underset{\sim}{k}}|}{\pi w_{\underset{\sim}{k}}} \psi_{\underset{\sim}{k}} \left(1 + \left(\frac{x}{w_{\underset{\sim}{k}}}\right)^2\right)^{-1} ,$$

$E^m_{\underset{\sim}{k}} = -J_{\underset{\sim}{k}}\psi_{\underset{\sim}{k}}$, and,

$$\left|\frac{1}{J_{\underset{\sim}{k}}} \frac{\partial J_{\underset{\sim}{k}}}{\partial x}\right| \sim \left|\frac{1}{n_k} \frac{\partial n_{\underset{\sim}{k}}}{\partial x}\right| \sim \left|\frac{1}{w_{\underset{\sim}{k}}}\right|$$

we find that

$$E^m_{\underset{\sim}{k}} \sim E^I_{\underset{\sim}{k}} \qquad (2\text{-}96)$$

and the "equipartition time" is given by

$$\tau_{ep}^{-1} = \frac{\rho_s v_A}{w_{\underset{\sim}{k}}} \left(\frac{\Delta'_{\underset{\sim}{k}}}{w_{\underset{\sim}{k}}} \right)^{1/2} \left(\frac{\delta B_r}{B_0} \right)_{rms} \qquad (2\text{-}97)$$

where $(\delta B_r)^2 = k_y^2 (\psi_{\underset{\sim}{k}})^2$. Taking the ratio of the shearless interaction time

$$\tau_{eq} = \left(\frac{1}{k_y^2 \rho_s v_A \left(\frac{\delta B}{B_0} \right)_{rms}} \right)$$

to the one with shear, we see that their ratio is $(k_y w_{\underset{\sim}{k}})^{-3/2}$. Hence, shear acts (through nonlocality) to shorten the interaction time (reflecting localization around the mode rational surface). From the one point equation (Eq. (2-76)) the nonlinear interaction time at "equipartition" is

$$\delta\gamma_k = \tau_{ep}^{-1} .$$

In the case of shear, this time is similar to the "Alfven" time of the shearless theory, but with $\Delta'_{\underset{\sim}{k}}$ regulating the interaction (i.e., progressive current filamentation). At equipartition (inside the tearing layer) we can alternatively write

$$\tau_{ep}^{-1} \cong k_y v_A (v_{Dy})_{rms} \qquad (2\text{-}98)$$

where

$$v_{Dy}^2 = \left(\frac{\partial n_{\underset{\sim}{k}}}{\partial x} \right)^2 >> (k_y n_{\underset{\sim}{k}})^2 = (v_{Dx})^2.$$

The equipartition time can now be viewed as a diamagnetic convection eddy turnover time. As in the shearless case, key to this "equipartitioning" is the inclusion of incoherent mode coupling and both back reaction and straining effects.

The second class of interactions corresponds to an unstable test mode, i.e., the effect of small scale background fluctuations on a large scale test mode. This regime is treated in the next section on saturation.

We conclude this section with a summary of the differences between the shearless and sheared theory. The principal differences are

(1) Line bending ($ik_\parallel$ terms) tends to damp magnetic energy while driving internal energy, thus funnelling magnetic energy to internal energy (but conserving their sum).

(2) Nonlocality ($k_y w_{\underset{\sim}{k}} < 1$) makes back reaction terms ($n^{(2)}_{\underset{\sim}{k}+\underset{\sim}{k}'}$) predominantly damp magnetic energy (coherently) while emitting to internal energy (incoherently).

(3) The inverse (to large scales) transfer of mean square flux is weakened by shear.

(4) The cascade of energy to small scales is strengthened by shear, since back reaction effects do not oppose the cascade (see 2 above).

(5) The nonlinear interaction time ($\delta\gamma^{-1}$) is altered significantly by shear, such that this time in much shorter when shear is present by $(k_y w)^{3/2}$.

2.6 Saturation Mechanisms

The stationary state of microtearing turbulence is addressed for both the cases of uniform and sheared magnetic field. As in Navier-Stokes turbulence,[33] energy is input (stirring) at large scales and transferred to small scales where the energy is dissipated. Physically, magnetic field lines are stretched by a diamagnetic strain field, thus increasing energy at small scales. Writing the equation for magnetic field

(no dissipation or forcing):

$$\frac{\partial \underset{\sim}{B}}{\partial t} + \underset{\sim}{v}_D \cdot \underset{\sim}{\nabla} \underset{\sim}{B} = \underset{\sim}{B} \cdot \underset{\sim}{\nabla} \underset{\sim}{v}_D, \tag{2-99}$$

we see that in the Lagrangian frame, that strain, $\underset{\sim}{\nabla} \underset{\sim}{v}_D$, is a source of magnetic field production. This process is similar to vortex stretching in 3-D Navier-Stokes fluids, because vorticity obeys Eq. (2-99), with magnetic field replaced by vorticity (and diamagnetic velocity replaced by fluid velocity). Hence, a possible saturation mechanism whereby stable modes at small scales nonlinearly absorb energy from unstable modes at large scales (stirring) exists. Magnetic fluctuation levels are derived for the cases of a uniform and sheared equilibrium magnetic field. For a sheared field, two cases are treated, corresponding to the size of the conductivity layer compared to the island width. Quantitatively, the island width over the conductivity layer width squared is

$$R_s = \frac{\delta \nabla_\parallel}{(\nabla_\parallel)_0} \sim \frac{(k'_\parallel)^{-1} \frac{\delta B_r}{B_0}}{w_{\underset{\sim}{k}}^2}$$

$$= \frac{\delta B_r}{B_0} \frac{\Omega_e}{\nu_e} \frac{L_T}{L_s} \tag{2-100}$$

where Ω_e is the electron gyrofrequency. When $R_s < 1$, a weakly turbulent (or quasi-marginal) state exists and is not considered here. $R_s \cong 1$ corresponds to a self-excited state or moderately turbulent regime. Finally, for $R_s > 1$ we have a strongly turbulent regime (highly excited state). The three regimes are termed weak, moderate and strong, respectively.

2.6.1 Saturation of the Self-Filamentation Mode

Recalling the discussion of the triplet interactions in Section 2.3.2, we now discuss the spectrum energy equations in a uniform magnetic field for small scale background modes interacting with a test mode k in the region where unstable modes exist. In wave-number space, this region occurs when

(1) $k \lesssim \nu_e(k_y/\omega_*^T)$, corresponding to the validity of the Chapman Enskog[25] equations

(2)
$$\eta < \left(\frac{k_y}{k}\right)^2 \left(\frac{\omega_*^T}{k_y}\right)^2 (1 + \alpha)\alpha\alpha',$$

for an unstable mode, and

(3) $$\eta < \rho_s v_A \frac{\delta B}{B_0} ,$$

where nonlinear interaction dominates resistive processes such that Reynold's number greater than 1 (inertial range).

From Section 2.3.1, we found that magnetic and internal energy equipartition at small scales ($E^m_{\underset{\sim}{k}} = E^I_{\underset{\sim}{k}}$). Physically, a stationary state at small scales required the stretching of magnetic field lines balancing the back reaction of $\underset{\sim}{B} \cdot \underset{\sim}{\nabla} J$ on Ohm's Law. This balance occurs when the energies equipartition. Applying the equipartition of energy to the spectrum energy equations (Eqs. (2-92) and (2-93)) at large scales:

$$\frac{\partial E^m_{\underset{\sim}{k}}}{\partial t} - 2\alpha\alpha' \frac{\omega^T_*}{\nu_e} \mathrm{Re}(\omega_{\underset{\sim}{k}}) E^m_{\underset{\sim}{k}}$$

$$= -(\rho_s/a)^2 \sum_{\underset{\sim}{p}+\underset{\sim}{q}=-\underset{\sim}{k}} (\underset{\sim}{p} \cdot \underset{\sim}{q} \times \hat{z})^2 \mathrm{Re}(\mathcal{L}_{\underset{\sim}{k},\underset{\sim}{p},\underset{\sim}{q}}) E^m_{\underset{\sim}{q}} E^m_{\underset{\sim}{k}}$$

$$+ T^m \qquad (2\text{-}101)$$

and

$$\frac{\partial E^I_{\underset{\sim}{k}}}{\partial t} = -(\rho_s/a)^2 \sum_{\underset{\sim}{p}+\underset{\sim}{q}=-\underset{\sim}{k}} (\underset{\sim}{p} \cdot \underset{\sim}{q} \times \hat{z})^2 \mathrm{Re}(\mathcal{L}_{\underset{\sim}{k},\underset{\sim}{p},\underset{\sim}{q}})$$

$$\left(\frac{p_\perp^2 - q_\perp^2}{q^2}\right) E^m_{\underset{\sim}{q}} E^I_{\underset{\sim}{k}} + T^I, \qquad (2\text{-}102)$$

where $\mathcal{L} = \mathcal{L}^{(1)} = \mathcal{L}^{(2)} \sim (\delta\gamma)^{-1}$,

$$T^m =$$

$$(\rho_s/a)^2 \sum_{\underset{\sim}{p}+\underset{\sim}{q}=-\underset{\sim}{k}} (\underset{\sim}{p} \cdot \underset{\sim}{q} \times \hat{z})^2 \mathrm{Re}(\mathcal{L}_{\underset{\sim}{k},\underset{\sim}{p},\underset{\sim}{q}}) \frac{k_\perp^2}{q_\perp^2} E^m_{\underset{\sim}{q}} E^I_{\underset{\sim}{p}}, \qquad (2\text{-}103)$$

and

$$T^I =$$

$$(\rho_s/a)^2 \sum_{p+q=-k} (\underset{\sim}{p} \cdot \underset{\sim}{q} \times \hat{z})^2 \mathrm{Re}(\mathcal{L}_{\underset{\sim}{k},\underset{\sim}{p},\underset{\sim}{q}}) \left(\frac{p_\perp^2 - q_\perp^2}{q_\perp^2}\right) E^m_{\underset{\sim}{p}} E^m_{\underset{\sim}{q}} . \qquad (2\text{-}104)$$

Here, T^m and T^I are the incoherent sources of Ohm's Law and continuity, respectively.

A stationary state is found when Ohm's Law and total energy are required to be time independent (up to ω_*^T rotation). From Section 3.4.1, Ohm's Law is:

$$\frac{\partial \psi_{\underset{\sim}{k}}}{\partial t} + i\omega_*^T \left(1 + \alpha + \frac{1\alpha\alpha'\omega}{\nu_e}\right) \psi_{\underset{\sim}{k}}$$

$$+ (\rho_s/a)^2 \sum_{\underset{\sim}{k}'} (\underset{\sim}{k} \cdot \underset{\sim}{k}' \times \hat{z})^2 \mathcal{L}_{k,k',k''} (E^I_{\underset{\sim}{k}'} - E^m_{\underset{\sim}{k}'})$$

$$+ (\rho_s/a)^2 \sum_{\underset{\sim}{k}'} (\underset{\sim}{k} \cdot \underset{\sim}{k} \times \hat{z})^2 \mathcal{L}_{\underset{\sim}{k},\underset{\sim}{k}',\underset{\sim}{k}''} \frac{k_\perp^2}{k_\perp'^2} E^m_{\underset{\sim}{k}'} = 0 \qquad (2\text{-}105)$$

where $\mathcal{L}_{\underset{\sim}{k},\underset{\sim}{k}',\underset{\sim}{k}''} = \delta\gamma_{\underset{\sim}{k}}^{-1}$ and resistivity is neglected (we are considering large scales, with Reynold's number larger than 1). Note that the third term on the left hand side of Eq. (2-105), is composed of a positive resistivity due to stretching of constant flus contours and a negative resistivity due to back reaction. The fourth term, although smaller than the third, is kept for resons which will become clear. This term is the positive anomalous resistivity piece of the back reaction. With short scale background, Eq. 2-105 becomes

$$\frac{\partial \psi_{\underset{\sim}{k}}}{\partial t} + i\omega_*^T \left(1 + \alpha + \frac{i\alpha\alpha'\omega}{\nu_e}\right) \psi_{\underset{\sim}{k}}$$

$$+ (\rho_s/a)^2 \sum_{\underset{\sim}{k}'} (\underset{\sim}{k} \cdot \underset{\sim}{k}' \times \hat{z})^2 \left(\frac{k_\perp}{k_\perp'}\right) E^m_{\underset{\sim}{k}'} \mathcal{L}^{(2)}_{\underset{\sim}{k},\underset{\sim}{k}',\underset{\sim}{k}''}$$

$$= 0 \qquad (2\text{-}106)$$

where $\mathcal{L}^{(2)}_{\underset{\sim}{k},\underset{\sim}{k}',\underset{\sim}{k}''} = \delta\gamma^{-1}_{\underset{\sim}{k}} = \tau_{ep}$, the equipartition time. A saturated state is found when Ohm's Law is time independent, and thus

$$\delta\gamma_{\underset{\sim}{k}} = (1 + \alpha)\alpha\alpha' \frac{(\omega^T_*)^2}{\nu_e} \quad , \tag{2-107}$$

i.e., linear growth balances the positive anomalous resistivity piece of the back reaction of $\underset{\sim}{B} \cdot \underset{\sim}{\nabla} J$ on Ohm's Law. Thus, our keeping of both pieces of the back reaction is justified, because the positive anomalous resistivity is the only remaining nonlinear term. This term is more compactly written as

$$\frac{\partial \psi_{\underset{\sim}{k}}}{\partial t} + \ldots = -\delta\gamma_{\underset{\sim}{k}}\psi_{\underset{\sim}{k}} \cdot$$

From Eqs. (2-101) and (2-102) the total energy at unstable large scales is:

$$\frac{\partial}{\partial t}\left(E^m_{\underset{\sim}{k}} + E^I_{\underset{\sim}{k}}\right) - \alpha\alpha'(1 + \alpha)\frac{(\omega^T_*)^2}{\nu_e} E^m_{\underset{\sim}{k}} \tag{2-108}$$

$$= -\delta\gamma_{\underset{\sim}{k}} E^m_{\underset{\sim}{k}} - \delta\gamma_{\underset{\sim}{k}} E^I_{\underset{\sim}{k}} + T^m + T^I$$

From Eq. (2-107) (the balance of back-reaction with linear growth) the second term on the left hand side cancels the first term on the right hand side of Eq. (2-108) (total energy) such that:

$$\frac{\partial}{\partial t}\left(E^{m}_{\underset{\sim}{k}} + E^{I}_{\underset{\sim}{k}}\right)$$

$$= -\delta\gamma_{\underset{\sim}{k}} E^{I}_{\underset{\sim}{k}} + T^{m} + T^{I} \qquad (2\text{-}109)$$

Hence, we find that total energy is time independent when:

$$E^{I}_{k} = \frac{T^{m} + T^{I}}{\delta\gamma_{\underset{\sim}{k}}} \,. \qquad (2\text{-}110)$$

The internal energy is proportional to incoherent emission and the nonlinear interaction time (diamagnetic eddy turnover time). Physically, stable modes at small scales nonlinearly absorb energy from unstable modes at large scales, which in turn is emitted incoherently to internal energy at large scales.

The magnetic field fluctuation level (Eq. (2-107)) can be rewritten as:

$$\frac{\delta B}{B_0} = (1 + \alpha)\alpha\alpha' \left(\frac{\beta_e}{2}\right)^{1/2} \frac{\Omega_e}{\nu_e} \left(\frac{\rho_e}{L_T}\right)^2 \qquad (2\text{-}111)$$

where

$$\beta_e = \frac{n_0 T_e 8\pi}{B_0^2} ,$$

ρ_e is the electron gyroradius and Ω_e is the electron gyrofrequency. Characteristic of this fluctuation level, is the proportionality to β_e (nonlinear pressure coupling), L_T^{-1} (linear source of free energy) and $\nu_e^{-1}\alpha\alpha'$ (time dependent thermal force, indicative of semicollisionality).

2.6.2 Saturation of the Microtearing Mode

In addition to the Reynold's number,

$$R_1 = \frac{\delta\gamma_k}{\frac{|\Delta'|\eta}{\pi W}} > 1,$$

indicates the incidence of an inertial-like range, a second parameter (Reynold's number),

$$R_s = \left(\frac{w_I}{w_k}\right)^2$$

can be defined, where w_I is the magnetic island width and w_k is conductivity layer width. $R_s > 1$ represents the dominance of nonlinear effects over linear ones, where roughly,

$$R_s = \frac{\delta\nabla_\parallel}{(\nabla_\parallel)_0} \quad \frac{\frac{\delta \underset{\sim}{B}}{B_0} \cdot \underset{\sim}{\nabla}}{k_\parallel} \quad .$$

Three regimes can then be delineated--weak, moderate and strong, corresponding to $R_s < 1$, $R_s \cong 1$, and $R_s > 1$. The first regime is where the radial scale goes as the mode width and $w_k > w_I$. The second (moderate) regime corresponds to the mode width approximately equal to the island width and the third regime has $w_I >> w_k$. Realistically, the second regime (mode width = island width) is most relevant for present tokamaks ($w_k \sim \rho_s \sim 1 - 2\text{cm} \sim w_I$) and will be emphasized in the next section on applications. To motivate this regime, we begin by discussing the strongly turbulent or mixing length regime.

As with the shearless theory, we require the time independence of the one point equations and total energy. Unlike the local theory, Ohm's Law and continuity must be solved as an eigenmode problem. We

also use the equipartition of magnetic and internal energies, corresponding to a balance of magnetic field line stretching and back reaction of $\underset{\sim}{B} \cdot \underset{\sim}{\nabla} J$.

The one point equations are ($k_y w_k < 1$ with background energies equipartitioned):

$$\frac{\partial \psi_{\underset{\sim}{k}}}{\partial t} - (1 + \alpha)\alpha\alpha' \frac{(\omega_*^T)^2}{\nu_e} \psi_{\underset{\sim}{k}}$$

$$+ i\omega_*^T(1 + \alpha)\psi_{\underset{\sim}{k}} \qquad (2\text{-}112)$$

$$= -c_k^{(1)} \frac{\partial^2 J_{\underset{\sim}{k}}}{\partial x^2} + (\rho_s/a)^2 n_{\underset{\sim}{k}} ,$$

$$\frac{\partial n_{\underset{\sim}{k}}}{\partial t} = a_{\underset{\sim}{k}} \frac{\partial^2 n_{\underset{\sim}{k}}}{\partial x^2} - ik_{\parallel} J_{\underset{\sim}{k}} \qquad (2\text{-}113)$$

and

$$J_{\underset{\sim}{k}} = \frac{\partial^2 \psi_{\underset{\sim}{k}}}{\partial x^2} ,$$

where $c_{\underset{\sim}{k}}^{(1)}$ and $a_{\underset{\sim}{k}}$ are given by Equations (2-78) and (2-81).

In the strong turbulence case, where $R_s \gg 1$, the radial dependences are roughly,

$$\left|\frac{\partial J_{\underset{\sim}{k}}}{\partial x}\right| \sim \frac{J_{\underset{\sim}{k}}}{\Delta} \quad , \quad \left|\frac{\partial n_{\underset{\sim}{k}}}{\partial x}\right| \sim \frac{n_{\underset{\sim}{k}}}{\Delta}$$

and

$$\frac{\partial^2 \psi_{\underset{\sim}{k}}}{\partial x^2} \sim \frac{\Delta'_{\underset{\sim}{k}}}{\Delta} \psi_{\underset{\sim}{k}}$$

(Δ' remains a global constraint) where Δ is the "mixing length." To find Δ, we solve Ohm's Law and continuity as an eigenmode problem, with $\partial/\partial t \sim \gamma = 0$ for stationarity.

The spectrum energy equations in the case of $|\underset{\sim}{p}| \sim |\underset{\sim}{q}| >> |\underset{\sim}{k}|$ (small scale background limit), $R_l > 1$ (inertial-like range) with $\omega_*^T < \nu_e$ (instability), $w_k k_y < 1$ (radial scales much smaller than poloidal scales), and energy equipartition of small scale background (see Eqs. (2-92) and (2-93)) are:

$$\frac{\partial E^m_{\underset{\sim}{k}}}{\partial t} + (\rho_s/a)^2 \int dx\ ik\ (J^*_{\underset{\sim}{k}} n_{\underset{\sim}{k}} - n^*_{\underset{\sim}{k}} J_{\underset{\sim}{k}})$$

$$- 2\int dx \frac{(\omega_*^T)^2}{\nu_e} (1+\alpha)\alpha\alpha' E^m_{\underset{\sim}{k}}$$

$$= - \sum_{\underset{\sim}{p}+\underset{\sim}{q}=-\underset{\sim}{k}} (\rho_s/a)^2 \mathrm{Re}(L^{(2)}_{\underset{\sim}{k},\underset{\sim}{p},\underset{\sim}{q}}) q_y^2 (\psi_{\underset{\sim}{q}})^2 \left(\frac{\partial J_{\underset{\sim}{k}}}{\partial x}\right)^2 + \mathcal{T}^m \qquad (2\text{-}114)$$

$$\frac{\partial E^I_{\underset{\sim}{k}}}{\partial t} - (\rho_s/a)^2 \int dx\ ik\ (J^*_{\underset{\sim}{k}} n_{\underset{\sim}{k}} - n^*_{\underset{\sim}{k}} J_{\underset{\sim}{k}})$$

$$= -(\rho_s/a)^2 \sum_{\underset{\sim}{p}+\underset{\sim}{q}=-\underset{\sim}{k}} \frac{R_e(L^{(1)}_{\underset{\sim}{k},\underset{\sim}{r},\underset{\sim}{q}})}{(1 + (x_p/w_{\underset{\sim}{p}})^2)} \frac{|\Delta'_{\underset{\sim}{p}}|}{\pi w_{\underset{\sim}{p}}} \frac{k_y^2}{p_y^2}$$

$$(\psi_q)^2 \left(\frac{\partial n_k}{\partial x}\right)^2 + \mathcal{T}^I \qquad (2\text{-}115)$$

where

$$\mathcal{T}^m = (\rho_s/a)^2 \int dx \sum_{\underset{\sim}{p}+\underset{\sim}{q}=-\underset{\sim}{k}} \frac{R_e(L^{(1)}_{\underset{\sim}{k},\underset{\sim}{p},\underset{\sim}{q}}) q_y^2 |\Delta'_{\underset{\sim}{k}}|}{(1 + (x_k/w_k)^2)\pi w_{\underset{\sim}{k}}}$$

$$(\psi_{\underset{\sim}{q}})^2 \left(\frac{\partial n_{\underset{\sim}{p}}}{\partial x}\right)^2 , \qquad (2\text{-}116)$$

$$\mathcal{T}^I = (\rho_s/a)^2 \int dx \sum_{\underset{\sim}{p}+\underset{\sim}{q}=-\underset{\sim}{k}} R_e(L^{(1)}_{\underset{\sim}{k},\underset{\sim}{p},\underset{\sim}{q}}) q_y^2 (\psi_{\underset{\sim}{q}})^2 \left(\frac{\partial J_{\underset{\sim}{p}}}{\partial x}\right)^2 \qquad (2\text{-}117)$$

and

$$L^{(1)} = L^{(2)} \sim \frac{1}{\delta\gamma_{\underset{\sim}{k}}} .$$

The general solution for constant ψ is given by Furth, Rutherland and Selberg. Normalizing Eqs. (2-112) and (2-113) with

$$x = \left(\frac{c_{\underset{\sim}{k}} a_{\underset{\sim}{k}}}{k'_{\|}(\rho_s/a)^2}\right)^{1/6} u, \qquad (2\text{-}118)$$

density such that

$$N = \frac{\left(-\frac{c_{\underset{\sim}{k}} a_{\underset{\sim}{k}}}{ik'_{\parallel}(\rho_s/a)^2}\right)^{1/6} (ik_{\parallel}(\rho_s/a)^2)^{5/6} n_{\underset{\sim}{k}}}{\psi_{\underset{\sim}{k}}(x = 0)(-i\omega + i\omega_*^T(1 + \alpha) - \frac{\alpha\alpha'}{\nu_e}(\omega_*^T)^2(1 + \alpha))}, \tag{2-119}$$

and $R_l > 1$ (i.e., ignoring resistive dissipation), then the "dispersion relation" is

$$\Delta'_{\underset{\sim}{k}} \psi_{\underset{\sim}{k}}(x = 0) = \left(\frac{a_{\underset{\sim}{k}}}{c_{\underset{\sim}{k}}}\right) \frac{\psi_{\underset{\sim}{k}}(x = 0) S_0}{k'_{\parallel}(\rho_s/a)} \times \tag{2-120}$$

$$\int_{-\infty}^{\infty} \frac{du}{u} \frac{\partial^2 N}{\partial u^2},$$

where S_0 is given by

$$S_0 = -i\omega + i\omega_*^T(1 + \alpha) - \frac{\alpha\alpha'}{\nu_e}(\omega_*^T)^2(1 + \alpha). \tag{2-121}$$

From Furth, et al.,

$$\int_{-\infty}^{\infty} \frac{du}{u} \frac{\partial^2 N}{\partial u^2} = \pi. \tag{2-122}$$

A "natural" mixing length, Δ, is found from the x normalization:

$$\Delta = \left(\frac{c_{\underset{\sim}{k}} a_{\underset{\sim}{k}}}{k_{\parallel}'(\rho_s/a)^2} \right)^{1/6} \tag{2-123}$$

Noting that (mode width $= \Delta$)

$$c_{\underset{\sim}{k}} \cong a_{\underset{\sim}{k}} = \frac{\rho_s v_A}{\Delta} \left(\frac{\Delta_{\underset{\sim}{k}}'}{\Delta} \right)^{1/2} \frac{\delta B_r}{B_0} = \delta\gamma_{\underset{\sim}{k}}, \tag{2-124}$$

we find that:

$$\Delta^2 = \frac{1}{k_{\parallel}'} \frac{\delta B_r}{B_0}, \tag{2-125}$$

or the magnetic island width. Plugging Δ into Eq. (2-120) and using Eqs. (2-124) and (2-122) yields

$$\delta\gamma(w_{\underset{\sim}{k}} = \Delta) = \frac{\rho_s v_A}{\pi\Delta} \sqrt{\frac{\Delta_{\underset{\sim}{k}}'}{\Delta}} = \alpha\alpha' \frac{(\omega_*^T)^2}{\nu_e} (1 + \alpha) \tag{2-126}$$

and

$$\omega = (1 + \alpha)\omega_*^T.$$

Hence, the strong turbulence (mixing length) regime, as in shearless theory, has nonlinear eddy turnover time $\delta\gamma$ balancing linear growth, with a correlation length given by the island width. Writing in a dimensionless

form, Eq. (2-126) reduces to:

$$\frac{\delta B_r}{B_0} \sim \left(\frac{\alpha\alpha'}{\pi} (1+\alpha) \left(\frac{\beta_e}{2}\right)\left(\frac{\Omega_e}{\nu_e}\right)\left(\frac{\rho_e}{L_T}\right)^2 \right)^4 (k_y L_s)^3 \qquad (2\text{-}127)$$

The total energy is (from Eqs. (2-114) and (2-115):

$$\frac{\partial}{\partial t}\left(E^m_{\underset{\sim}{k}} + E^I_{\underset{\sim}{k}}\right) = 0 = \int dx \frac{(\omega^T_*)^2}{\nu_e} \alpha\alpha'(1$$

$$+ \alpha) \int dx \sum_{p+q=-k} (\rho_s/a)^2 R_e\left(L^{(2)}_{\underset{\sim}{k},\underset{\sim}{p},\underset{\sim}{q}}\right) q_y^2 (\psi_{\underset{\sim}{q}})^2 \left(\frac{\partial J_{\underset{\sim}{k}}}{\partial x}\right)^2$$

$$+ \mathcal{J}^m + \mathcal{J}^I \qquad (2\text{-}128)$$

$$- \int dx \sum_{\underset{\sim}{p}+\underset{\sim}{q}=-\underset{\sim}{k}} \frac{(\rho_s/a)^2 R_e\left(L^{(1)}_{\underset{\sim}{k},\underset{\sim}{p},\underset{\sim}{q}}\right)}{(1+(x_p/w_{\underset{\sim}{p}})^2)} \frac{k_y^2}{p_y^2} \frac{|\Delta'_{\underset{\sim}{p}}|}{\pi w_{\underset{\sim}{p}}} (\psi_{\underset{\sim}{q}})^2 \left(\frac{\partial n_{\underset{\sim}{k}}}{\partial x}\right)^2$$

Demanding stationarity of total energy, with radial scales going as Δ, and using the one-point dispersion relation (Eq. (2-126)), we find

$$E^I_{\underset{\sim}{k}} \sim \left(\frac{\mathcal{J}^m + \mathcal{J}^I}{\delta\gamma_k}\right)\Bigg|_{w_{\underset{\sim}{k}}=\Delta} . \qquad (2\text{-}129)$$

This result parallels the shearless result, with the incoherent emission coming from the damping of unstable large scale modes by small scale stable modes. The

damping of small scale stable modes is via the back-reaction of $\nabla_{\|} J$ on Ohm's Law and the subsequent transfer of energy to small scales can be viewed as the driving of the majority of unstable modes (peak in energy) to regions where they are stable, by the process of progressive current filamentation (Δ' coupling of non-linear terms).

The mixing length, Δ, can be equivalently found by imposing:

$$(1)\ \nabla_{\|} J = (\nabla_{\|})_0 J_{\underset{\sim}{k}} + \delta\nabla_{\|} J_{\underset{\sim}{k}} = 0 \qquad (2\text{-}130)$$

$$(2)\ \nabla_{\|} n_{\underset{\sim}{k}} = (\nabla_{\|})_0 n_{\underset{\sim}{k}} + \delta\nabla_{\|} n_{\underset{\sim}{k}} = 0. \qquad (2\text{-}131)$$

Implicit in the conditions (1) and (2) is the form of $\delta\gamma$, which results from equipartitioning at small scales and is not derivable in this simple mixing length theory. If we impose universal equipartition of magnetic and internal energy, then, along with condition (1) or (2) above,

$$\delta\gamma = \frac{\rho_s v_A}{\Delta} \left(\frac{\Delta'_k}{\Delta}\right)^{1/2},$$

and

$$\frac{\partial}{\partial t}\int d\underset{\sim}{x}\ \psi^2 = (\rho_s/a)^2 \int d\underset{\sim}{x}\psi(\nabla_\parallel)_0 n$$
$$+ 2\int d\underset{\sim}{x}\alpha\alpha'(1+\alpha)\frac{(\omega_*^T)^2}{\nu_e}\psi^2 = 0, \tag{2-132}$$

the magnetic fluctuation level, Eq. (2-127), is found. Although not consistent with the dynamical behavior of the spectrum energy equations, universal energy equipartitioning is reasonable when $k_y w_k \ll 1$.

Finally, when we are in the moderate turbulent regime when mode width equals island width, a simple fluctuation level follows:

$$\frac{\delta B_r}{B_0} \sim \frac{L_s}{L_T}\frac{\nu_e}{\Omega_e}\ . \tag{2-133}$$

This result corresponds to a self-excited regime and seems most natural. The only conditions necessary to obtain Eq. (2-133) are:

$$(1)\ \nabla_\parallel J = 0 \tag{2-134}$$

$$(2)\ \nabla_\parallel n = 0 \tag{2-135}$$

$$(3)\ \frac{\partial}{\partial x} \sim w_{\underset{\sim}{k}},\ x \sim w_{\underset{\sim}{k}}\ . \qquad (2\text{-}136)$$

We pay particular attention to this result in the next section, where the scalings and transport properties of Eq. (2-133) are examined.

2.7 Discussion

Having obtained magnetic fluctuation levels, we now compare our results with earlier attempts (2.7.1) and consider the effects on thermal (heat) transport near the edge (2.7.2).

Only a small number of authors[14,48,58,62,65] have attributed edge transport to microtearing. The most recent results are phenomenological in nature and will be discussed in 2.7.2, along with transport. Earlier theoretical results[14,58,62] are discussed below.

2.7.1 Previous Theory

All nonlinear theoretical models of microtearing have been quasi-linear, except for one. Although Samain[62] and Rebut[58] have indicated that their

results involve microturbulence, they concentrate on island topology and are, in reality, extending the results of Hazeltine,[29] Biskamp,[5] Rutherford[60] and Scott.[63] Rebut emphasizes the stochastic nature of chains of overlapping islands and their ergodic properties. He assumes magnetic island chains separated by stochastic magnetic field regions and discusses heat and particle flows through this fixed magnetic field structure. Microtearing is invoked because of its temperature gradient driven magnetic fluctuation. No self-consistent model of the nonlinear dynamics of microtearing is used. Most important, he presupposes the topology of magnetic island structure near the plasma edge, without discussion of the dynamical maintenance of this topology.

The model of Drake, et al.,[14] is in our opinion, the only self consistent attempt at a theory of microtearing turbulence. His model is kinetic, with shear retained only in the local theory. A "one point" multihelicity closure finds a saturation level for magnetic field. The saturation is hypothesized as being related to an "energy flow" from short to long wavelengths, due to electron motion along fluctuating field lines. Drake finds the fluctuation level:

$$\frac{\delta B}{B_0} \sim \frac{\rho_e}{L_T}$$

where ρ_e is the electron gyroradius. He relates the effects of magnetic fluctuations on temperature which in turn effects the time dependent thermal force. Hence, a nonlinear time dependent thermal force saturates the instability.

Drake's result can be criticized for a number of reasons. First, his nonlinear theory does not take into account the effects of radial eigenmode structure (i.e., shear and line bending). Basically, ignoring the radial structure corresponds to ignoring the effects of magnetic island topology. Second, a two point theory was not performed and hence any conclusion pertaining to energy (or mean square flux) transfer are not appropriate since incoherent mode coupling has been omitted. Although his direction of mean square flux cascade agrees with our result (for shearless theory) its source is not the $\nabla_\parallel J$ back-reaction, but corresponds to a weak turbulence effect (from $\omega - \omega'$ resonance). Third, effects of nonlinear broadening (Alfven effect on nonlinear interaction time) are not considered. Neither is there any discussion of energy

equipartitioning. Last, he does not include effects of driven magnetic fluctuations ($\psi_{k+k'}$ effects). A consistent one point theory would not conserve mean square flux, while Drake's does.

Although Rebut and Drake do not correctly describe microtearing turbulence, each makes certain important points. Rebut's inclusion of magnetic island topology effects emphasizes that shear (line bending) plays a role in the nonlinear as well as the linear theory. Drake's emphasis on employing a "self-consistent" statistical many mode turbulence theory, incorporating linear assumptions, is the best way to approach the problem of microtearing turbulence. Our result is therefore an improved hybrid of the positive features of Drake and Rebut.[14,58]

2.7.2 Transport

Recently, a number of experimental papers have appeared which attempt to relate magnetic fluctuations to global plasma confinement.[44,48,65] Most recently published is a paper by Ohyabu, et al.[48] where edge magnetic fluctuations are correlated with global L vs. H mode confinement. Observations are reported

from Doublet III consisting of low frequency (5-50 kHz) magnetic fluctuation measurements. The signals are incoherent (signals uncorrelated between probes at different spatial positions) and broadband. Changes in magnetic fluctuation level are observed in transitions from L (low) to H (high) confinement modes of operation. A model of microtearing modes is proposed, where the temperature threshold for linear stabilization corresponds to the L to H mode transition. The stabilization condition used is $\omega_*^T \sim \nu_e$. Consistent with mode numbers of unstable microtearing modes, a lower bound of $m \sim 8$ is found for magnetic fluctuations. Island widths are estimated to be about 2 cm. A comparison of the island width and distance between mode rational surfaces (1.3 cm) indicates overlapping of islands with enhanced thermal transport. Using a "Rechester-Rosenbluth"[59] thermal diffusivity, χ_e is calculated from

$$\left(\frac{\delta B}{B}\right)^2 \nu_e q R \qquad (2\text{-}137)$$

(we shall discuss the dubious nature of this form later). Finally, energy confinement times for L-mode

regimes are:

$$\tau_E \sim (P_{Heat})^{-1/2} I_p \qquad (2\text{-}138)$$

where P_{Heat} is the beam power (input power) and I_p is the plasma current. L-mode scaling is also independent of torroidal magnetic field (B_T). On the other hand, H-mode confinement time does not vary with input power and does not vary with electron density. Current scaling of H-mode τ_E is not clear but seems to increase with current. As with L-mode, no torroidal magnetic field dependence is found with the H-mode τ_E. Also note that the H-mode transition has thresholds in density and beam power.

For a number of reasons, the theoretical interpretation of Ohyabu is flawed. First, as emphasized in Section 2.2, in addition to the stabilizing trend which begins when $\omega_*^T > \nu_e$, the resistive damping, aided by shear, can stabilize the microtearing mode. Both mechanisms have an electron temperature threshold T_c, for which $T > T_c$ stabilizes the mode (note that there also is a temperature gradient threshold). Near the edge, where shear lengths can be small, strong

shear stabilization can occur (possibly connected to separatrixes). Second, the use of

$$\chi_e \sim \left(\frac{\delta B}{B}\right)^2 v_e q R$$

for a collisional edge plasma is inappropriate. Further, in general, this $\chi_\parallel$ should be $v_e D_m$ (where D_m is instability, mode dependent) in the collisionless regime. From Rechester and Rosenbluth,[59]

$$D_m = L_0 \left(\frac{\delta B_r}{B}\right)^2$$

(where L_0 is the parallel autocorrelation length of radial magnetic fluctuations) and $L_0 = \pi R$. This is not the χ_e of Ohaybu.[48] Therefore for a collisional plasma, the more appropriate χ_e is

$$\chi_e \sim \frac{v_e D_m}{L_0}\left(\frac{v_e}{\nu_e}\right)$$

or

$$\chi_e \sim \frac{v_e^2}{\nu_e}\left(\frac{\delta B}{B}\right)^2 . \qquad (2\text{-}139)$$

In light of the above misuse of parallel correlation lengths, we consider the thermal transport due to fluctuating radial magnetic field which in turn is generated by the saturated state of the microtearing mode. Radial magnetic fluctuations lead to the destruction of flux surfaces and enhanced radial thermal transport.[58] In a collisional plasma, the heat flux along the magnetic field is $q_{\parallel} = - \nabla_{\parallel} T$, which leads to an anomalous thermal diffusivity given by Eq. (3-139). Assuming island widths comparable to mode widths (moderate turbulence), we have from Eq. (2-133)

$$\chi_e \sim \left(\frac{L_s}{L_T}\right)^2 \left(\frac{\nu_e}{\Omega_e}\right) v_e^2. \qquad (2\text{-}140)$$

Simplifying with

$$q \sim \frac{B_0}{RI_p}$$

and

$$L_s = \frac{qR}{\hat{s}} \quad (\hat{s} = r \frac{dq}{dr}/q),$$

then χ_e scales as

$$\chi_e \sim \frac{n_0}{L_T^2} \hat{s}^{-2} I_p^{-2} T_e^{-1/2}, \tag{2-141}$$

or

$$\chi_e \sim \frac{n_0}{L_T^2} q^2 R^2 \hat{s}^{-2} B_0^{-2} T_e^{-1/2} .$$

Note that χ_e increases radially as a function of q (related to inverse current) and T_e. As a consequence of the observed temperature profile $T_e(r)/T_e(0)$ insensitivity to $T_e(0)$ and heating methods,[10,53,58] the concept of "profile consistency" has evolved (as discussed in the introduction). The dependences of χ_e derived here on L_T and T_e are consistent with this concept. Using the power balance

$$\frac{\chi_e n T_e}{L_T^2} = P_{Heat}, \tag{2-142}$$

where P_{Heat} is the power imparted to the electrons, then

$$L_T \sim q^{1/2} P_{Heat}^{-1/4} . \tag{2-143}$$

Thus, the temperature profile is maintained by the q profile (but not power of temperature), and, in this sense, is "self-consistent."

We now consider the case of an Ohmically heated tokamak, where

$$P_{Heat} \sim \eta I_p^2. \tag{2-144}$$

The electron thermal diffusivity then scales as

$$\chi_e \sim \frac{qR}{\hat{S}} \frac{I_p}{B_T} T_e^{-3/2}$$

$$\sim \hat{S}^{-1} T_e^{-3/2}. \tag{2-145}$$

Note the lack of B_T dependence and the stabilizing effect of shear ($\hat{S}^{-1}$). The scalings of temperature scale length, magnetic fluctuation level and energy confinement time are:

$$L_T \sim I_p^{-1} \hat{S}^{-1/2} n_o^{1/2} T_e^{1/2}$$

$$\sim Rq\beta_e^{1/2} \hat{S}^{-1/2}, \tag{2-146}$$

$$\frac{\delta B_r}{B_T} \sim \hat{s}^{-1/2} T_e^{-2} n_o^{1/2} \qquad (2\text{-}147)$$

and

$$\tau_E \sim a^2 \chi_e^{-1} \sim a^2 T_e^{3/2} \hat{s}. \qquad (2\text{-}148)$$

We emphasize that these scalings are for the plasma edge and should not be interpreted global scalings.

In a neutral beam heated tokamak, such as Doublet III, the power balance is

$$\frac{\chi_e n_o T_e}{L_T^2} = P_{Heat} \sim P_{Beam}. \qquad (2\text{-}149)$$

Considering microtearing modes responsible for the magnetic fluctuations, in the L-mode, we obtain (using Eq. (2-146))

$$\chi_e \sim I_p^{-1} P_{Heat}^{1/2} \hat{s}^{-1} T_e^{-3/4}$$

$$\sim q R B_T^{-1} P_{Heat}^{1/2} \hat{s}^{-1} T_e^{-3/4}. \qquad (2\text{-}147)$$

The scalings of L_T, δB, and τ_E are:

$$L_T \sim n_o^{1/2} I_p^{-1/2} P_{Heat}^{-1/4} \hat{S}^{-1/2} T_e^{1/8} \quad , \tag{2-150}$$

$$\frac{\delta B}{B_T} \sim I_p^{-1/2} P_{Heat}^{1/4} \hat{S}^{-1} n_o^{1/2} T_e^{-13/8} \quad , \tag{2-151}$$

and

$$\tau_E \sim a^2 I_p P_{Heat}^{-1/2} \hat{S}^{1} T_e^{3/4} . \tag{2-152}$$

Comparing Eq. (2-138) with (2-150), we see that some of the dependences (I_p, P_{Heat}) of Ohyabu are reproduced, but the strong T_e dependence suggests that our edge confinement time does not quite compare favorably to Ohyabu.[48] This is reasonable since our result is not a global confinement time, where core plasma effects must be considered. A better comparison is the magnetic fluctuation level (Eq. (2-133)). For the edge of Doublet III[48] in L-mode operation, R ~ 1.44 m, B_T ~ 1 T, T_e ~ 200 eV, q~2.6, $\hat{S}$ ~ 2, $n_o \sim 1 \times 10^{13}$ cm^{-3}, and L_T ~ 5 cm, and the resulting magnetic fluctuation level is $\delta B/B_T \sim 1.5 \times 10^{-4}$ (and edge χ_e is 7×10^4 cm^2/s). Note that this level of $\delta B/B$ agrees with the 2×10^{-4} level of Doublet III.

As a possible mechanism of L to H mode transition, consider the stability threshold of the microtearing mode. As in ASDEX,[71] and electron temperature threshold exists, i.e., when the electron temperature increases, the microtearing mode is stabilized. Another possible stabilization mechanism is strong shear (discussed in Section 2.2). Hence, in regions where strong shear overlaps with the electron temperature gradient (free energy source) the magnetic fluctuation level should go down (corresponding to a transition from L to H mode). This idea is similar to the discussion in Malacarne, et al.[44] for JET, where the physics of x-points (separatrixes) is important. This connection to shear is reflected in the $\hat{s}^{-1}$ dependence of the magnetic fluctuation level of the saturated microtearing mode.

2.8 Conclusion

The nonlinear dynamics of microtearing turbulence is studied analytically with the goal of understanding the broadband magnetic fluctuations near a tokamak edge. These fluctuations are electron temperature gradient driven and hence provide a mechanism for

the rigidity of the electron temperature profile.[10,53,58] Recent observations[44,48] of L to H mode transition correlated with edge magnetic fluctuations suggest that the transition might be due to the stabilization of the microtearing mode. For both of these reasons, microtearing turbulence is a reasonable candidate for the explanation of the anomalous electron thermal energy loss near the edge.

Here, we have studied microtearing turbulence using a one- and two-point renormalized (statistical) turbulence theory. A stationary state is found and magnetic energy spectra are derived for this state. The analytical predictions are then applied to the problem of edge magnetic transport. The principal results are (repeating from the introduction):

1. One-point and two-point equations are derived for the microtearing mode in a multihelicity environment for uniform and sheared magnetic field, using an iterative closure scheme.
2. The dominant anomalous effect in Ohm's Law is a "hyperresistivity" due to the back reaction of current compression on diagmagnetic convection in Ohm's Law.

3. At small scales, magnetic and internal energy equipartition.
4. At large scales, the energies are in general not equipartitioned.
5. Evidence, through equilibrium statistical mechanics, is found for energy transfer to small scales and mean square flux transfer to large scales.
6. High m stable modes saturate the low m (~10) unstable modes, with energy going to small scales.
7. The back reaction of $\nabla_{\parallel} J$ (current compression) on Ohm's Law saturates the unstable micro-tearing mode. This effect takes the form of a hyperresistivity.
8. By requiring that the total energy be time independent, the saturation level of the magnetic field in the case of a uniform equilibrium magnetic field (B_0) is:

$$\frac{\delta B}{B_0} \sim (1 + \alpha)\alpha\alpha' \left(\frac{\beta_e}{2}\right)^{1/2} \frac{\Omega_e}{\nu_e}\left(\frac{\rho_e}{L_T}\right)^2 .$$

9. In the moderate or strong turbulence regime, a mixing length theory is found and

subsequent magnetic field saturation levels are derived.

10. For the case of moderate turbulence (mode width equals island width), the saturation level is

$$\frac{\delta B_r}{B_T} \sim \frac{L_s}{L_T} \frac{\nu_e}{\Omega_e}$$

This regime is most relevant for present-day tokamaks. The corresponding thermal diffusivity (appropriate to the plasma edge) is

$$\chi_e \sim \frac{V_e^2}{\nu_e}\left(\frac{\delta B_r}{B}\right)^2$$

and scales as $S^{-2} L_T^{-2} n_o I_p^{-2} T_e^{-1/2}$. The temperature scale length scales as $L_T \sim q^{1/2} P_{Heat}^{-1/4} T_e^{1/8}$. Thus, L_T is tied to the q profile and not to the input power. These results are consistent with the concept of "profile consistency,"[10,53,58] since χ_e increases radically, toward the plasma edge.

11. For an Ohmically maintained temperature profile, the confinement time is:

$$\tau_E \sim \frac{a^2}{\chi_e} \sim a^2 S T_e^{3/2} .$$

12. For neutral beam heated plasma, the L-mode confinement time is:

$$\tau_E \sim a^2 T_e^{3/4} S^{1/2} P_{Heat}^{-1/2} I_p \quad .$$

This result is in partial agreement with the scaling of Ohyabu[48] τ_E. The magnetic fluctuation level, for Doublet III parameters, agrees with Ohyabu's measurements.

13. Strong shear and higher electron temperatures stabilize the microtearing mode, indicating possible mechanisms for transition from L to H mode.

Finally, we discuss possible future work. First, the nonlinear theory should be extended to include both temperature and electrostatic fluctuations for completeness, and to find the effects on particle transport. Second, additional effects, such as trapped particles, can be invoked to increase the robustness of the instability. Third, the nonlinear theory should be checked against a numerical solution using a 3-D mode,

In addition to being a check of the analytic theory, this code is an extension of the 2-D equations solved numerically in Chapter III. A curious question is whether intermittent behavior found in the next chapter is found in 3-D.

C H A P T E R I I I

A COMPUTATIONAL STUDY OF CONSTRAINED RELAXATION OF 2-D MICROTEARING

3.1 Introduction

The phenomenon of spatially "patchy" or temporally "spikey" flows in turbulence has been broadly categorized under the class of intermittency and is a breakdown of statistical homogeneity of turbulent flow, i.e., deviations from gaussianity. Gaussian flow is characterized by large lower order moments (average, standard deviation), but has negligible higher order moments (skewness, kurtosis, etc.). Experimental studies, since 1947,[4] have indicated nonnegligible third order (skewness) and fourth order (kurtosis or flatness) moments of the fluid velocity gradient.

Deviations from gaussianity are important because virtually all analytic theories of turbulence are quasi-gaussian (perturbations about gaussian flows). Nongaussianity breaks down the basic statistical assumption of turbulence as "space filling."[17] Lack of spacial homogeneity raises the question of the existence of spatially coherent structure in the flow, i.e., shocks (1-D) and vorticies (2-D).

McWilliams,[45] in a numerical simulation of 2-D Navier Stokes fluids, found coherent structures or

vortices appearing out of seemingly random initial conditions. These vortices were long-lived (compared to an eddy turnover time), and only ceased to exist when they interacted with other vorticies. The stronger vortex would "swallow" the weaker vortex, yet the remaining vortex did not gain in amplitude. As a quantitative measure of this "spatial intermittency," McWilliams calculated the spatial fourth moment (kurtosis) of vorticity and graphed it as a function of time. Kurtosis of vorticity is defined as:

$$\langle(\delta\omega)^4\rangle/(\langle(\delta\omega)^2\rangle)^2$$

where $\langle\ \rangle$ is a spatial average, ω is the vorticity, and $\delta\omega = \omega - \langle\omega\rangle$. Physically, the kurtosis of a vorticity is the ratio of the distance between vorticies over their width. McWilliams found high values of kurtosis (much greater than 3), indicating a patchy pattern associated with "spatial intermittency" and possible deviations from gaussianity.

Further, these structures were characterized by a positive value of strain minus enstrophy, i.e.,

$$Q = -2 \text{ trace}((\underset{\sim}{\nabla}\underset{\sim}{v})^2) = \omega^2 - S^2. \qquad (3\text{-}1)$$

We see that vorticity (ω) is the antisymmetric piece of $\underset{\sim}{\nabla}\underset{\sim}{v}$, while S (strain) is the symmetric piece. When $Q > 0$, then enstrophy dominates strain and vortices result. For $Q < 0$, vortices are sheared apart, i.e., they do not persist. Weiss[72] showed that Q has dynamical significance, with $Q < 0$ corresponding to cascading turbulence (i.e., growing vorticity gradient). $Q > 0$ corresponded to oscillatory behavior of vorticity gradient. McWilliams, via contour plots, confirmed Weiss's theoretical results and further showed that the regions of strongest cascading (most positive Q) occur just outside the isolated vortices.

An additional (traditional) sign of intermittency has been spectra steeper than explained theoretically.[37] In 2-D Navier-Stokes fluids, energy spectra steeper than k^{-3}, have been attributed to intermittency.[37,45] Although McWilliams seemed to observe steeper spectra, other simulations do not see this.[7] Recently,[3,30] energy spectra has been argued not to be indicative of coherent structures. Instead, phase information, lost in ensemble averaging, is important to the analysis of coherent structures in flows.

By imposing differing spectral falloffs (k^{-2}, k^{-3}, etc.), but keeping phase information on images of structures, Armi[3] showed that spectral shape is relatively unimportant. Present closure theories do not account for the lost phase information (due to ensemble averaging). Hence, spectra can not be a reliable measure of intermittency.

With 2-D Navier Stokes fluids indicating intermittent behavior, a natural question is whether MHD or similar systems show this behavior. Magnetohydrodynamics (MHD) is the extension of Navier-Stokes fluids to conducting fluids, i.e., coupling to magnetic fields. Von Neuman[70] sought MHD as an alternative form of turbulence, with resistivity acting as viscosity and "magnetic eddies" giving rise to turbulent motion.

The analogy of Navier-Stokes fluids with MHD fluids has been discussed recently in a paper by Moffatt.[46] He considers an infinitely conducting, but viscous MHD fluid as a vehicle for proving that analytic 3-D initial conditions of Navier Stokes fluids can lead to nonanalytic final conditions, i.e., singularities in fluid flow. This "constrained relaxation" conserves magnetic helicity and hence bounds the

magnetic energy from above. (Helicity is a measure of the degree of linkage of magnetic field lines.) Moffatt postulates that the final state is "force free," i.e., the $\underset{\sim}{J} \times \underset{\sim}{B}$ force is zero such that $\underset{\sim}{J} = \alpha \underset{\sim}{B}$, where J is the current and B is the magnetic field. A spatially constant α region is postulated to be "ergodic," while spacially dependent α corresponds to "current sheets" or singularities. Hence, the magnetic field in the final state has regions of ergodicity interspersed with current sheets.

By examination of McWilliams[45] and Moffatt's[46] papers, a model problem is suggested. Could the constrained relaxation of 2-D MHD (incompressible), whose equations (without resistivity) are:

$$\frac{\partial \underset{\sim}{v}}{\partial t} + \underset{\sim}{v} \cdot \underset{\sim}{\nabla} \underset{\sim}{v} = -\underset{\sim}{\nabla} p + \underset{\sim}{J} \times \underset{\sim}{B} + \mu \nabla_i^2 \underset{\sim}{v}, \tag{3-2}$$

$$\frac{\partial \underset{\sim}{B}}{\partial t} = \underset{\sim}{\nabla} \times \underset{\sim}{v} \times \underset{\sim}{B}, \tag{3-3}$$

$$J = \underset{\sim}{\nabla} \times \underset{\sim}{B}, \quad \underset{\sim}{\nabla} \cdot \underset{\sim}{v} = 0,$$

and

$$\underset{\sim}{\nabla} \cdot \underset{\sim}{B} = 0,$$

show intermittent behavior? Because of incompressibility and two dimensionality, the magnetic field ($\underset{\sim}{B}$) can be written in terms of the vector potential (ψ) such that $\underset{\sim}{B} = \underset{\sim}{\nabla} \times \psi\hat{z}$ (z is the ignorable coordinate) and v (fluid velocity) is usually expressed in terms of stream function (ϕ) such that $v = \underset{\sim}{\nabla}\phi \times \hat{z}$. We see that the constraint is the conservation of mean square flux or

$$\frac{\partial}{\partial t} \int d\underset{\sim}{x}(\psi)^2 = 0.$$

Further, by replacing magnetic field with velocity $\underset{\sim}{v}$ in Equation (3-3), we see that current is analogous to vorticity and magnetic field is analogous to fluid velocity. This suggests that coherent structures might appear in current, analogous to vortices found by McWilliams.[45]

Numerical simulations[18,51] have hinted at intermittent behavior in 2-D MHD. Current sheet formation has been observed for low mode number initial conditions (which in general do not simulate strongly turbulent flows). Frisch, et al.[18] attributes this sheet formation to the alignment of $\underset{\sim}{\nabla}\Psi$ and $\underset{\sim}{\nabla}J$ (or the force free condition of $J = \alpha\psi$) such that $\underset{\sim}{\nabla}\Psi \times \hat{z} \cdot \underset{\sim}{\nabla}J$ is

$$= (\rho_s/a)^2 \int dx \sum_{\underset{\sim}{p}+\underset{\sim}{q}=-\underset{\sim}{k}} \left\{ \left(n^*_{\underset{\sim}{k}} i k_y \frac{\partial \psi_{-\underset{\sim}{q}}}{\partial x} - i q_y \psi_{-\underset{\sim}{q}} \frac{\partial n^*_{\underset{\sim}{k}}}{\partial x} \right) J^{(2)}_{\underset{\sim}{k}+\underset{\sim}{q}} + \left(\frac{\partial n^*_{\underset{\sim}{k}}}{\partial x} i q_y J_{-\underset{\sim}{q}} - \frac{\partial J_{-\underset{\sim}{q}}}{\partial x} i k_y n^*_{\underset{\sim}{k}} \right) \psi^{(2)}_{\underset{\sim}{k}+\underset{\sim}{q}} + \left(\frac{\partial J_{-\underset{\sim}{p}}}{\partial x} i q_y \psi_{-\underset{\sim}{q}} - \frac{\partial \psi_{-\underset{\sim}{q}}}{\partial x} i p_y J_{-\underset{\sim}{q}} \right) n^{(2)}_{\underset{\sim}{p}+\underset{\sim}{q}} + \text{c.c.} \right\}, \tag{2-89}$$

where

$$E^I_{\underset{\sim}{k}} = \frac{1}{2} (\rho_s/a)^2 (n_k)^2.$$

As with mean square flux, nonlocality can alter the relative magnitude of different terms. The addition of linear line bending ($k_\parallel$) damps magnetic energy linearly (when the mode is unstable) such that magnetic energy is converted into internal energy, i.e.,

$$\frac{\partial E^m_{\underset{\sim}{k}}}{\partial t} + \ldots = -2(\rho_s/a)^2 \int dx \frac{k_\parallel^2 (J_{\underset{\sim}{k}})^2 (\mathrm{Im}(\omega_{\underset{\sim}{k}}) + \delta\gamma_{\underset{\sim}{k}})}{|\omega_{\underset{\sim}{k}} + i\delta\gamma_{\underset{\sim}{k}}|^2}$$

$$= - \frac{\partial E^I_{\underset{\sim}{k}}}{\partial t} + \ldots$$

Thus, line bending conserves total energy. As with mean

minimized. Note that no intermittency diagnostics, such as kurtosis, were reported in any of these simulations.

On the other hand, we have a model problem in the 2-D uniform electron temperature, microtearing model. This model is very similar to 2-D MHD with fluid velocity replaced by diamagnetic velocity

$$\underset{\sim}{v}_D = \underset{\sim}{\nabla} \times n\hat{z} \tag{3-4}$$

(where n is the fluctuating electron density) and velocity evolution replaced by

$$\frac{\partial \underset{\sim}{v}_D}{\partial t} = \underset{\sim}{\nabla} \times (\underset{\sim}{J} \times \underset{\sim}{B}) + \nu_2 \nabla_1^2 \underset{\sim}{v}_D, \tag{3-5}$$

i.e., electron continuity. Note that the convective nonlinearity, $\underset{\sim}{v} \cdot \underset{\sim}{\nabla} v$, is absent, thus reducing computation time, ν_2 is a cross field viscosity (discussed in next section).

The computational study of the relaxation of 2-D microtearing is motivated by the results of McWilliams'[45] coherent structures and Moffatt's[46] constrained relaxation. Further, studies of nongaussian behavior

of the 2-D microtearing equations is the first step toward understanding the breakdown of the quasi-gaussian closure used in Chapter II.

To this end, we present preliminary results of a computational simulation of 2-D microtearing with a uniform temperature profile.

The principal results are:

(1) For the viscosity dominated system (viscosity much greater than resistivity), current filaments are found to appear out of initially random conditions, analogous to the vortices of McWilliams.

(2) Large values of kurtosis for current indicate a kind of spatial "intermittency."

(3) The filaments are long lived and force free ($J = \alpha\psi$). α is nonconstant at filaments whose lifetime is the length of the code run.

(4) Filaments of like sign tend to attract (i.e., attracting current rods) and merge similar to McWilliams.

(5) The quantity $Q = -2$ trace $(\nabla \underset{\sim}{B})$, the difference between current squared and the magnitude of "shear stress" on the magnetic field, is

correlated with the long-lived filament. No theoretical interpretation is proposed, though.

(6) A transfer of mean square flux to large scales is tied to the appearance of the current filaments.

(7) Assuming that the current field is composed of cylindrical current rods, we find that the magnetic energy goes as k^{-4}. This result is compared with the simulation spectra. No evidence of steepening is found.

(8) Preliminary comparisons[68] with a quasi-gaussian closure theory are made.

This chapter is organized as follows. The next section introduces the basic equations of microtearing followed by a section discussing the numerical method of solution and diagnostics. The fourth section presents the results of the numerical solution followed by a discussion of the spectra, comparison with closure, and a conclusion.

3.2 Basic Model

The model of two dimensional microtearing in a uniform magnetic field (self filamentation) is outlined in the second section of Chapter II (Section 2.2).

Assuming a uniform electron temperature profile and adding cross field transport, the model equations for microtearing relaxation are Ohm's Law, electron continuity, and Ampere's Law, which are:

$$\frac{\partial \psi}{\partial t} + \underset{\sim}{v}_D \cdot \underset{\sim}{\nabla}\psi = \eta J, \tag{3-6}$$

$$\frac{\partial n}{\partial t} + \nabla_{\parallel} J = \nu_2 \nabla_{\perp}^2 n, \tag{3-7}$$

and

$$J = \nabla_{\perp}^2 \psi, \tag{3-8}$$

where

$$\underset{\sim}{v}_D = (\rho_s/a)^2 \underset{\sim}{\nabla} n \times \hat{z},$$

$$\nabla_{\parallel} = \underset{\sim}{\nabla}\psi \times \hat{z} \cdot \underset{\sim}{\nabla},$$

$$\nabla_{\perp}^2 = \frac{\partial^2}{\partial x^2} + \frac{\partial^2}{\partial y^2} \quad ,$$

ψ is the parallel vector potential, n is the electron density, and J is the current. η and ν_2 are collisional

resistivity and cross field particle diffusivity, respectively. From Braginskii,[8] we find that

$$\nu_2 \nabla_\perp^2 n = -\rho_e \nu_e \underset{\sim}{\nabla} \cdot \; n_0 \frac{\underset{\sim}{\nabla} n}{n_0} \tag{3-9}$$

and hence

$$\eta/\nu_2 \sim \frac{c^2}{\omega_{pe}^2 \rho_e^2} \cdot$$

In this chapter, $\eta \ll \nu_2$, i.e., where the collisionless skin depth is much smaller than electron gyroradius. Eqs. (3-6), (3-7) and (3-8) are similar to those of 2-D MHD (as discussed in Section 3.1). If we replace diamagnetic flux convection with $\underset{\sim}{E} \times \underset{\sim}{B}$ fluid convection in Ohm's Law, then we obtain Ohm's Law for 2-D MHD. The equation for vorticity, ω, in 2-D MHD is

$$\frac{\partial \omega}{\partial t} + \underset{\sim}{v} \cdot \underset{\sim}{\nabla} \omega = \nabla_\parallel J + \nu \nabla_\perp^2 \omega, \tag{3-10}$$

where $\omega = \underset{\sim}{\nabla} \times \underset{\sim}{v}$, and $\nabla_\parallel J$ is the coupling to the magnetic field through the J × B force. Note that continuity (Eq. (3-7)) is related to vorticity evolution with $\omega \rightarrow -n$ and $v \rightarrow v_D$. Thus, density is not convected

by diamagnetic drifts since $\underset{\sim}{v}_D \cdot \underset{\sim}{\nabla} n = 0$. Roughly, we see that vorticity dynamics is replaced by electron density dynamics when comparing 2-D MHD and microtearing.

As found in Section 2.2, the quadratic quantities of mean square flux (ψ^2), total energy

$$\frac{1}{2}(\nabla_\perp \psi)^2 + \frac{1}{2}(\rho_s/a)^2 n^2 ,$$

and cross helicity ($n\psi$) are conserved in the absence of dissipation (ν_2 and η). The conservation laws are, respectively:

$$\frac{1}{2}\frac{\partial}{\partial t}\int dxdy\psi^2 = -\eta \int dxdy(\nabla_\perp \psi)^2, \qquad (3\text{-}11)$$

$$\frac{1}{2}\frac{\partial}{\partial t}\int dxdy((\nabla_\perp \psi)^2 + (\rho_s/a)^2 n^2)$$

$$= -\eta \int dxdy J^2 - \nu_2(\rho_s/a)^2 \int dxdy(\nabla_\perp n)^2 \qquad (3\text{-}12)$$

and

$$\frac{1}{2}\frac{\partial}{\partial t}\int dxdyn\psi = -(\eta + \nu_2) \int dxdy\ \underset{\sim}{B} \cdot \underset{\sim}{v}_D, \qquad (3\text{-}13)$$

where $\underset{\sim}{B} = \underset{\sim}{\nabla}\Psi \times \hat{z}$. When $\eta/\nu_2 << 1$, only mean square flux is conserved, thus flux is frozen into the diamagnetic fluid. We call this case "constrained relaxation" because although density fluctuations (and total energy) are relaxed visciously, the area average of mean square flux constrained to be constant (on the other hand, no such constrained problem exists for $\eta \sim \nu_2$ or $\eta >> \nu_2$).

3.3 Numerical Preliminaries

Eqs. (3-6), (307), and (3-8) are solved as an initial value problem in a doubly periodic domain of width 2π. The model is investigated numerically using a pseudospectral (Fourier expansion) code. By pseudospectral,[49,52] we mean that all derivatives are performed in wavenumber (k) space and all convolutions (i.e., nonlinearities) are performed in configuration space thereby saving N^2 - N log N operations over a simple spectral code. Characteristic of this method are "aliasing errors,"[49,52] which result from grid points not distinguishing between wavenumber k and its "aliases" $k \pm mN$, where $|k| < N/2$ and m is a nonzero integer. If a_k is the continuous Fourier transform of a

function and b_k is the discrete transform, then

$$b_k - a_k = \sum_{\substack{m \\ m \neq 0}} a_{mN+k}, \tag{3-4}$$

where the term on the right hand side is the "aliasing term." When performing convolutions, this "aliasing term" can lead to "aliasing instabilities."[54] By truncating the upper 2/3 of wavenumbers, such that $|k| > N/3$, then no aliasing errors result.[49,52] We thus truncate in a square, such that $|k_x| < N/3$ and $|k_y| < N/3$.

The method of time stepping employed is the second order Runge-Kutte method:[2,11]

$$y^{m+\frac{1}{2}} = y^m + \frac{\Delta t}{2} f(y^m) \tag{3-15}$$

$$y^{m+1} = y^m + \Delta t \; f(y^{m+\frac{1}{2}}) \tag{3-16}$$

where

$$\frac{\partial y}{\partial t} = f(y)$$

is the equation being solved, Δt is the time step, and m is the time index. We use a variable time step, such that Δt is tied to the nonlinear interaction time, or "eddy turnover time." Quantitatively,

$$(\Delta t)^{-1} > \text{Max}(k_{max}^2 (E^m)^{1/2}, k_{max}^2 (E^I)^{1/2}) \qquad (3\text{-}17)$$

where

$$E^m = \sum_{k=1}^{N} k^2 \psi_k^2,$$

and

$$E^I = \sum_{k=1}^{N} (\rho_s/a)^2 n_k^2.$$

Here, ψ_k and n_k are the spectral components of flux and density, respectively, N is the number of grid points, and k_{max} is the maximum wavenumber. This modified Euler method is widely used in nonlinear simulations.[11,21] Stability is discussed in a paper by Dahlburg, et al.,[11] using a Von Neuman stability analysis. In our case, the equation

$$\frac{\partial \psi}{\partial t} + v_0 \frac{\partial \psi}{\partial x} = 0$$

or advection equation is weakly unstable. The e-folding time, t_E, for the numerical instability is given by:

$$t_E \approx \frac{8}{(kv_0)^4(\Delta t)^3} \qquad (3\text{-}18)$$

where k is spacial scale length. By requiring

$$\Delta t = \frac{\delta}{kv_0} ,$$

where $\delta < 1$, then none of the runs (times the order of 100 Alfven times) discussed in this work, show instability, provided the run time is less than

$$\frac{8\delta^{-3}}{(kv_0)^{-1}} .$$

Typically, for our runs, this time (t_E) is the order 300 Alfven times (with $\delta \sim .3$, $kv_0 \sim \tau_A^{-1}$), or $8\delta^{-3}$ large eddy turnover times $(kv_0)^{-1}$. The nonlinear equipartitioning time is

$$\tau_{EP} \sim \frac{\tau_A}{k^2(\rho_s/a)(E^m)^{1/2}} \qquad (3\text{-}19)$$

which is typically 10 times smaller than the large scale diamagnetic eddy turnover time. Hence, the advective instability e-folding time corresponds to about 30 large scale eddy turnover time, and about 300 equipartitioning times.

With the addition of resistivity, the advective instability can be stabilized, provided that (from Von Neuman stability analysis):[55]

$$GG^* < 1, \qquad (3\text{-}20)$$

where

$$GG^* = 1 - 2\Delta t\eta k^2 + 2(\Delta t\eta k^2)^2$$

$$- (\Delta t)^3(v_0^2\eta k^4 + \eta k^6)$$

$$+ \frac{1}{4}(\Delta t)^4((kv_0)^2 + \eta^3 k^4)^2.$$

Using

$$\Delta t \sim \frac{\delta}{kv_0} ,$$

we find that for numerical stability,

$$\frac{2\delta}{R} + \frac{R\delta^3}{4} < 2 + \delta^2 \qquad (3\text{-}21)$$

where

$$R = \frac{kv_0}{\eta k^2} .$$

In our code, typically R ~ 10-100 and δ = .3 and thus Eq. (3-20) is easily satisfied.

Unfortunately, our runs have $\delta \ll \nu_2$, which does not stabilize the advective instability. With finite ν_2, the additional condition of

$$\Delta t < \frac{2}{\nu_2 k^2}$$

must be satisfied for continuity to be numerically stable. Using

$$R \sim \frac{kv_0}{\nu_2 k^2},$$

then for stability $\delta < 2R$, which is easily satisfied (our runs have $R \sim 10$). In conclusion, with the eddy turnover time always greater than Δt, then the time integration scheme (Eqs. (3-15), (3-16)) is numerically stable, up to a e-folding time of the advective instability.

The initial condition is the same as McWilliams,[45] with a gaussian random realization (random phase) for each Fourier component of ψ. The magnetic energy spectral component, E_k^m is proportional to

$$\frac{k}{k^4 + 6^4} \qquad (3\text{-}22)$$

and the internal energy spectral component (E_k^I) is given such that the energies are equipartitioned. A point crucial to the results of McWilliams (and of this work) is that the initial condition be broadband in k, as opposed to a low mode number "Taylor Green" vortex type initial condition.[18] These initial conditions (spectra) are plotted in Figures 3.1 and 3.2.

Throughout the runs, the Reynold's numbers were between 10 and 100. Our definition of Reynold's number is

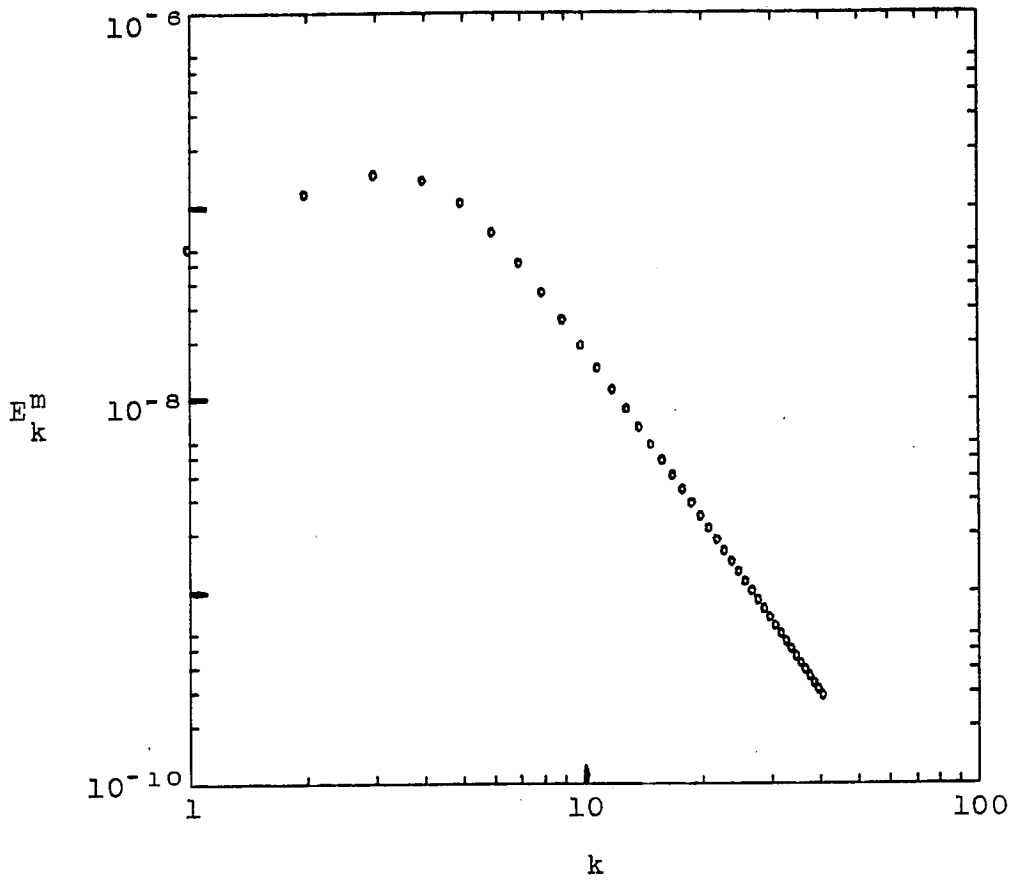

FIGURE 3.1. Spectrum of magnetic energy at t = 0.

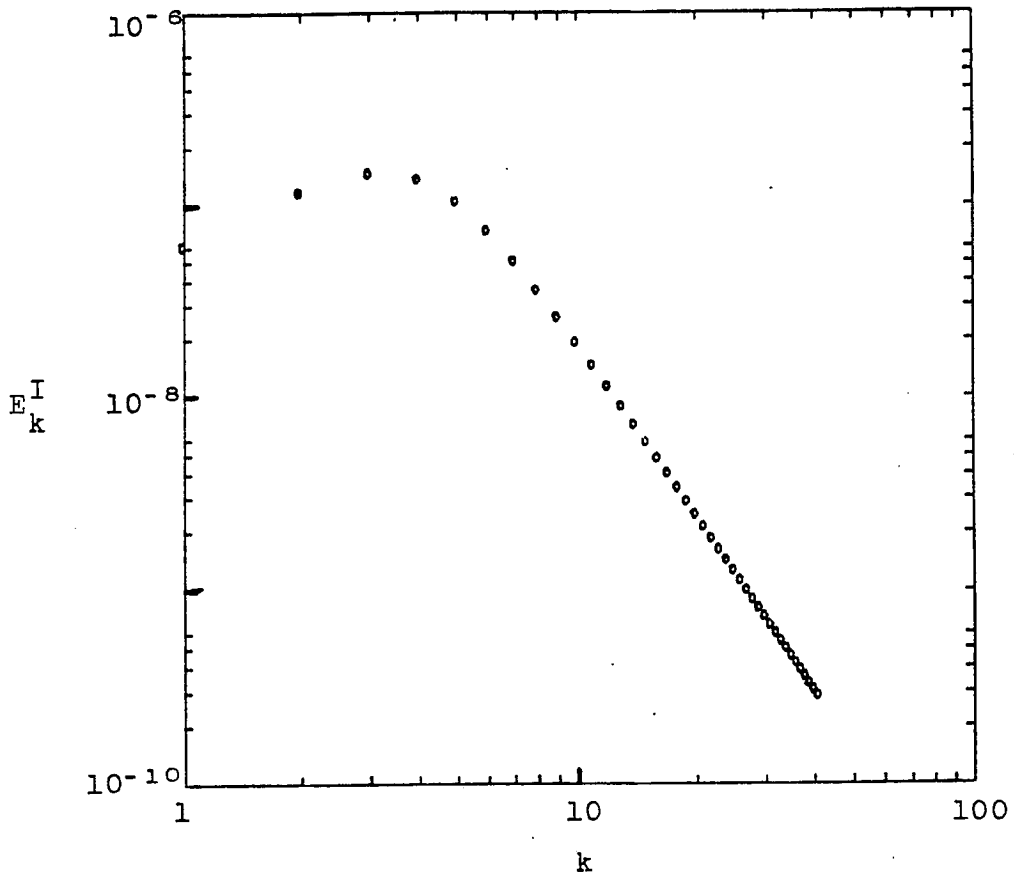

FIGURE 3.2. Spectrum of internal energy at t = 0

$$R = \int dx dy \, \frac{\nabla_{\parallel} J}{\nu_2 \nabla_{\perp}^2 n} \, , \tag{3-23}$$

i.e., the ratio of nonlinear to linear terms in the continuity equation. Roughly,

$$R \sim \frac{E^m(\rho_s/a)}{2\pi \nu_2 (E^I)^{1/2}} \, . \tag{3-24}$$

Physically, $R \sim R_1 R_2$, where R_1 is the ratio of magnetic to internal energy and

$$R_2 = \frac{k v_D}{k \nu_2 (\rho_s/a)}$$

where $v_D \cong (\rho_s/a)^2 kn$. R_1 is the inverse ratio of the time for a diamagnetic eddy to turnover on a radius k^{-1} and the viscious damping time. If we define

$$R_3 = \frac{k^2 (E^m)^{1/2}}{\nu k^2} (\rho_s/a) \, ,$$

then alternatively,

$$R \sim R_3 \left(\frac{E^m}{E^I} \right)^{1/2} = R_3 R_1^{1/2} .$$

R_3 is the ratio of the viscious damping time to an "Alfven time."[35]

Runs of $k_{max} \sim 11, 22, 44$ (dealiased) with $\eta >> \nu$ and $\eta << \nu$ have been performed. The main results of this chapter are reported for the highest resolution and largest Reynold's number runs, such that $k_{max} = 44$, $(\rho_s/a)^2 = 1$, $\eta = 0$, and $\nu_2 = .001$.

The diagnostics used in our code are briefly discussed below. First, we graph spatially averaged quantities as a function of time every 40 time steps. These time history plots are broken into three pieces corresponding to three sequential (in time) runs (Figure 3.3 is an example of this diagnostic). We graph magnetic energy and internal energy, defined, respectively, as

$$E^m(t) = \frac{\int dx\,dy(-J(x,y)\psi(x,y))}{(2\pi)^2}$$

$$= \langle -J\psi \rangle$$

and

$$E^I(t) = \langle (\rho_s/a)^2 (n(x,y))^2 \rangle .$$

The integral is the discrete sum over each spatial gridpoint. Other time history diagnostics are mean square flux,

$$\mathcal{A}(t) = \langle(\psi(x,y))^2\rangle$$

and kurtosis of current,

$$\mathcal{K}(J) = \frac{\langle(J - \langle J\rangle)^4\rangle}{\langle(J - \langle j\rangle)^2\rangle^2} .$$

Mean square flux is conserved throughout the computer run and, in addition to being a constraint, provides a test of the numerics. In our case, mean square flux is conserved up to 1 percent (and hence is not reported in this work). Kurtosis is motivated by the analogy of vorticity in 2-D Navier Stokes flow with current in 2-D MHD (as discussed in the introduction). High values of kurtosis (much greater than 3) could indicate spatially intermittent current flow. The second type of diagnostic is graphs of spectra. We graph the spectral components of magnetic energy (E_k^m), internal energy (E_k^I), current squared (J_k^2), and mean square flux (ψ_k^2). Figure 3-1 is an example of our spectral graphs.

All graphs are log-log and only diagonal ($k_x = k_y$) components of spectra are plotted. The off diagonal spectra show no appreciable difference from the diagonal ones.

Contour plots are our most extensively used diagnostic. We plot two dimensional "slices" of the three dimensional quantities (amplitude, x, and y) by breaking the total range (of current J for example) into 10 equal pieces (number of contours). Lines of constant J (for example) are plotted on a two dimensional plane, with positive values as solid lines and negative values as dotted lines. This diagnostic provides high resolution visual information on the qualitative behavior of a flow. With contour plots, we can see the spatially intermittent behavior of a flow. Most important, contour plots contain phase information which is lost in spatial averages and spectra. Figure 3.6 is an example of a contour plot of flux, ψ. Note that the range of current is given by its maximum and minimum values. To quantify the contour plots, we "cut" across the plot at constant y. This "cut" is a graph of (for example current J) J (amplitude) vs. x (spatial coordinate). This diagnostic can show the

shape of coherent structures and can "correlate" quantities, such as current (j) and flux (ψ). Motivated by McWilliams,[45] we graph cuts of the gaussian curvature of flux (ψ) across current coherent structures. This quantity is defined as: -2 trace $((\nabla\underset{\sim}{B})^2)$. As discussed in the introduction, we also graph cuts of force free behavior. Specifically, we graph cuts of $\alpha = J/\psi$ and $\underset{\sim}{B} \cdot \nabla J$. Cuts also provide temporal information about coherent structures, i.e., their amplitude and width as a function time. With cuts, we can characterize coherent structure quantitatively and still retain phase information (Figure 3.20 is an example of a cut). The results of these diagnostics are presented in the next section.

3.4 Numerical Results

3.4.1 Decaying Flow

We now present the results of our highest resolution run. With $\nu_2 = .001$, $k_{max} = 44$, and Reynold's numbers of 10-100, the rate of energy decay is slow, as shown by the time series graphs in Figures 3.3 and 3.4. (Note that time history is broken into

three parts, corresponding 0 to 43, 43 to 74, and 74 to 118 Alfven times.) These plots indicate that magnetic energy (Figure 3.3) and internal energy (Figure 3.4) have almost reached an equilibrium. Presumably, with longer running time, we could reach an equilibrium. However, the e-folding time of the advective instability would also be reached. Finally, mean square flux is not graphed because it is conserved within 1 percent.

Contour plots of ψ (vector potential) indicate an accumulation of flux at large scales, as shown by Figures 3.5-3.8. Density plots (Figures 3.9-3.12) indicate behavior relatively uncorrelated with flux.

Consider the spectrum equation derived for mean square flux in Section 2.4 (Equation (2-54)):

$$\frac{\partial \mathcal{A}_{\underset{\sim}{k}}}{\partial t} + \eta k^2 \tag{3-24}$$

$$= (\rho_s/a)^2 \sum_{\underset{\sim}{p}+\underset{\sim}{q}=-\underset{\sim}{k}} (\underset{\sim}{p} \cdot \underset{\sim}{q} \times \hat{z})^2 \times$$

$$\left\{ \frac{(q_\perp^2 - k_\perp^2)}{q^2} \, \mathrm{Re}\left(\mathcal{L}^{(2)}_{\underset{\sim}{k},\underset{\sim}{p},\underset{\sim}{q}}\right) E^m_{\underset{\sim}{q}} \mathcal{A}_{\underset{\sim}{k}} \right.$$

$$\left. - k_\perp^2 \mathrm{Re}\left(\mathcal{L}^{(1)}_{\underset{\sim}{k},\underset{\sim}{p},\underset{\sim}{q}}\right) E^I_{\underset{\sim}{q}} \mathcal{A}_{\underset{\sim}{k}} + \mathrm{Re}\left(\mathcal{L}^{(1)}_{\underset{\sim}{k},\underset{\sim}{p},\underset{\sim}{q}}\right) E^I_{\underset{\sim}{p}} E^m_{\underset{\sim}{q}} \right\}$$

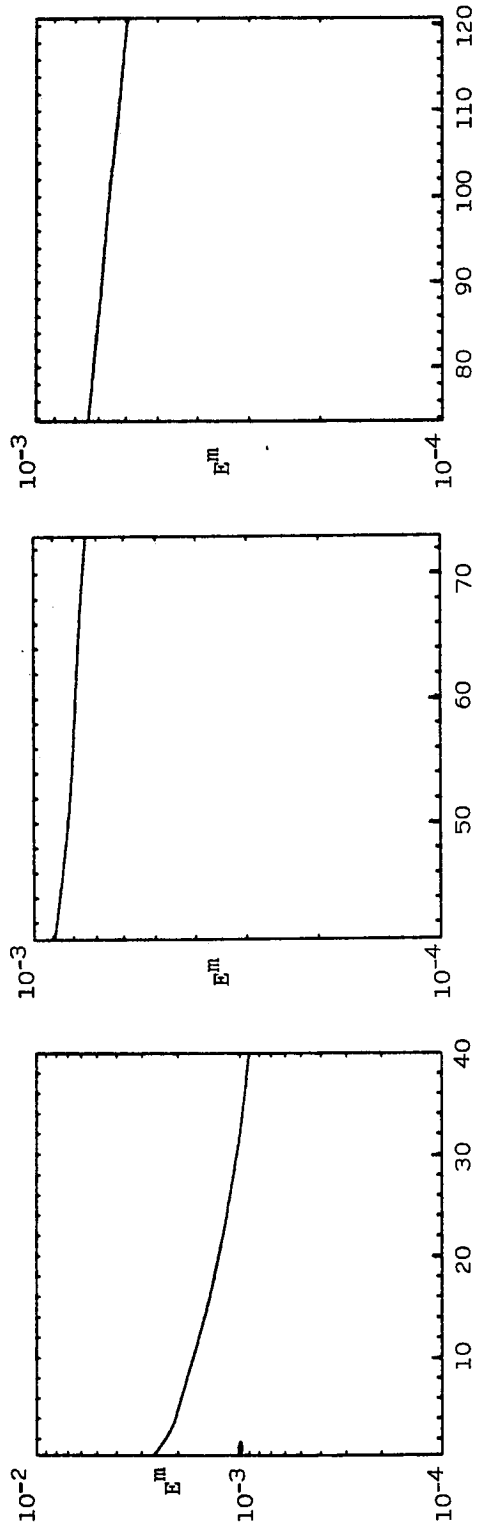

FIGURE 3.3. Time history (series) of magnetic energy (E^m). t is the Alfven time.

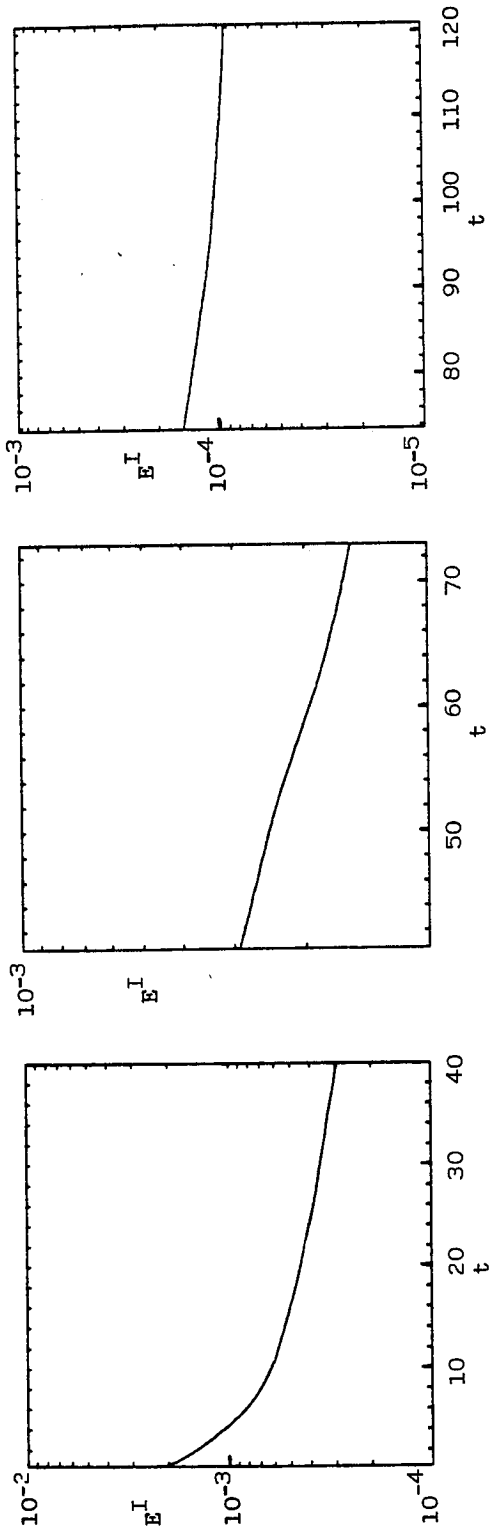

FIGURE 3.4. Time history (series) of internal energy (E^I). t is in Alfven times.

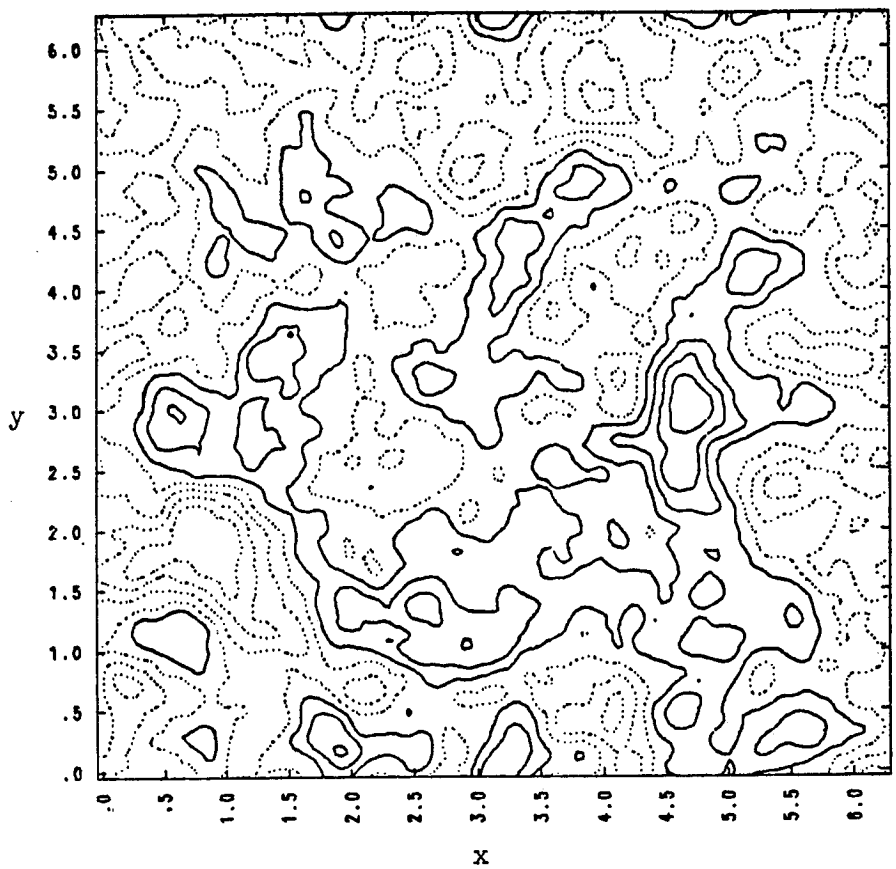

FIGURE 3.5. Contour plot of flux Ψ at t = 0.

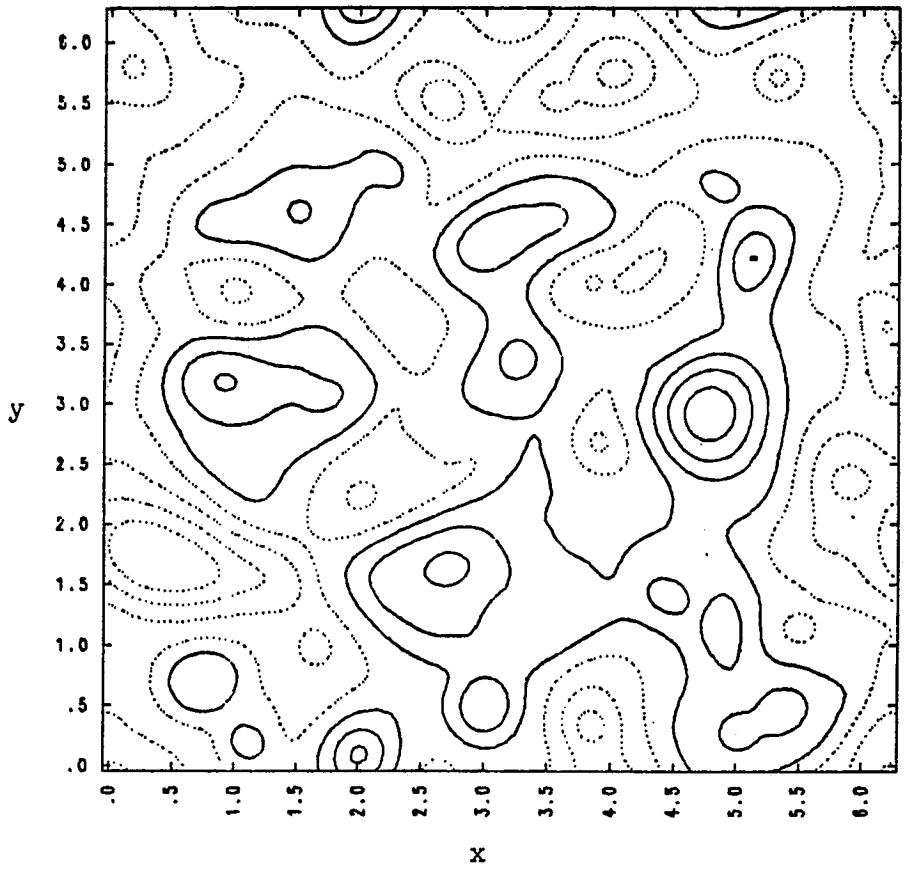

FIGURE 3.6. Contour plot of flux ψ at t = 29.

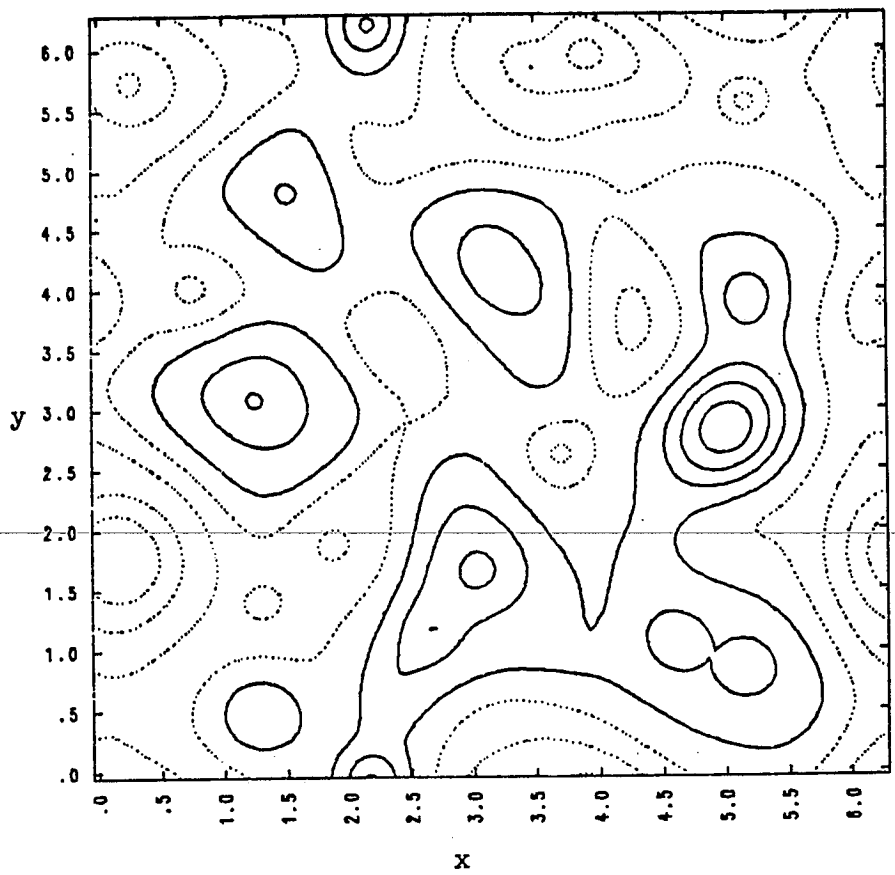

FIGURE 3.7. Contour plot of flux ψ at t = 83.

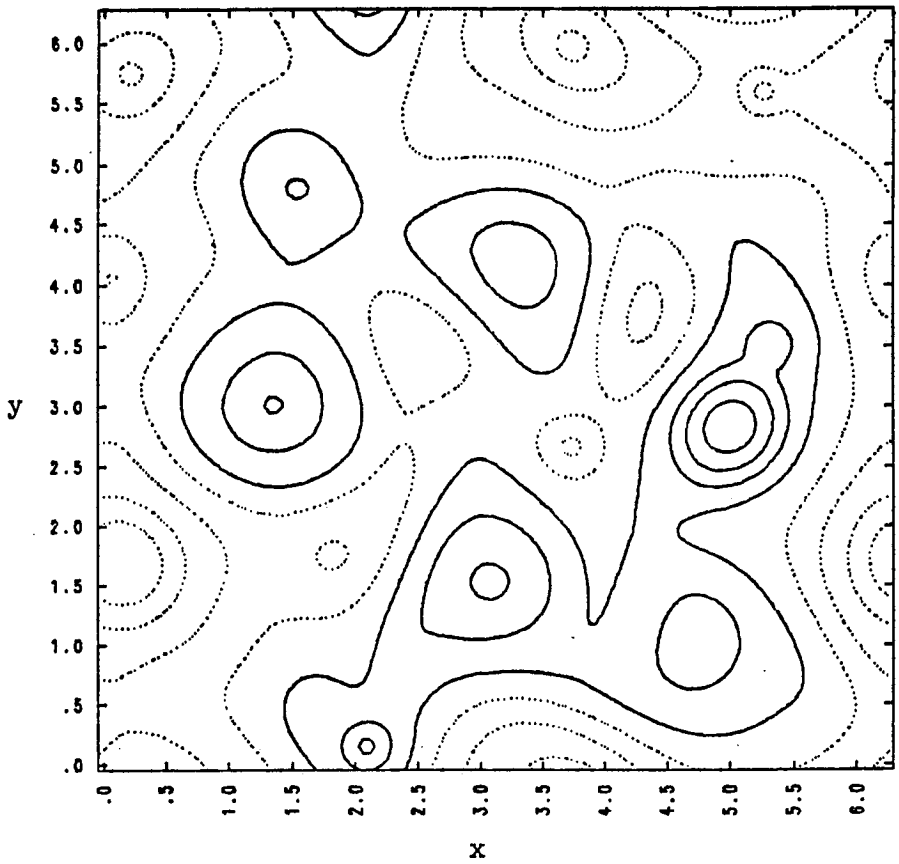

FIGURE 3.8. Contour plot of flux Ψ at t = 118.

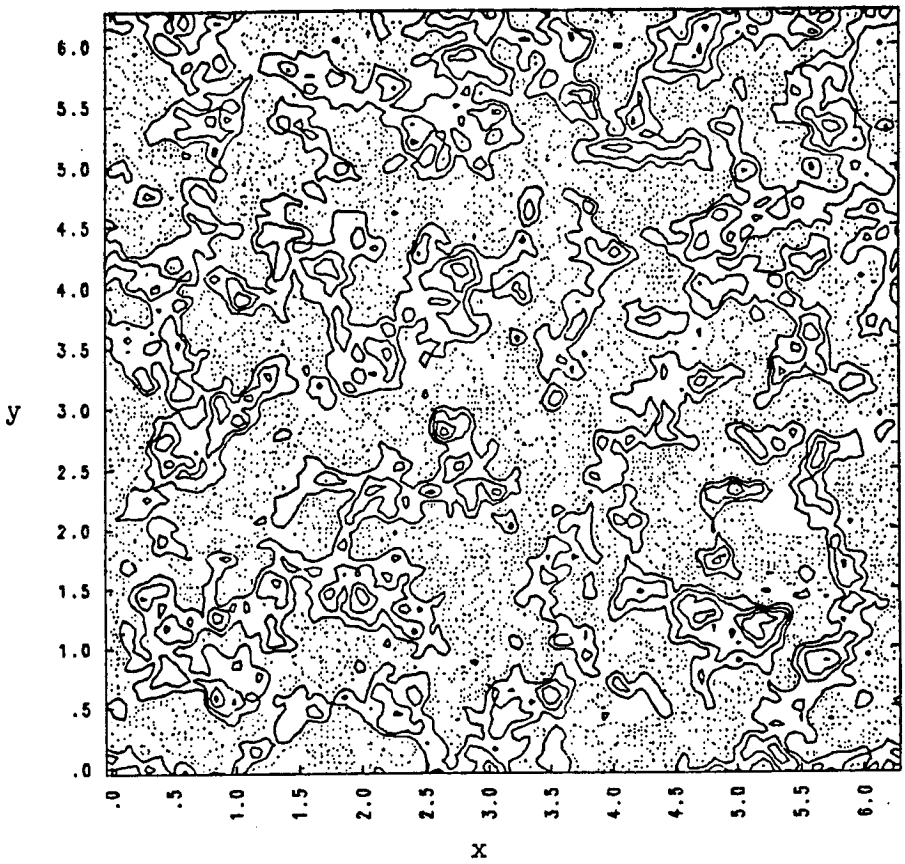

FIGURE 3.9. Contour plot of density n at t = 0.

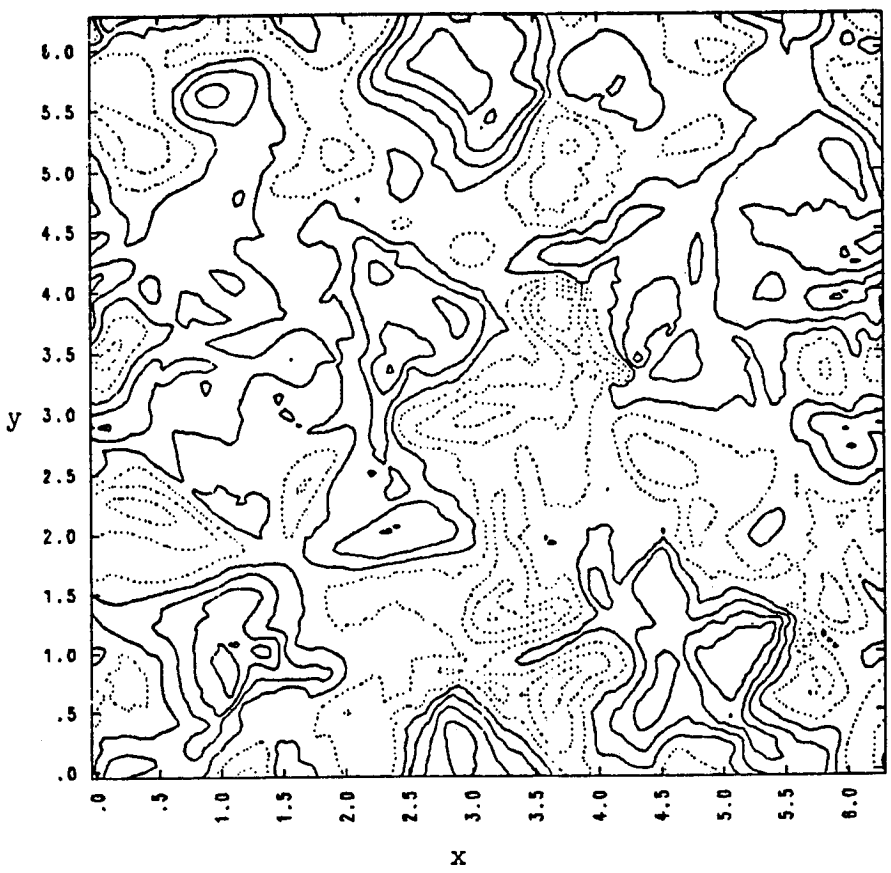

FIGURE 3.10. Contour plot of density n at t = 29.

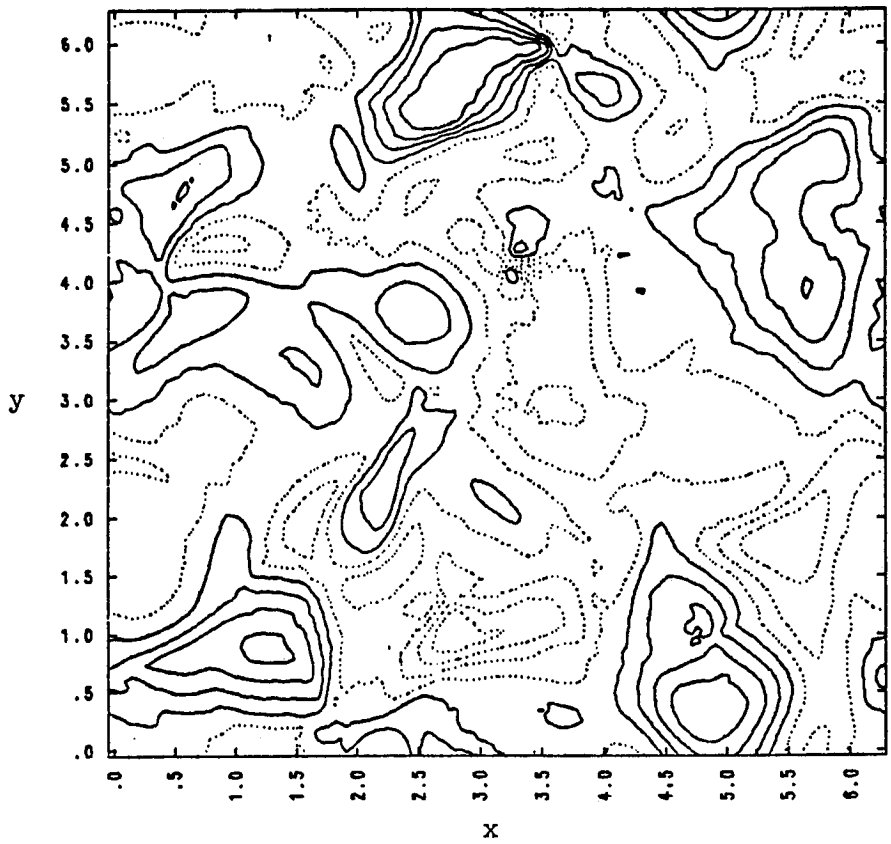

FIGURE 3.11. Contour plot of density n at t = 83. Compare to Figure 3.15, i.e., no correlation of density with current filaments.

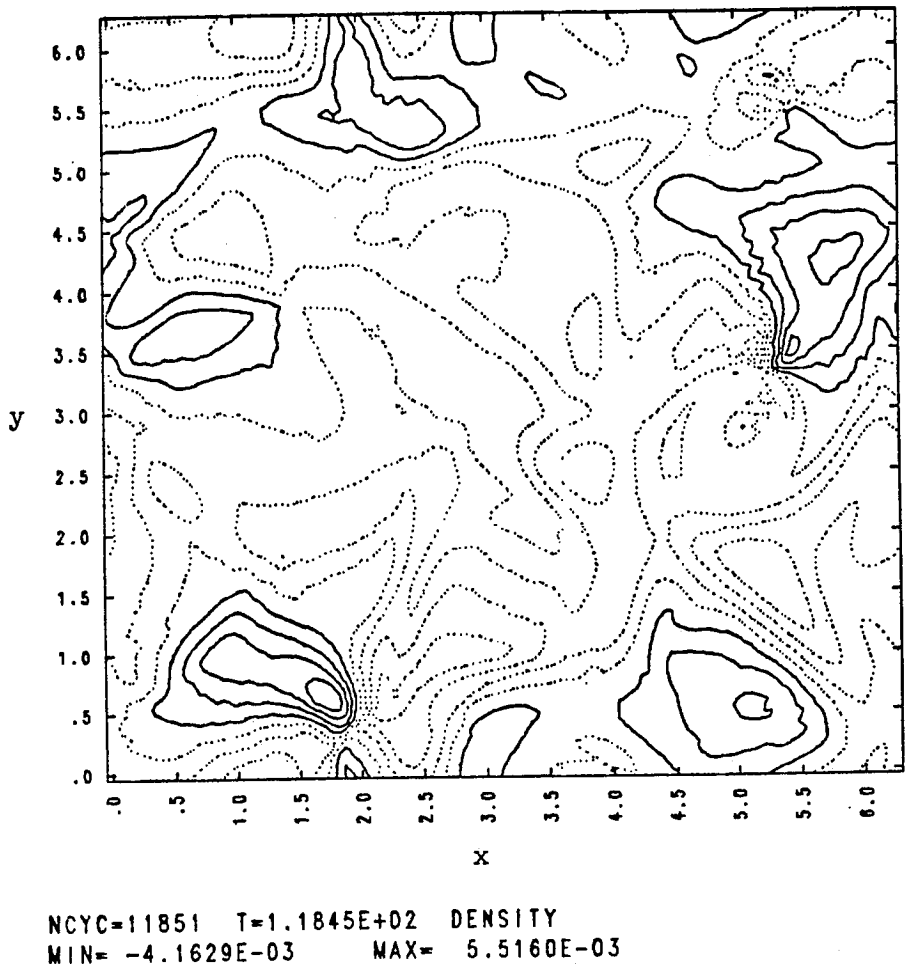

FIGURE 3.12. Contour plot of density n at t = 118.

where

$$\mathcal{L}^{(1)}_{\underset{\sim}{k},\underset{\sim}{k}',\underset{\sim}{k}''} = \frac{1}{\delta\gamma^{(1)}_{\underset{\sim}{k}} + \delta\gamma^{(1)}_{\underset{\sim}{k}'} + \delta\gamma^{(1)}_{\underset{\sim}{k}''}} ,$$

$$\mathcal{L}^{(2)}_{\underset{\sim}{k},\underset{\sim}{k}',\underset{\sim}{k}''} = \frac{1}{\delta\gamma^{(2)}_{\underset{\sim}{k}} + \delta\gamma^{(2)}_{\underset{\sim}{k}'} + \delta\gamma^{(2)}_{\underset{\sim}{k}''}} ,$$

$$\delta\gamma^{(1)}_{\underset{\sim}{k}} = \rho_s v_A k_\perp^2 \left(\frac{\delta B}{B_0}\right) ,$$

$$\delta\gamma^{(2)}_{\underset{\sim}{k}} = \delta\gamma^{(1)}_{\underset{\sim}{k}} + \nu_2 k^2 ,$$

$\mathcal{A}_{\underset{\sim}{k}}$ is the spectrum amplitude of mean square flux, $E^m_{\underset{\sim}{k}}$ is the spectrum amplitude of magnetic energy, and $E^I_{\underset{\sim}{k}}$ is the spectrum amplitude of internal energy. Note that the effect of viscious dissipation is included in the propagator $\mathcal{L}^{(2)}$. Consider $E^I_{\underset{\sim}{k}}$ to be visciously damped ($\delta\gamma^{(2)} \sim \nu_2 k_\perp^2$, i.e., dissipation range of $E^I_{\underset{\sim}{k}}$). Constrained relaxation ($\nu_2 >> \eta$) forces mean square flux to be conserved and $E^m_{\underset{\sim}{k}} >> E^I_{\underset{\sim}{k}}$. The latter result decouples mean square flux evolution from internal energy so that the second term (random convection due to diamagnetic drift) and the third term (incoherent source which conserves mean square flux against random convection) are much smaller than the first term (back reaction of

continuity on Ohm's Law). Eq. (3-24) thus simplifies to:

$$\frac{\partial a_{\underset{\sim}{k}}}{\partial t} \approx$$

$$\sum_{\underset{\sim}{p}+\underset{\sim}{q}=-\underset{\sim}{k}} (\underset{\sim}{p} \cdot \underset{\sim}{q} \times \hat{z})^2 \frac{(q_\perp^2 - k_\perp^2)}{q^2} \mathrm{Re}(\mathcal{L}^{(2)}_{\underset{\sim}{k},\underset{\sim}{k}',\underset{\sim}{k}''}) E^m_{\underset{\sim}{q}} a_{\underset{\sim}{k}} \qquad (3\text{-}25)$$

Mean square flux is hence damped at small scales ($k \gg q$) and driven at large scales ($k \ll q$) such that flux is transferred to large scales. This transfer is in qualitative agreement with the simulation results for flux given Figures 3.5-3.8. Thus, the decaying of magnetic and internal energy, with total mean square flux unchanged, but flowing to large scales is the expected behavior of our 2-D flow when $\eta \ll \nu_2$.

What is unexpected, is the property illustrated in the contour plot in Figures 3.13-3.16. The current field has evolved from a random initial distribution (spacially uniform) to a finite set of discrete, isolated current filaments. Figure 3.17 shows a sample contour plot for current when $\eta \gg \nu_2$, which is clearly radically different from the $\eta \ll \nu_2$ case. Further, Figure 3.18 shows magnetic flux, which is not appreciably

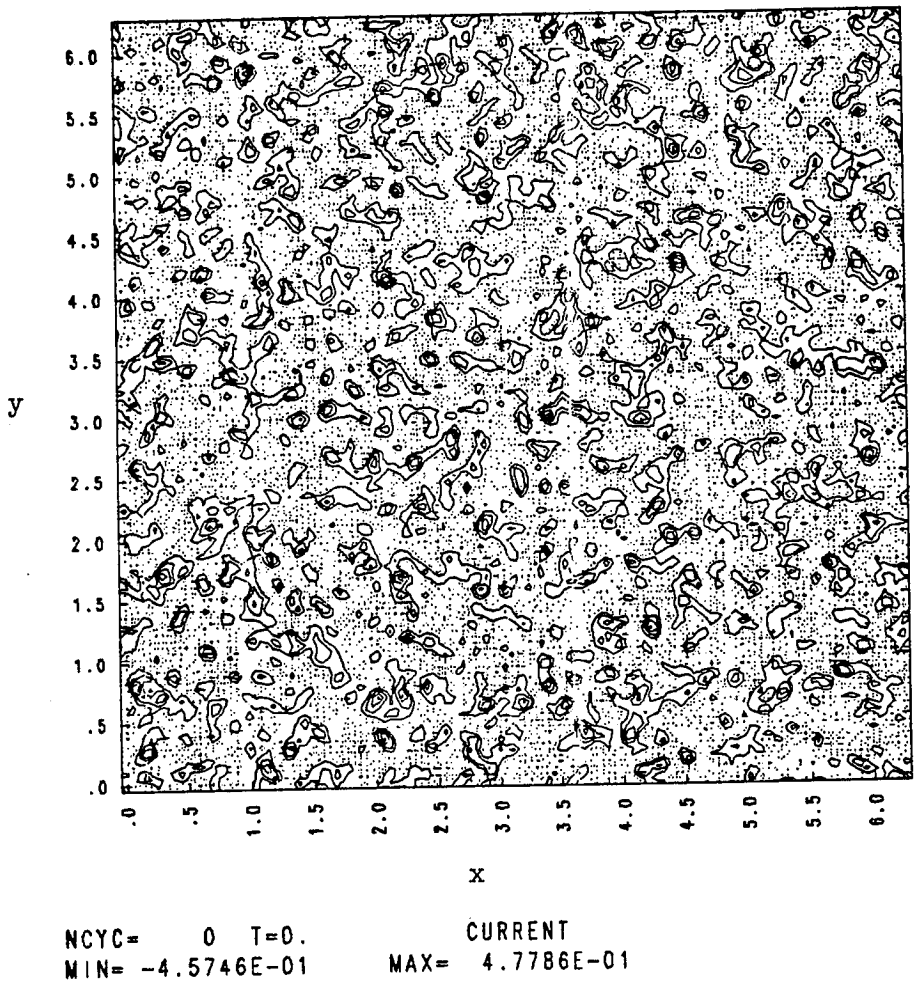

FIGURE 3.13. Contour plot of current J at t = 0.

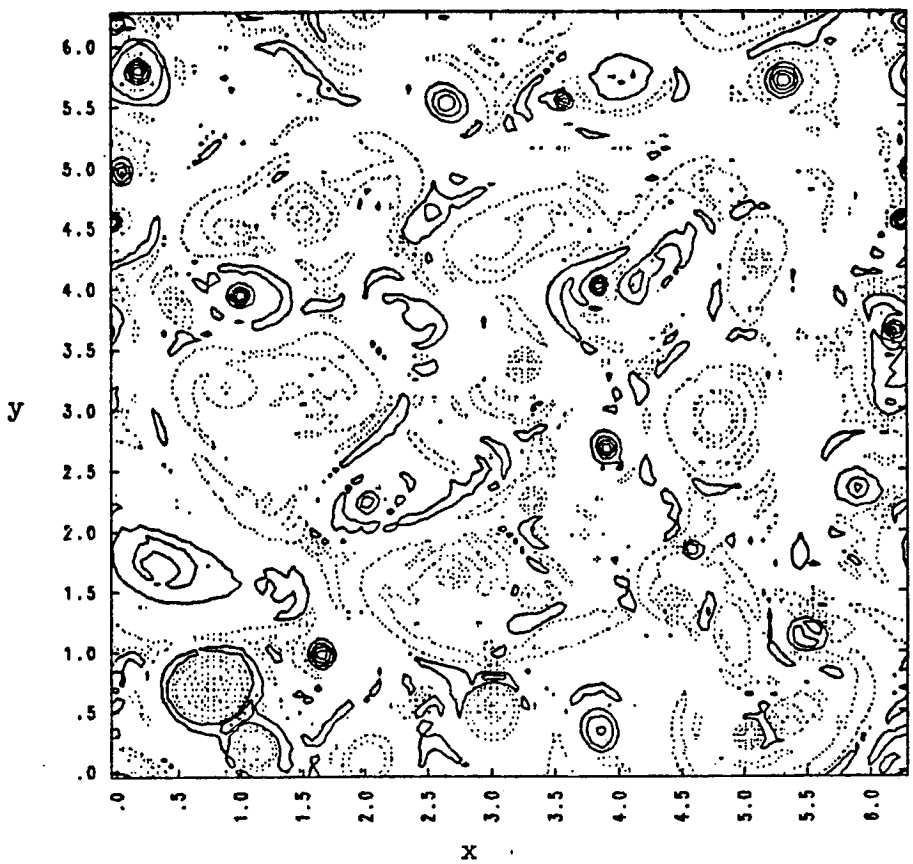

FIGURE 3.14. Contour plot of current (J) at t = 29. Note filament in upper right-hand corner.

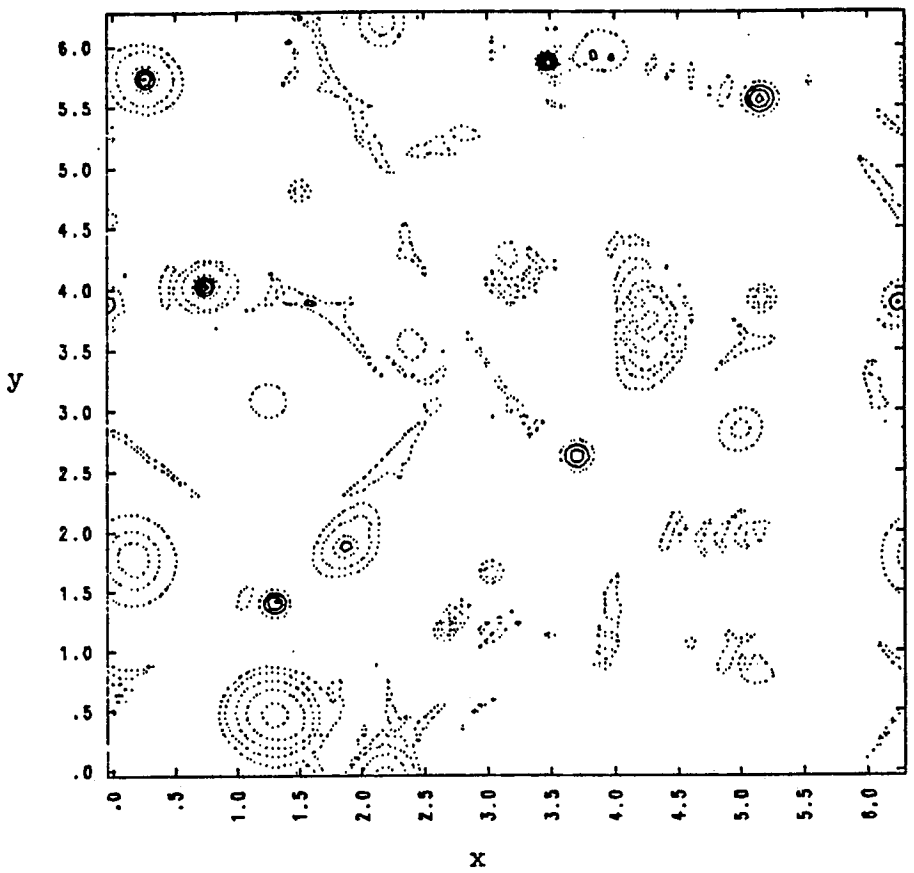

FIGURE 3.15. Contour plot of current J at t = 83. Note filament in upper right-hand corner.

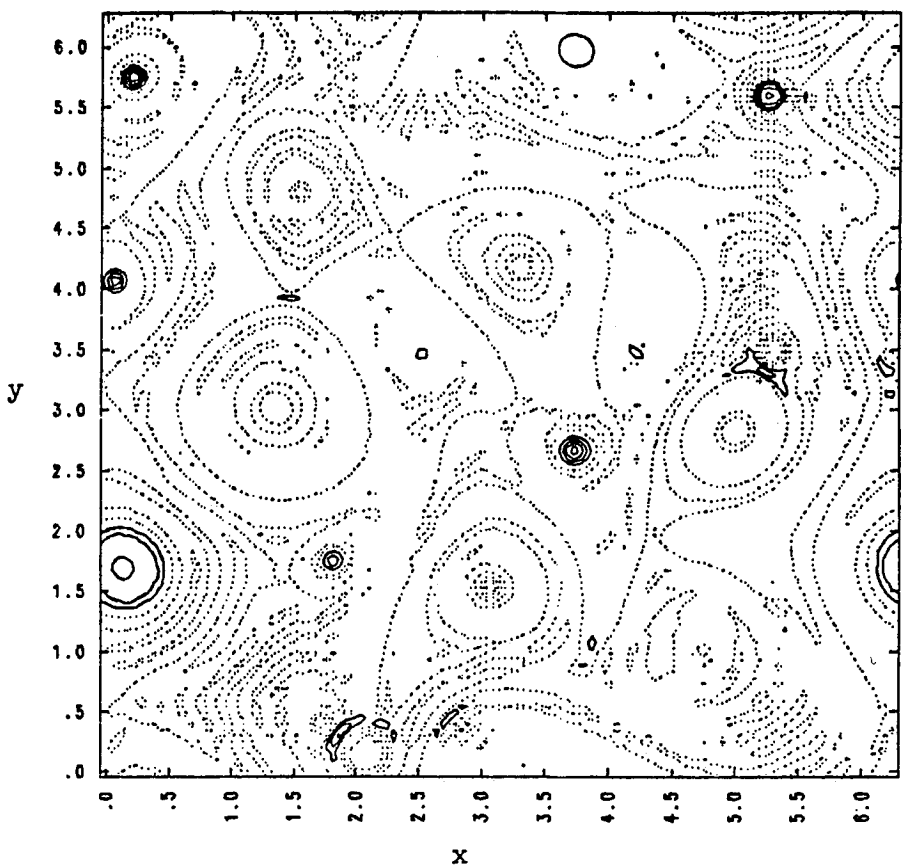

FIGURE 3.16. Contour plot of current J at t = 118. Note filament in upper right-hand corner.

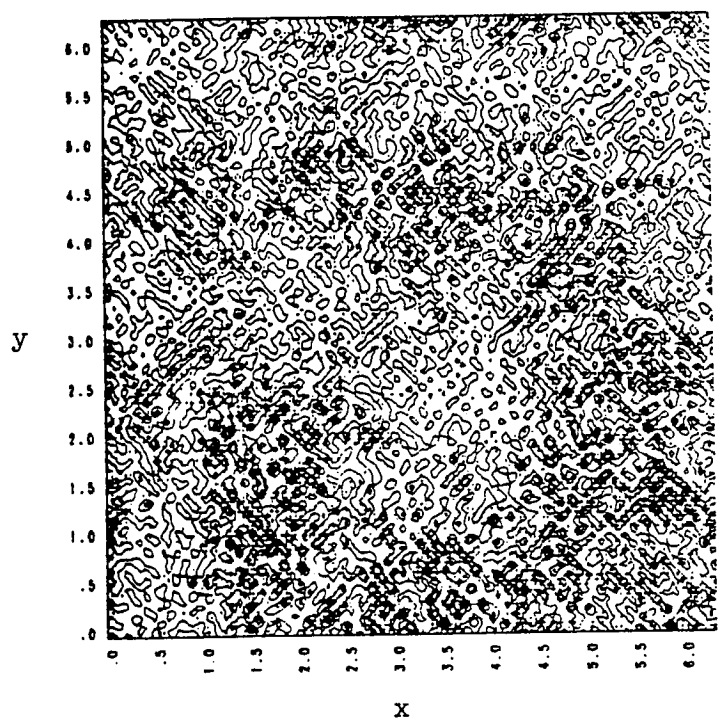

FIGURE 3.17. Contour plot of current, J, at t = 83 when $\eta = 10^{-3}$ and $\nu_2 = 0.0$. Note resemblance to initial condition (Fig. 3.13).

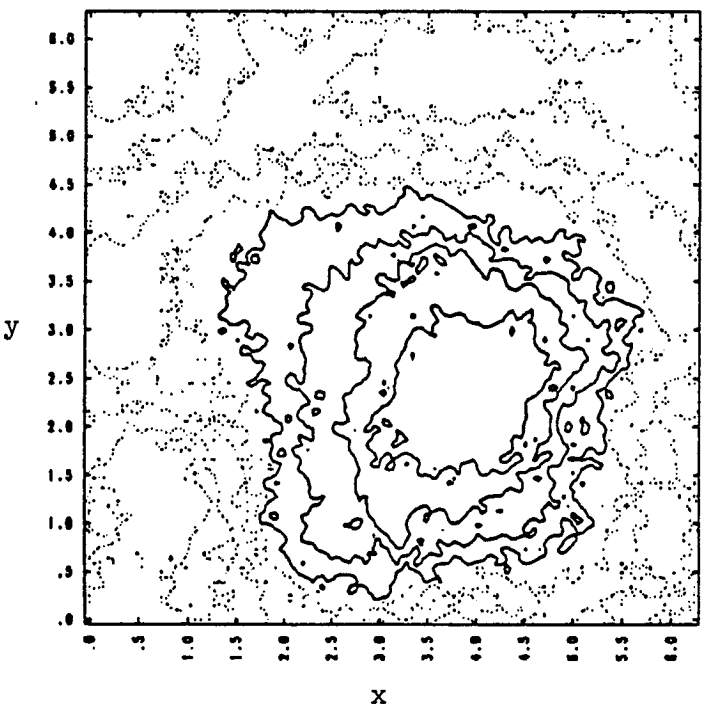

FIGURE 3.18. Contour plot of flux, ψ, at t = 83 when $\eta = 10^{-3}$ and $\nu_2 = 0.0$.

different from the initial condition. The absence of cascading can be traced to a lack of the conservation of mean square flux.

The maxima and minima of the flux contours correspond to the current filaments, while density seems uncorrelated with the current filaments (except in the special case of filament interaction, discussed in the next subsection). We thus see that the current filamentation is tied to the accumulation of flux at large scales and that the "density expulsion" from isolated filaments indicates the ejection of diamagnetic flows away from regions of current structures.

In addition to the temporal evolution of energy, a novel diagnostic is used.[45] This diagnostic indicates strong temporal variation, unlike energy, and is a qualitative measure of the spatial "spottiness" or intermittency of the current. Figure 3.19 shows the time history of the fourth moment of the current, or kurtosis $\mathcal{K}$ (sometimes called flatness). $\mathcal{K}$ is defined by

$$\mathcal{K}(f) = \langle \delta f^4 \rangle / \langle \delta f^2 \rangle^2$$

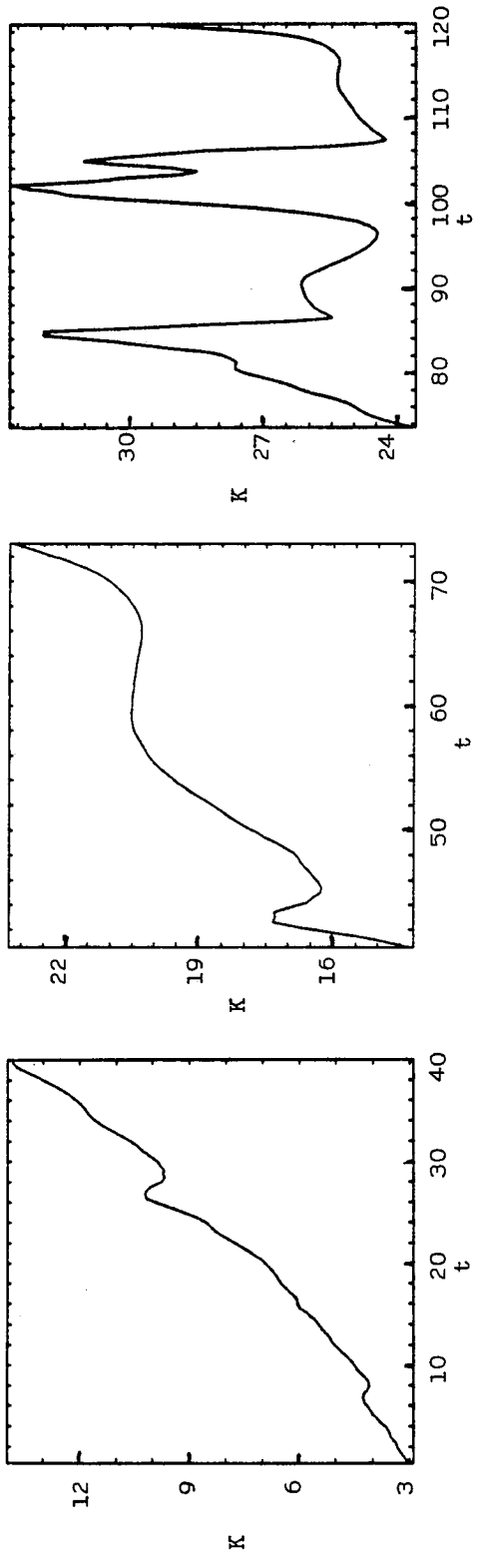

FIGURE 3.19. Time history (series) of kurtosis (K) of current (J). t is in Alfven times.

where $\langle\ \rangle = \int dxdy$ and $\delta f = f - \langle f \rangle$. For a gaussian distribution of f, $\mathcal{K} = 3$. From the spacial distributions of density and flux, we see that they are nearly gaussian.

The kurtosis of current, though, is of the order of 20, indicating a strong deviation from gaussianity. Geometrically, $\mathcal{K}(J)$ measures the square of the ratio of distance between current filaments to their width. This can be crudely confirmed by visual inspection of Figures 3.13-3.16. From the current contours and the geometrical interpretation, we see that a high kurtosis indicates a sort of spatial intermittency. Quasi-gaussian closure theories (iterating from "near" a gaussian), such as used in Chapter II, may be invalid in describing the dynamics of systems of high kurtosis.[30] Numerical comparisons of closure theories and direct simulations are hence needed (see Section 3.6).

Finally, in addition to being a strong function of time, kurtosis is a function of resolution. For runs of $k_{max} \sim 6$ or less, the flatness is the order 3-4, indicating nearly gaussian behavior. With increasing k_{max}, the kurtosis (for equal times) reaches values of about 10 for $k_{max} \sim 11$ and 20 for $k_{max} \sim 22$. This

resolution dependence indicates that a sufficient range of scales is examined, indicating that lower resolution limits nonlinear interactions in a bounded system (i.e., nonlocal transfers, such as the inverse transfer of mean square flux to large scales, depend on the disparity of wavenumbers of interacting modes).

3.4.2 Characterization of Current Filaments

In this subsection, we present results on the characterization of the individual filaments. First, each filament has a long lifetime. Looking at current contours throughout the run ($k_{max} \sim 44$, $\nu_2 \sim .001$), we see that an individual filament can be followed backwards in time to the initial condition. Figures 3.13-3.16 display current fields for various times. As an example, we consider the filament in upper right hand corner. This filament is present throughout the run. By "cutting" through the filament at constant y (Figures 3.20-3.22) we see that the integrity of the structure remains intact, but decreases slightly in amplitude (~10% over the entire run). This filament also remains almost stationary in space. Note that outside filament,

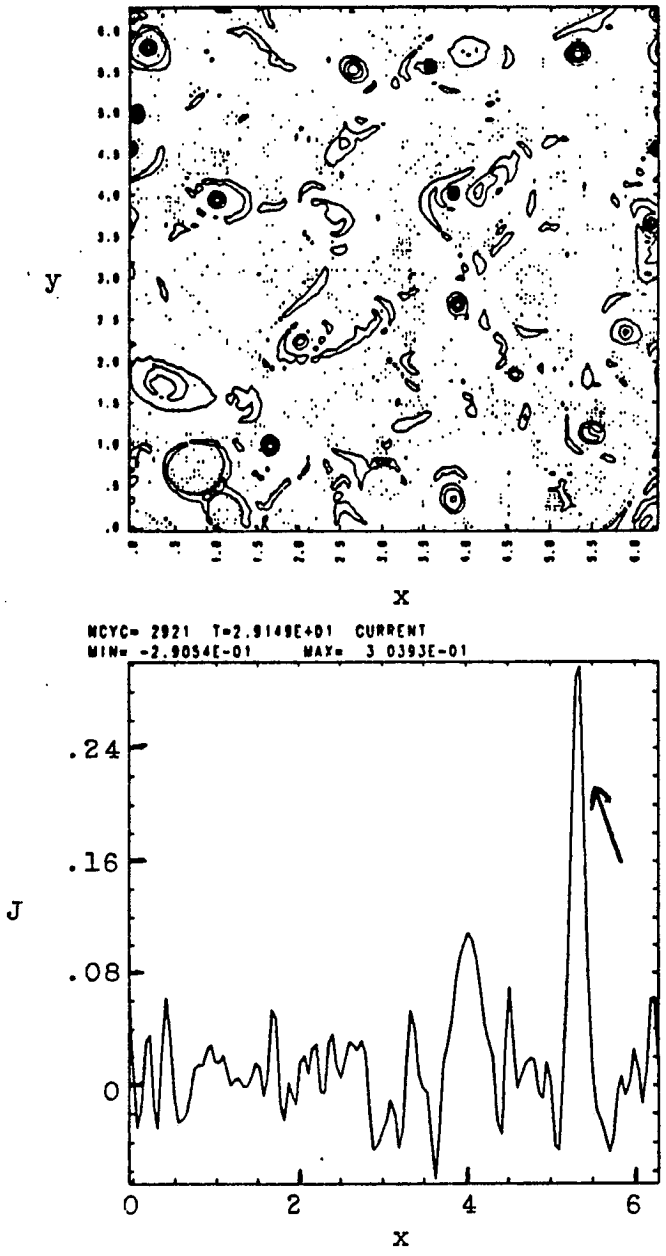

FIGURE 3.20. Cut (bottom), with y = constant of current filament (see arrow at top) at t = 29 (J is current magnitude). See Figure 3.14.

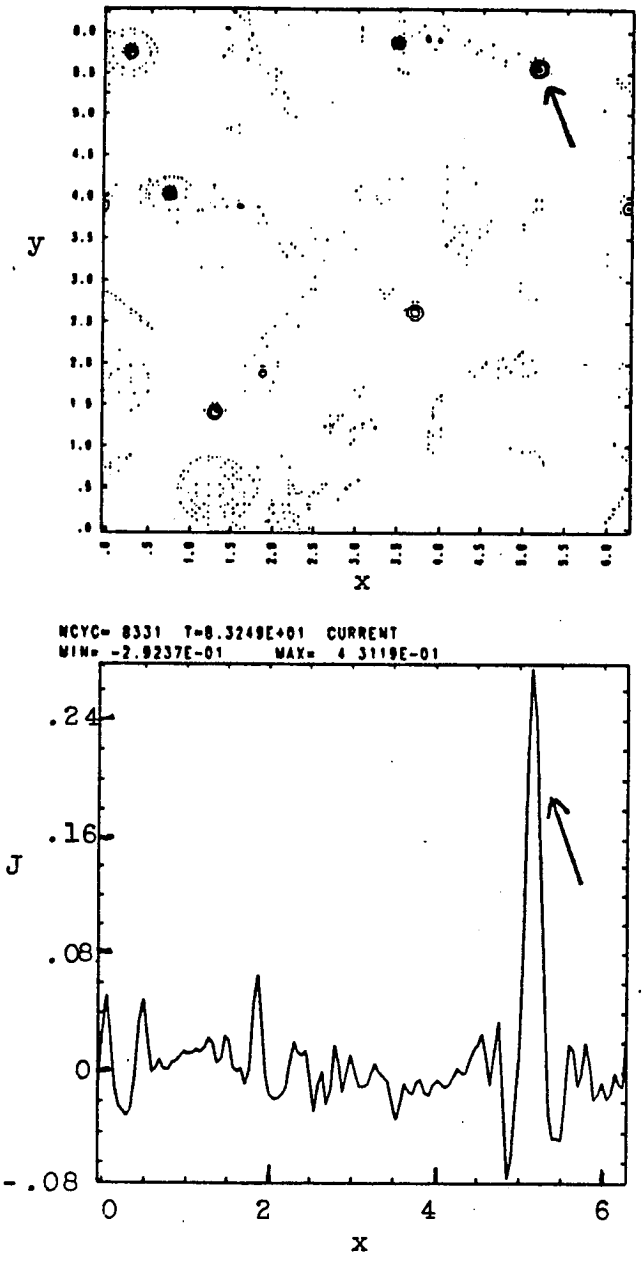

FIGURE 3.21. Cut (bottom), with y = constant, across current filament (see arrow at top) at t = 83 (J is current magnitude). See Figure 3.15.

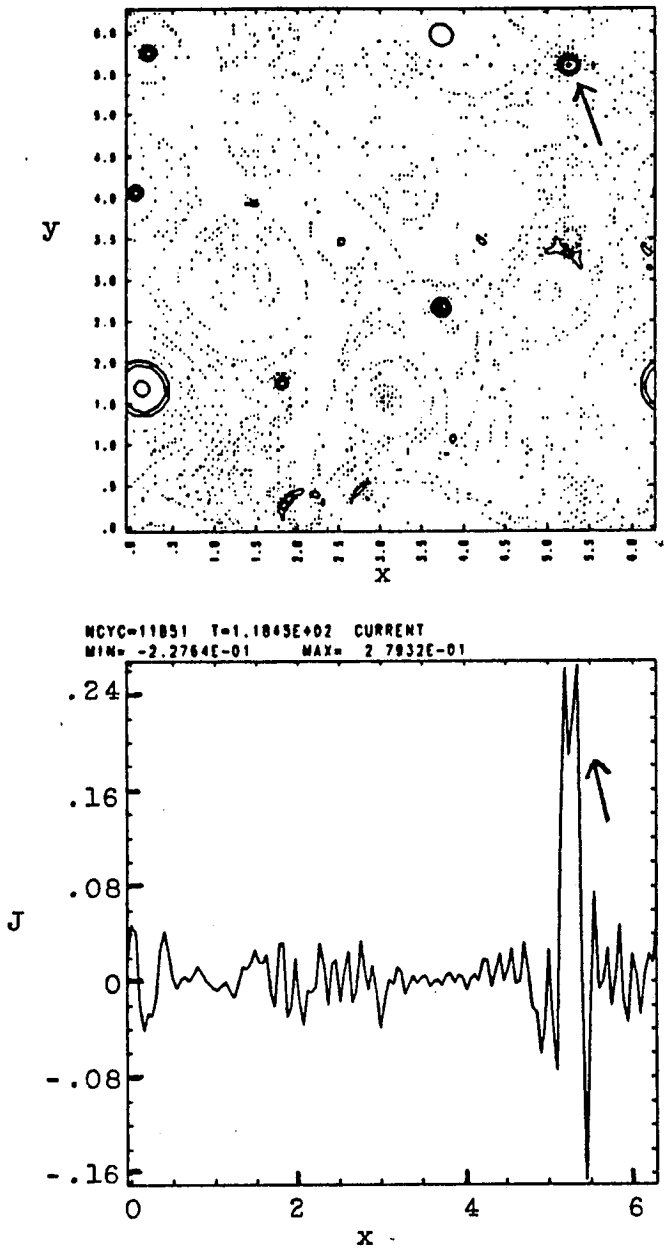

FIGURE 3.22. Cut (bottom), with y = constant, of current filament (see arrow at top) at t = 118 (J is the current magnitude). See Figure 3.16.

the current amplitude is much smaller (and varies on the order of an eddy turnover time).

We next consider the "force free" behavior of the filament. For microtearing, the force free condition is $J = \alpha\psi$ where $\underset{\sim}{B} \cdot \underset{\sim}{\nabla}\alpha = 0$. We graph $\underset{\sim}{B} \cdot \underset{\sim}{\nabla}J$ cuts across the filament in Figure 3.24 (Figure 3.23 is current cut at $t = 83$), ($t = 83\tau_A$) as well as α in Figure 3.25. First, we see that $\underset{\sim}{B} \cdot \underset{\sim}{\nabla}J \cong 0$ at the structures, but fluctuates wildly outside of the structures. Global nonzero $\underset{\sim}{B} \cdot \underset{\sim}{\nabla}J$ probably indicates that the simulation has not completely relaxed. (Hence, not relaxed to a force free state). Note that outside the current filament, α is approximately constant, while inside the filament α is nonconstant. The nonconstancy of α indicates, therefore, that the force free state, $J \sim J_0(\alpha^{1/2}r)$ (J_0 is zeroth order Bessel function) is not applicable to our current filaments. From the amplitude, we find a measure of the scale of a filament. $\alpha^{1/2}$ is a measure of the maximum wavenumber of the filament. For our isolated structure $\alpha^{1/2} \sim 10$, corresponding to a width of one tenth of the width of the domain (2π). Since the maximum wavenumber of the code is 44, then there is an average of 4 gridpoints resolving this structure.

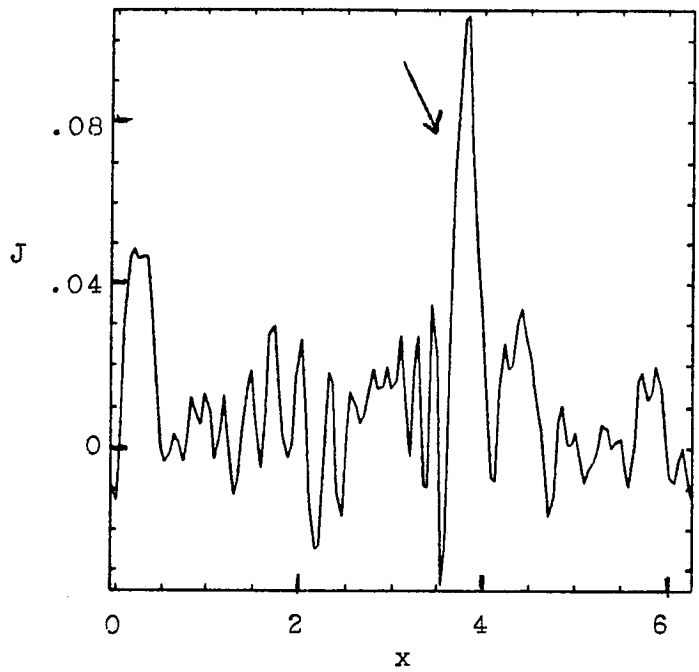

FIGURE 3.32. Cut (y is constant) across remaining filament in Figure 3.29 (t = 93). Note that final amplitude J (current) is less than either original filament.

might play a role in the interaction. I is the current analogue of fluid circulation, i.e., total current (J is actually the current density). Finally, by plotting density throughout the current interaction (Figures 3.33-3.35) we see that strong diamagnetic flows are set up near the point where they interact, indicating strong convection of flux in the interaction. (This point of interaction is an x-point in the magnetic field.)

Summarizing, we observe long-lived, force free current filaments, surround by smaller amplitude (compared to the filament) fluctuating current. These filaments interact with those of like sign (i.e., attracting current rods) such that one remains of equal or smaller amplitude. Further, the filaments are not solitary, in that one filament remains after interaction. The appearance of the current structures is tied to an accumulation of mean square flux at large scales (attributed to the constrained relaxation condition, $\nu_2 >> \eta$). Globally, the filaments represent spatial intermittency, measured by high values (>>3) of the fourth moment, kurtosis.

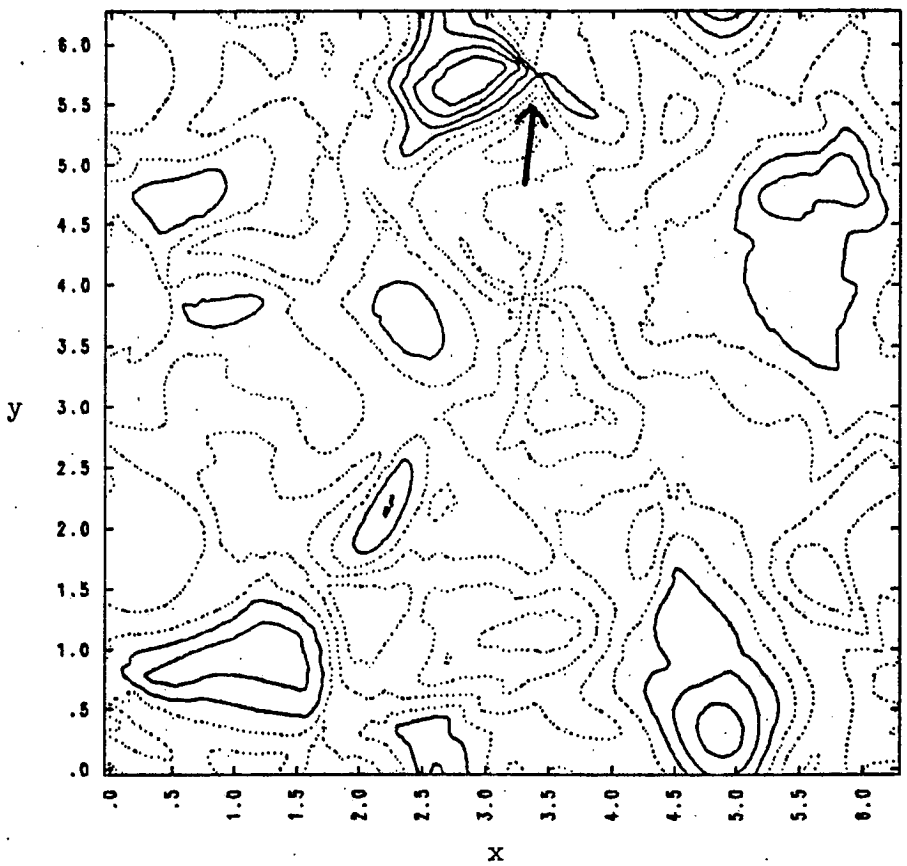

FIGURE 3.33. Contour plot of density (n) at t = 69. Arrow indicates site of strong diamagnetic flow, correlated with filament interaction (See Figs. 3.27 and 3.20).

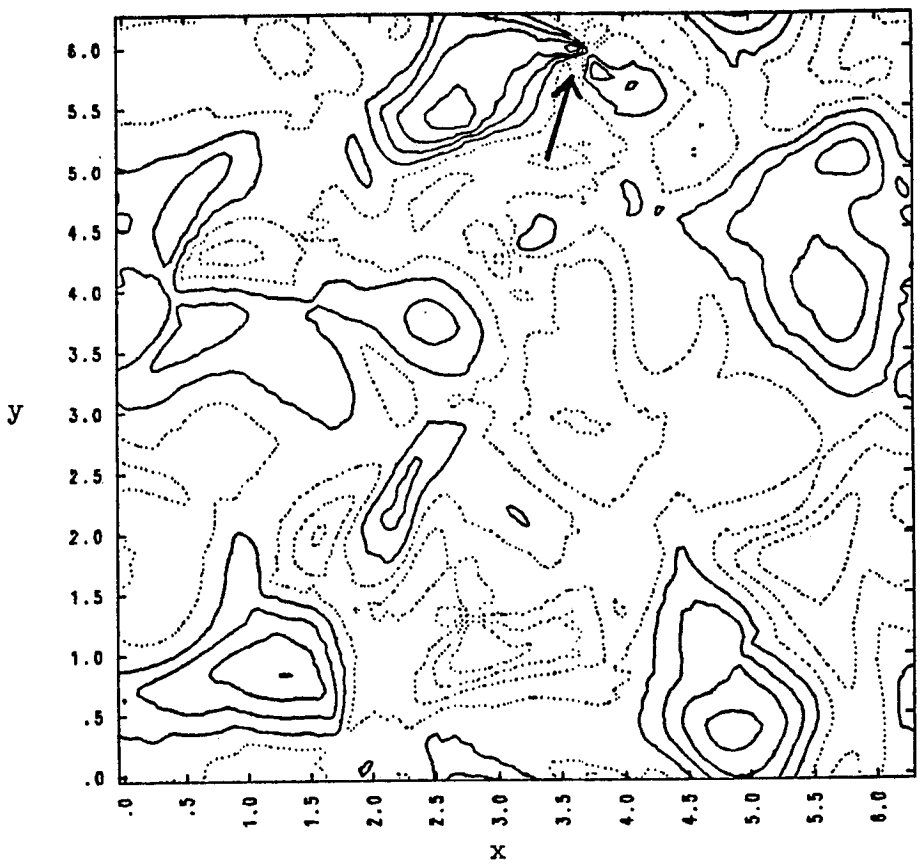

FIGURE 3.34. Contour plot of density (n) at t = 86. Arrow denotes site of strong diamagnetic (drift) flow, correlated with the site of current interaction. (See Figs. 3.28 and 3.31).

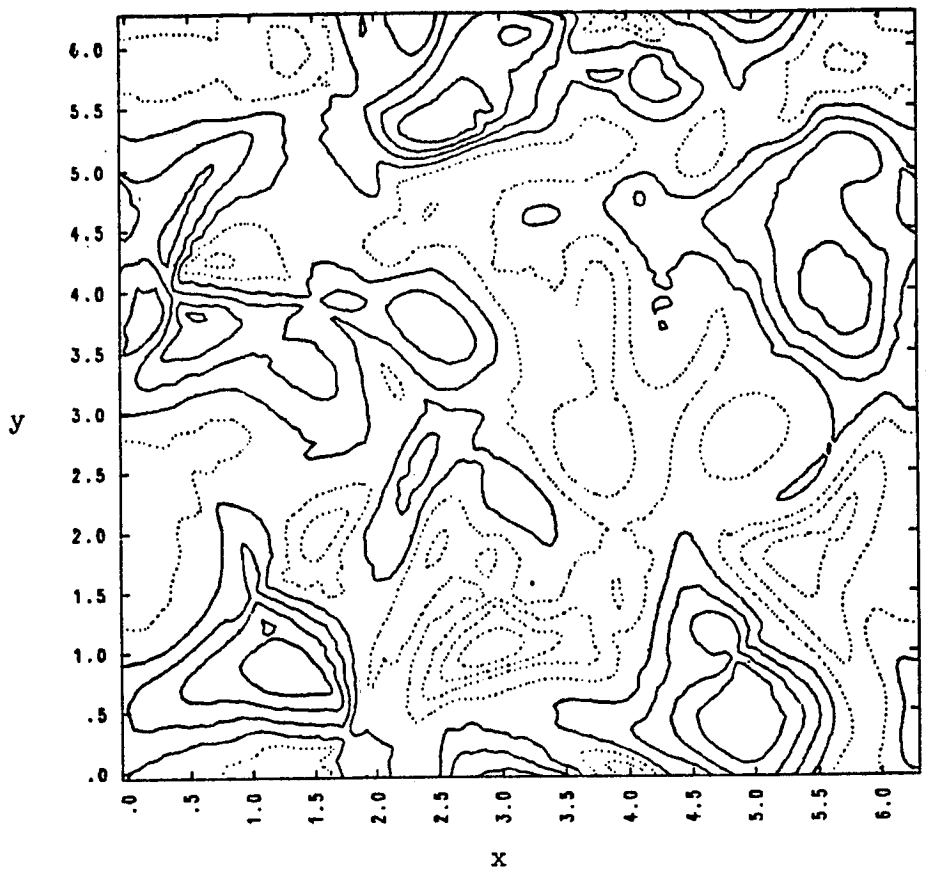

FIGURE 3.35. Contour plot of density (n) at 5 = 93. Note that strong diamagnetic flow has relaxed, corresponding to completion of filament interaction (See Figs. 3.29 and 3.32).

3.5 Spectra

In this subsection, we present spectra and discuss their relevance. High values of kurtosis have been associated with the steepening (note cautionary remarks in introduction) of energy spectra.[45] To obtain an estimate for the magnetic energy spectrum, we consider the analytic methods of Saffman.[61] In his paper, he calculates the energy spectrum for 2-D Navier-Stokes fluids. The vorticity field is considered to have discrete jumps along a line, with a spacially constant background in between. These jumps are thought to arise from the strong vorticity gradients generated by rearrangement of vortices by fluid turbulence, due to the conservation of vorticity along trajectories. The energy is found to be k^{-4}, which is steeper than k^{-3} spectrum found by Lilly.[43]

As found by Moffatt,[46] current and magnetic field are analogous to vorticity and fluid velocity. On the other hand, current is not conserved along trajectories

$$\left(\frac{\partial J}{\partial t} + \underset{\sim}{v}_D \cdot \underset{\sim}{\nabla} J \neq 0 \right).$$

Therefore we assume that the current field to be composed of a discrete current filaments of diameter a and constant amplitude such that each has a discontinuous boundary,[61] i.e., a field of cylindrical filaments. The current gradient is

$$\frac{\partial J}{\partial x} = \sum_{i}^{N} j_i \delta(x - x_i) - N\bar{j} \qquad (3\text{-}26)$$

where N is the number of discontinuities per unit length along a line and $\bar{j}$ is the average filament height. x_i is the point along a line at which the filament's edges appear. We see that for $i \neq j$, $b = \overline{(x_i - x_j)}$ is the average distance between filaments. From the definition of kurtosis $\mathcal{K} \cong b^2/a^2$, we find that

$$N \cong \frac{2}{b} (1 + 1/\mathcal{K}^{1/2})^{-1} . \qquad (3\text{-}27)$$

Defining $\mathcal{O}(k)$ such that

$$\int_{-\infty}^{+\infty} dxdy\ J(x,y)J(x + \epsilon, y)$$

$$= \int_{-\infty}^{+\infty} dk\ \exp(ik\epsilon)\,\mathcal{O}(k) \qquad (3\text{-}28)$$

we find

$$\mathcal{O}(k) = N\overline{j^2}/2\pi k^2, \tag{3-29}$$

where $(\overline{j^2})^{1/2}$ is the mean square current amplitude. To find the magnetic energy spectra, we use

$$\mathcal{O}(k) = \frac{1}{\pi}\int_{-\infty}^{+\infty} ds(k^2 + s^2)^{1/2} E_k^m(\sqrt{k^2 + s^2}) \tag{3-30}$$

and

$$E_k^m = \frac{N\overline{j^2}}{4k^4} \quad . \tag{3-31}$$

This result is valid when

$$\frac{1}{L} << k << \frac{1}{\delta} \ , \tag{3-32}$$

where δ is a dissipation scale associated with the filament boundary width and L is on the order of the system size. δ is a measure of the width of the current jump and is found by balancing parallel compression with viscious dissipation in regions of large current gradient, i.e., around filaments. In particular, balancing $\nabla_\parallel J$

with $\nu_2 \nabla_I^2 n$ in the region of strong current gradient,

$$\frac{\delta}{L} \overline{j^2} \sim \frac{\nu_2 \sqrt{E^I}}{\delta^2} \qquad (3\text{-}33)$$

or

$$\delta \sim \left(\frac{\nu_2 L \sqrt{E^I}}{j^2} \right)^{1/3} \qquad (3\text{-}34)$$

where E^I is the total internal energy and L is the scale of the magnetic field ($L^{-1} \sim N$). Similarly, for point-like filaments,

$$E_k^m \sim \frac{\overline{B^2} N}{4k^2} , \qquad (3\text{-}35)$$

where $\overline{B^2}$ is the mean square magnetic field and N is the number of filaments per unit length.

Assuming a discontinuity in J is equivalent to assuming current sheets in a current field, these point filaments correspond to one dimensional behavior, or the microtearing equivalent of "burgerlance." [61] Therefore, when analyzing spectra from simulation, k^{-4} behavior implies a current field of sheet like discontinuities (heavy side functions) while k^{-3} behavior

corresponds to point like discontinuities (δ functions). Note that this interpretation is based on the results of Saffman, and should be viewed with the cautionary remarks at the end of this section.

In Figures 3.36-3.39 we graph spectra of magnetic energy, internal energy, mean square flux and current squared, at t = 83. Figures 3.40 and 3.41 show spectra (energy) at t = 118 (the end of the run). No steepening of spectra can be seen. (This is not the final word, because the point scatter is great). Looking at t = 118, we find that, by visual fit,

$$E_k^m \sim k^{-(3.9\pm.5)}$$

and

$$E_k^I \sim k^{-(4.6\pm.5)}.$$

Thus, we see that the current field can be interpreted as being closer to being composed of current sheets, than of delta functions. We conclude this section, with a word of caution concerning spectral anslysis of intermittent flows[3] (as discussed in the introduction).

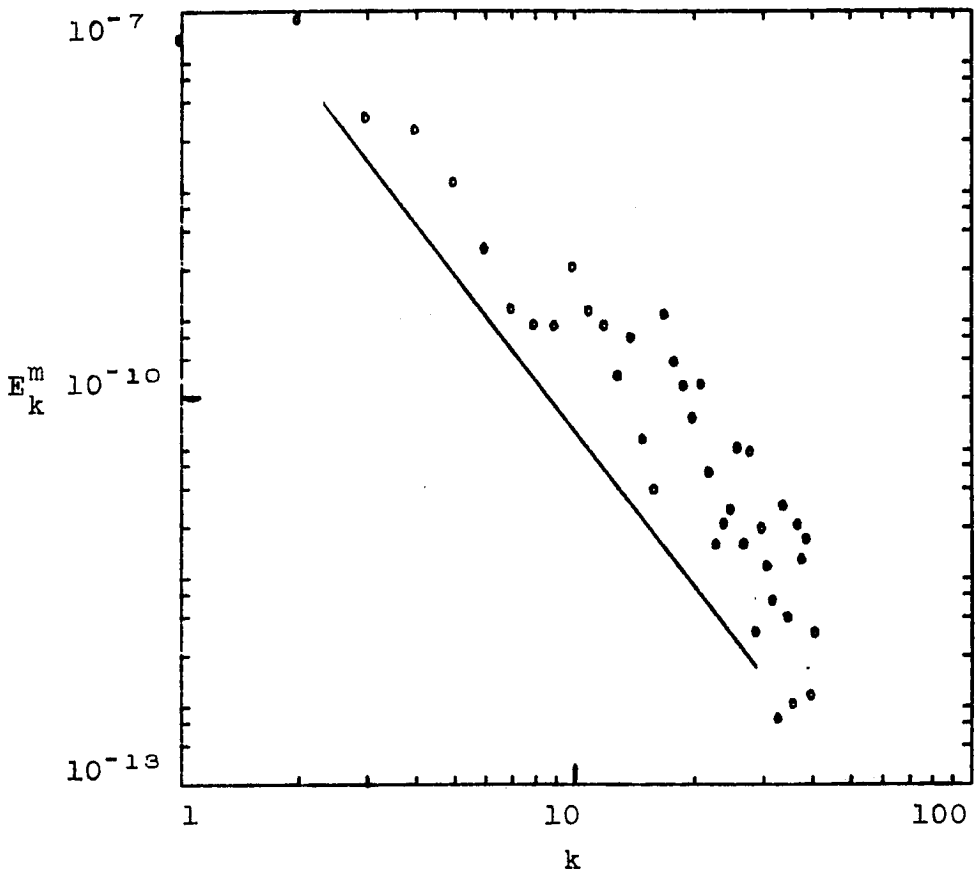

FIGURE 3.36. Spectrum of magnetic energy (E_k^m) at $t = 83$. Solid line is $E_k^m \sim k^{-4}$.

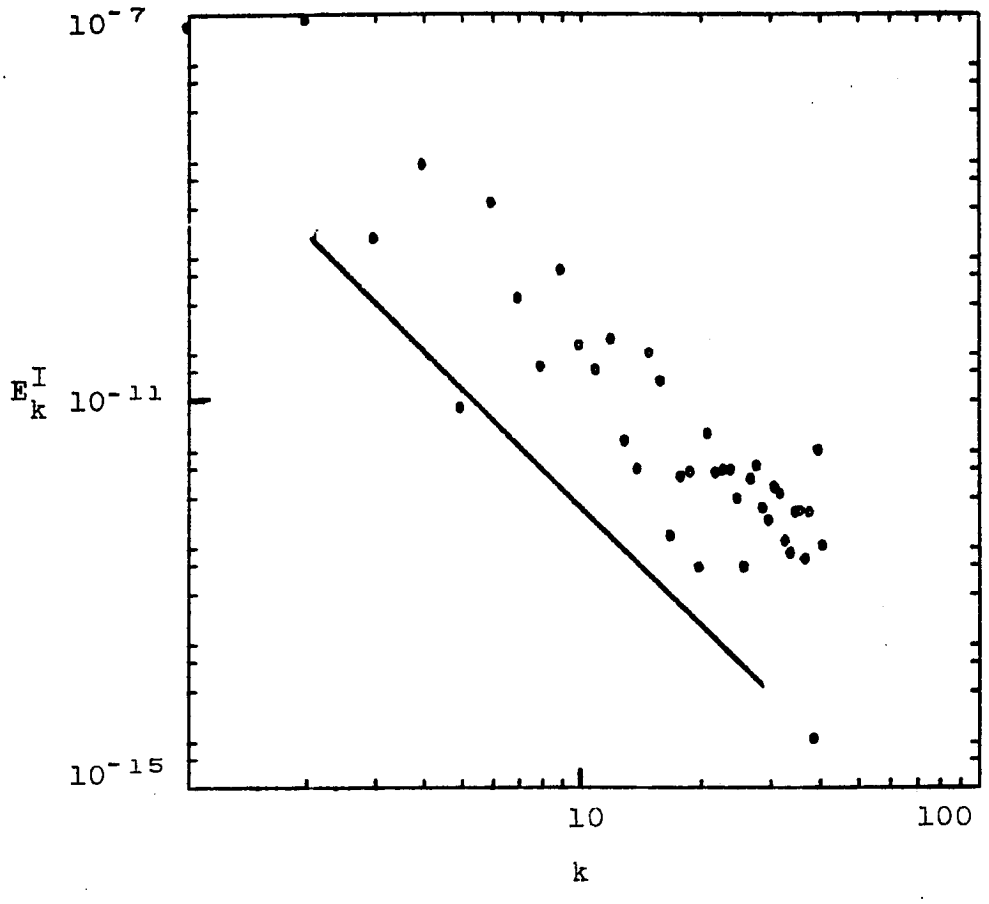

FIGURE 3.37. Spectrum of internal energy (E_k^I) at t = 83. Solid line is $E_k^I \sim k^{-4}$.

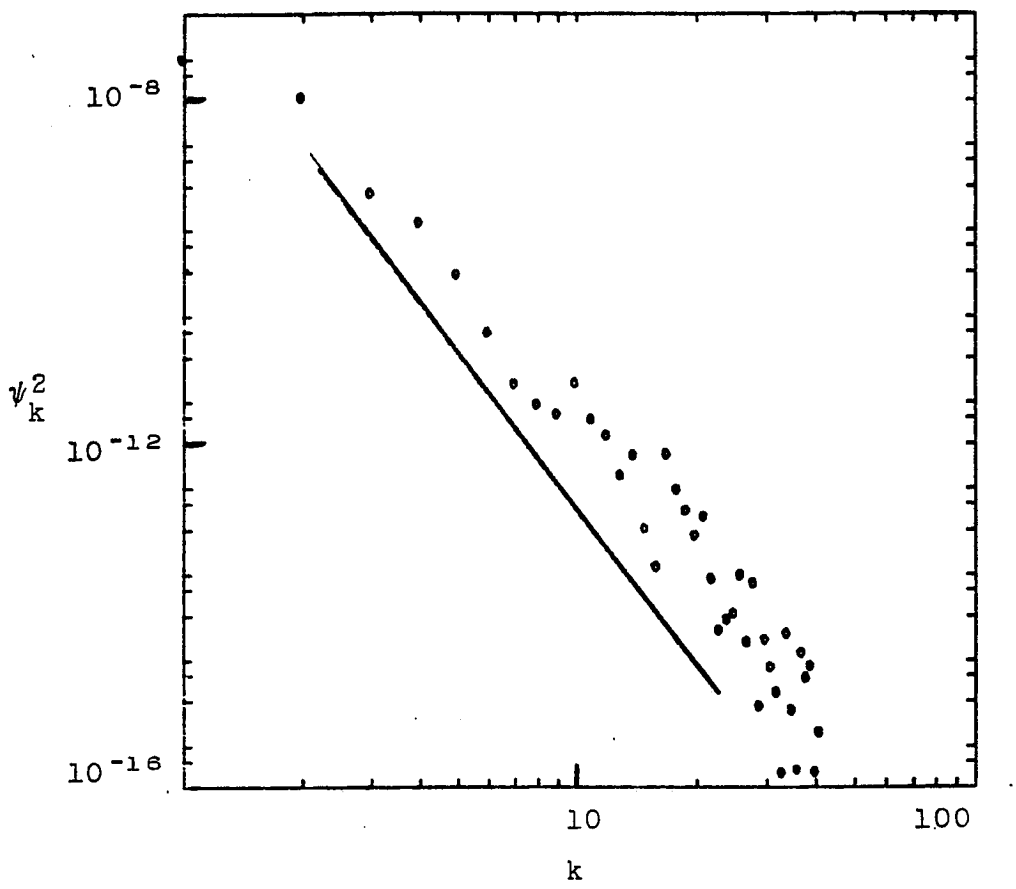

FIGURE 3.38. Spectrum of mean square flux (ψ_k^2) at t = 83. Solid line is $\psi_k^2 \sim k^{-6}$.

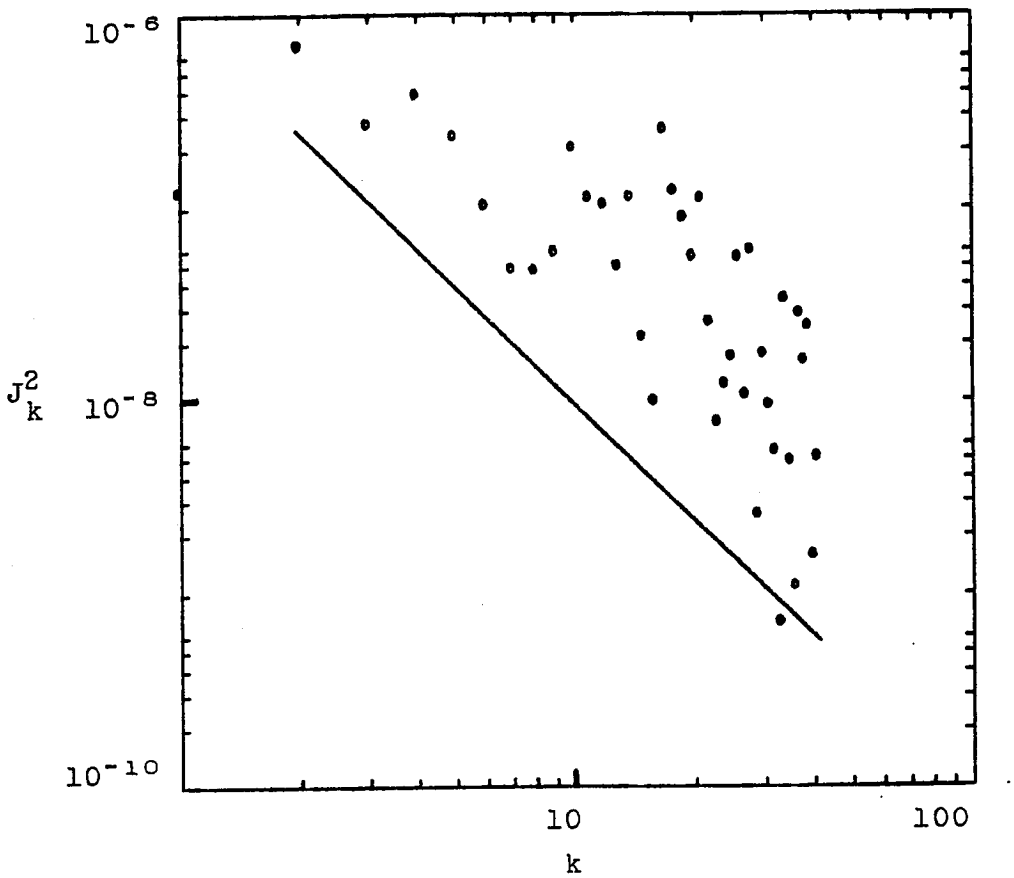

FIGURE 3.39. Spectrum of current squared (J_k^2) at $t = 83$. Solid line is $J_k^2 \sim k^{-2}$.

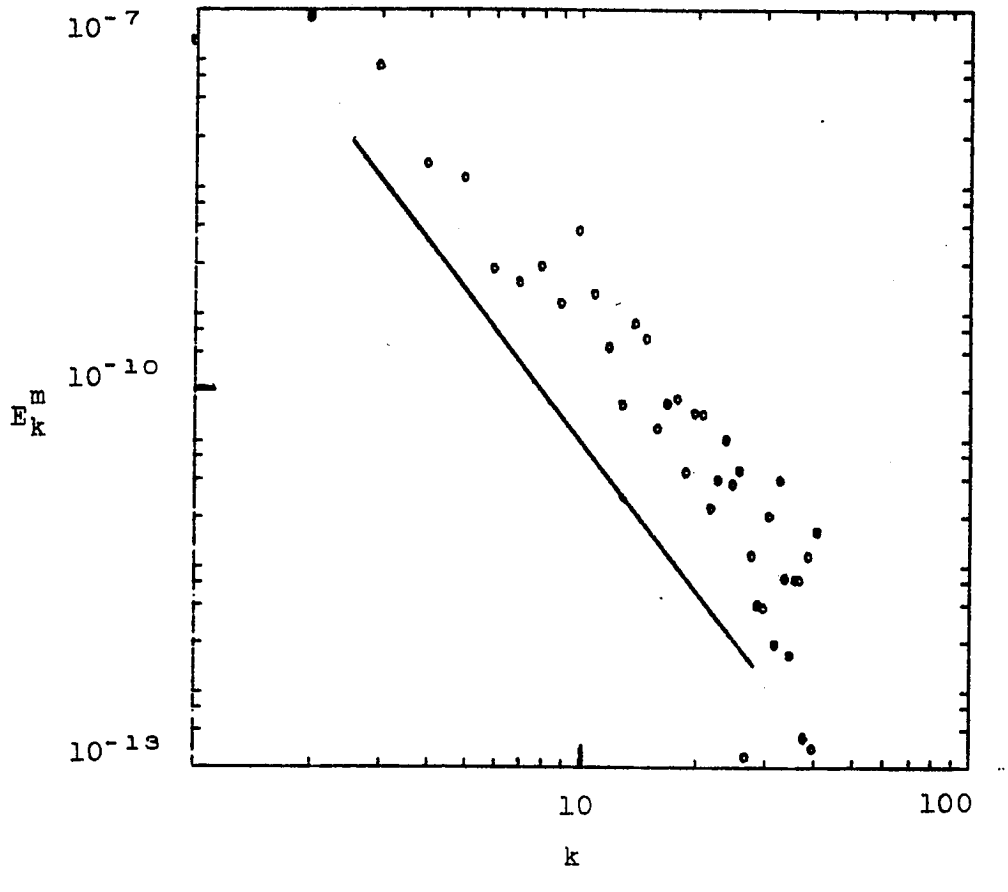

FIGURE 3.40. Spectrum of magnetic energy (E_k^m) at t = 118. Solid line is $E_k^m \sim k^{-4}$.

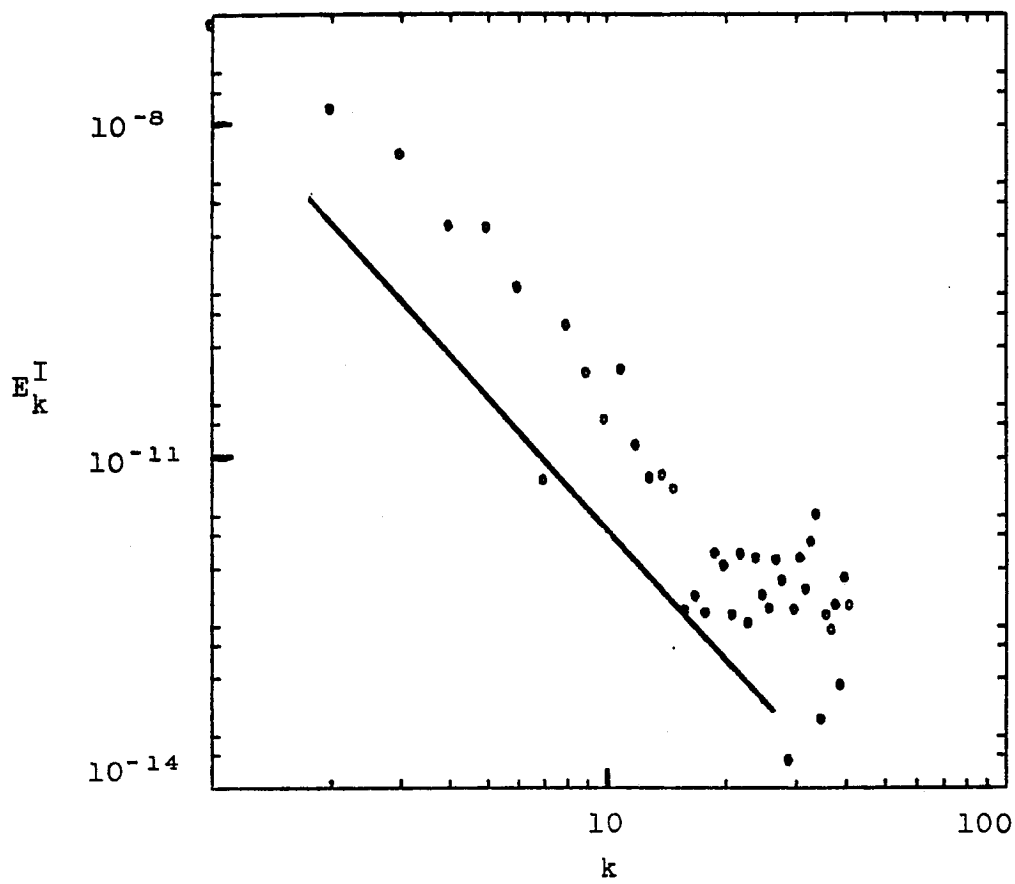

FIGURE 3.41. Spectrum of internal energy (E_k^I) at $t = 118$. Solid line is $E_k^I \sim k^{-4}$.

Spectra analysis of energy necessarily omits phase information concerning structures in a flow (i.e., for wavelike flows, spectra analysis is fine, but for individual coherent structures this is not enough information). Consider a flow with coherent structures (Figure 3.14) and impose (filter in) a random phase, but keep the energy spectra the same. Then, the resulting flow would not display these structures (see Figure 3.13 for example), but would be statistically homogeneous. To properly describe the coherent structures spectrally, one must graph all moments (higher order statistical quantities). Interpretation in terms of closure theories would then be impossible and interpretation of an infinite number of spectra would be extremely difficult. We thus do not emphasize the role of spectra in this work.

3.6 Closure Comparison Discussion

In this section, we discuss the results of a recent closure comparison with our simulation.[68] Closure simulations have been used in 2-D MHD,[56] but without regards to possible effects of intermittency. We

therefore wish to see if intermittency in 2-D micro-tearing has any effect on spectra and decay rates of energy predicted by closure derived spectrum equations.

Recently, the direct numerical simulation of 2-D Navier-Stokes (see McWilliams[45]) was compared[30] to a two point moment closure (and test-field model[38]). The closure was found to overestimate enstrophy and energy transfer to small and large scales, respectively. Discrepancies were found in the energy and enstrophy spectra at intermediate wavenumbers. This discrepancy is attributed to the vorticity (and energy) tied up in the isolated vortices of the direct numerical simulation (DNS), thus impeding the transfer of energy (to large scales) and enstrophy to small scales. Differences were also found in the time history of skewness (third moment of vorticity), energy, and enstrophy. The decay rates for energy and skewness were larger in the DNS, while the enstrophy decay rate was smaller for the DNS. Last, the DNS predicts kurtosis values much greater than 3. The closure has no computed value of kurtosis.

Similar comparisons of our DNS with the closure (EDQM[50]) of Chapter II can be made. Motivated by

McWilliams, we should compare decay rates of energy, current squared, and skewness of current. We also should compare spectra of energy, mean square flux and current squared.

For completeness, we present Eqs. (2-60) and (2-61) of Chapter II (spectrum equations). These two equations, with an appropriate eddy damping rate, constitute the closure theory for comparison. The equations for magnetic and internal energies are, respectively:

$$\frac{\partial E^m_{\underset{\sim}{k}}}{\partial t} - \eta J^2_{\underset{\sim}{k}} = (\rho_s/a)^2 \sum_{\underset{\sim}{p}+\underset{\sim}{q}=-\underset{\sim}{k}} (\underset{\sim}{p} \cdot \underset{\sim}{q} \times \hat{z})^2 \left\{ \frac{(q_\perp^2 - k_\perp^2)}{q_\perp^2} \operatorname{Re}\left(\mathcal{L}^{(2)}_{\underset{\sim}{k},\underset{\sim}{p},\underset{\sim}{q}}\right) E^m_{\underset{\sim}{q}} E^m_{\underset{\sim}{k}} \right.$$

$$- \operatorname{Re}\left(\mathcal{L}^{(1)}_{\underset{\sim}{k},\underset{\sim}{p},\underset{\sim}{q}}\right) E^I_{\underset{\sim}{q}} E^m_{\underset{\sim}{k}}$$

$$\left. + (k_\perp^2/q_\perp^2) \operatorname{Re}\left(\mathcal{L}^{(1)}_{\underset{\sim}{k},\underset{\sim}{p},\underset{\sim}{q}}\right) E^I_{\underset{\sim}{p}} E^m_{\underset{\sim}{q}} \right\} \qquad (3\text{-}35)$$

and

$$\frac{\partial E^I_{\underset{\sim}{k}}}{\partial t} + 2\nu_2 k_\perp^2 E^I_{\underset{\sim}{k}} = (\rho_s/a)^2 \sum_{\underset{\sim}{p}+\underset{\sim}{q}=-\underset{\sim}{k}} (\underset{\sim}{p} \cdot \underset{\sim}{q} \times \hat{z})^2 \frac{(p_\perp^2 - q_\perp^2)}{q_\perp^2} \operatorname{Re}\left(\mathcal{L}^{(1)}_{\underset{\sim}{k},\underset{\sim}{p},\underset{\sim}{q}}\right) E^m_{\underset{\sim}{q}} E^I_{\underset{\sim}{k}}$$

$$- \operatorname{Re}\left(\mathcal{L}^{(2)}_{\underset{\sim}{k},\underset{\sim}{p},\underset{\sim}{q}}\right) E^m_{\underset{\sim}{p}} E^m_{\underset{\sim}{q}} , \qquad (3\text{-}35)$$

where $E^m_{\underset{\sim}{k}}$ is the spectral amplitude of magnetic energy and $E^I_{\underset{\sim}{k}}$ is the spectral amplitude of internal energy. $\mathcal{L}^{(1)}$ and $\mathcal{L}^{(2)}$ are nonlinear propagaions, proportional to the nonlinear scrambling times of Ohm's Law and continuity, respectively. When the energies equipartition, the propagators are the same and equal to

$$1/(k_\perp^2 v_A \rho_s (\delta B/B_0)_{rms}), \qquad (3\text{-}37)$$

an effective "Alfven time." For constrained relaxation, the nonequipartitioning introduces internal energy into the propagators, making Eq. (3-37) necessarily inappropriate. The appropriate propagators can be estimated from the one point equations for flux ($\psi_{\underset{\sim}{k}}$) and density ($n_{\underset{\sim}{k}}$). The renormalized one point equations are derived in Section 2.4, with the viscosity zero, and are (with finite ν_2):

$$\frac{\partial \psi_{\underset{\sim}{k}}}{\partial t} + \eta k_\perp^2 \psi_{\underset{\sim}{k}} = -(c_{\underset{\sim}{k}} + d_{\underset{\sim}{k}})\psi_{\underset{\sim}{k}} \tag{3-38}$$

and

$$\frac{\partial n_{\underset{\sim}{k}}}{\partial t} + \nu_2 k_\perp^2 n_{\underset{\sim}{k}} = -a_{\underset{\sim}{k}} n_{\underset{\sim}{k}}, \tag{3-39}$$

where

$$c_{\underset{\sim}{k}} = (\rho_s/a)^2 \sum_{\underset{\sim}{k}'} (\underset{\sim}{k} \cdot \underset{\sim}{k} \times \hat{z})^2 \mathcal{L}^{(2)}_{\underset{\sim}{k},\underset{\sim}{k}',\underset{\sim}{k}+\underset{\sim}{k}'} (k_\perp^2 - k_\perp'^2) |\psi_{\underset{\sim}{k}'}|^2$$

$$\sim (\rho_s/a)^2 k_\perp^2 \sum_{\underset{\sim}{k}'} \mathcal{L}^{(2)}_{\underset{\sim}{k},\underset{\sim}{k}',\underset{\sim}{k}+\underset{\sim}{k}'} E^m_{\underset{\sim}{k}'} k_\perp'^2 \left(1 - \frac{k_\perp'^2}{k_\perp^2}\right),$$

$$d_{\underset{\sim}{k}} = (\rho_s/a)^2 \sum_{\underset{\sim}{k}'} (\underset{\sim}{k} \cdot \underset{\sim}{k}' \times \hat{z})^2 \mathcal{L}^{(1)}_{\underset{\sim}{k},\underset{\sim}{k}',\underset{\sim}{k}+\underset{\sim}{k}'} |n_{\underset{\sim}{k}'}|^2$$

$$\sim k_\perp^2 \sum_{k'} \mathcal{L}^{(1)}_{k,k',k+k'} |v_{D_{k'}}|^2,$$

and

$$a_{\underset{\sim}{k}} = (\rho_s/a)^2 \sum_{\underset{\sim}{k}'} (\underset{\sim}{k} \cdot \underset{\sim}{k}' \times \hat{z})^2 \mathcal{L}^{(1)}_{\underset{\sim}{k},\underset{\sim}{k}',\underset{\sim}{k}+\underset{\sim}{k}'} (k_\perp''^2 - k_\perp'^2) |\psi_{\underset{\sim}{k}'}|^2 \sim (\rho_s/a)^2 \sum_{\underset{\sim}{k}'} E^m_{\underset{\sim}{k}'} \mathcal{L}^{(1)}_{\underset{\sim}{k},\underset{\sim}{k}',\underset{\sim}{k}+\underset{\sim}{k}'}.$$

Consistently keeping coherent pieces in the propagators, as in Dupree and Tetreault, we have from Eqs. (3-38) and (3-39)

$$\mathcal{L}^{(1)}_{\underset{\sim}{k},\underset{\sim}{k}',\underset{\sim}{k}+\underset{\sim}{k}'} = \frac{1}{\delta\gamma^{(1)}_{\underset{\sim}{k}} + \delta\gamma^{(1)}_{\underset{\sim}{k}'} + \delta\gamma^{(1)}_{\underset{\sim}{k}+\underset{\sim}{k}'}}$$

and

$$\mathcal{L}^{(2)}_{\underset{\sim}{k},\underset{\sim}{k}',\underset{\sim}{k}+\underset{\sim}{k}'} = \frac{1}{\delta\gamma^{(2)}_{\underset{\sim}{k}} + \delta\gamma^{(2)}_{\underset{\sim}{k}'} + \delta\gamma^{(2)}_{\underset{\sim}{k}+\underset{\sim}{k}'}}$$

where

$$\delta\gamma^{(1)}_{\underset{\sim}{k}} = \eta k_\perp^2 + c_{\underset{\sim}{k}} + d_{\underset{\sim}{k}}$$

and

$$\delta\gamma^{(2)}_{\underset{\sim}{k}} = \nu_2 k_\perp^2 + a_{\underset{\sim}{k}}.$$

These propagators are still functions of themselves, and can be approximated by quasi-empirical eddy damping times,[50,56] found by inspecting the one point equations. These times are

$$\delta\gamma^{(1)} \sim \delta\gamma^{(2)} \sim (\eta + \nu_2)k_\perp^2$$

$$+ k_\perp^2 \rho_s v_A \Big(\sum_{\underset{\sim}{k'}} E^m_{\underset{\sim}{k'}}\Big)^{1/2}$$

$$+ \rho_s v_A \Big[\sum_{\underset{\sim}{k'}} (k_\perp k'_\perp)^2 E^m_{\underset{\sim}{k'}}\Big]^{1/2}$$

$$+ |k_\perp| \Big(\sum_{k'} (v_D)^2_{\underset{\sim}{k'}}\Big)^{1/2} .$$

The closure comparisons were performed recently with preliminary results indicating close agreement between closure and direct simulation. Figures 3.42-3.45 show comparisons of energy damping rates at t = 118, of magnetic and internal energies. Figures 3.46 and 3.47 show spectra of the closure runs. Note the agreement with the slopes of Figures 3.40 and 3.41, although scatter in the spectra precludes reliable results. Comparisons of spectra of mean square flux and current squared still need to be performed. Graphs of skewness (not presented here) time history in the DNS indicate strong nongaussianity (nonzero skewness) and need to be compared with the closure (along with current time history). A complete table of results will be presented in future publications.

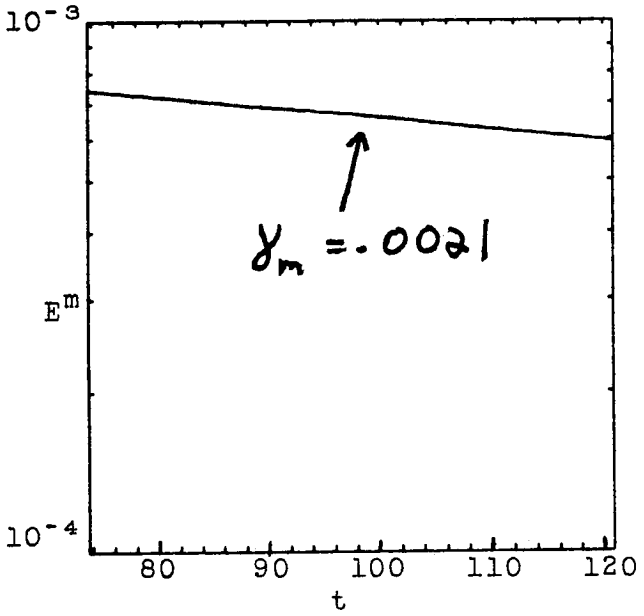

FIGURE 3.42. Time history of DNS magnetic energy (E^m) from t = 73 to t = 120. Damping rate is γ_m = .0021 (see Figure 3.3).

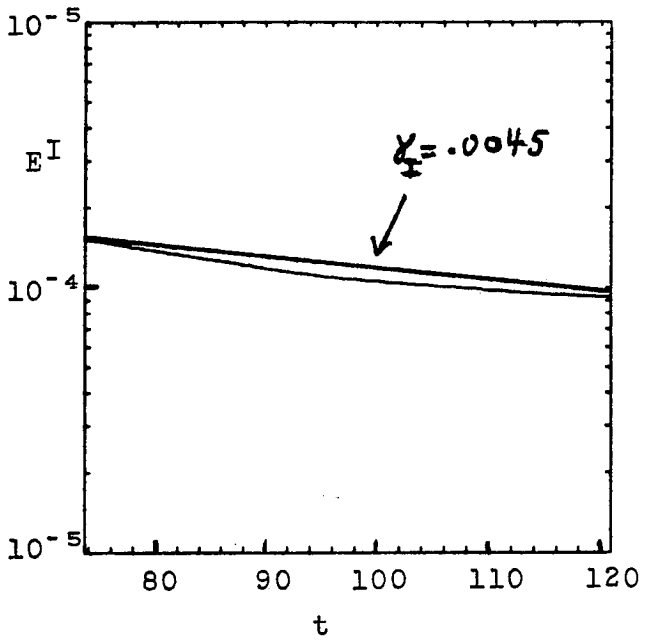

FIGURE 3.43. Time history of DNS internal energy (E^I) from t = 73 to t = 120. Damping rate is γ_I = .0045 (see Figure 3.4).

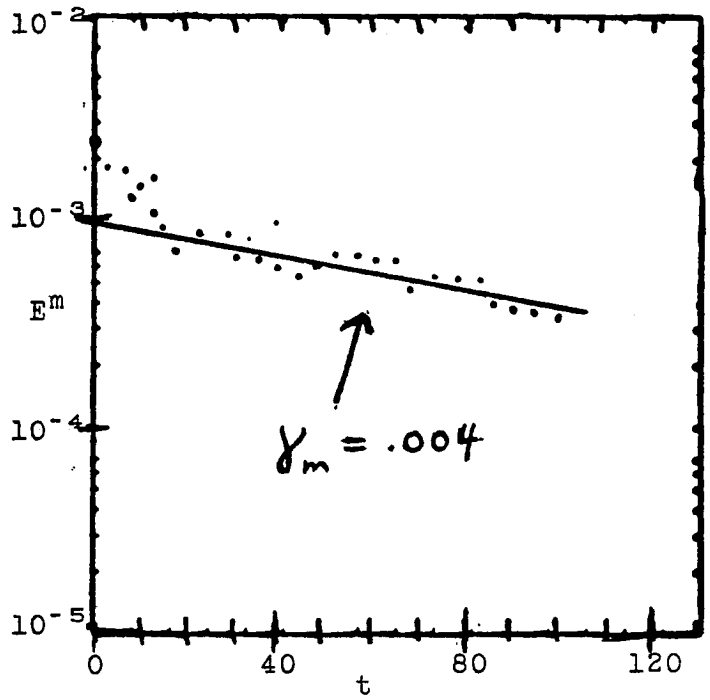

FIGURE 3.44. Time history of closure magnetic energy (E^m). Damping rate is $\gamma_m = .004$.

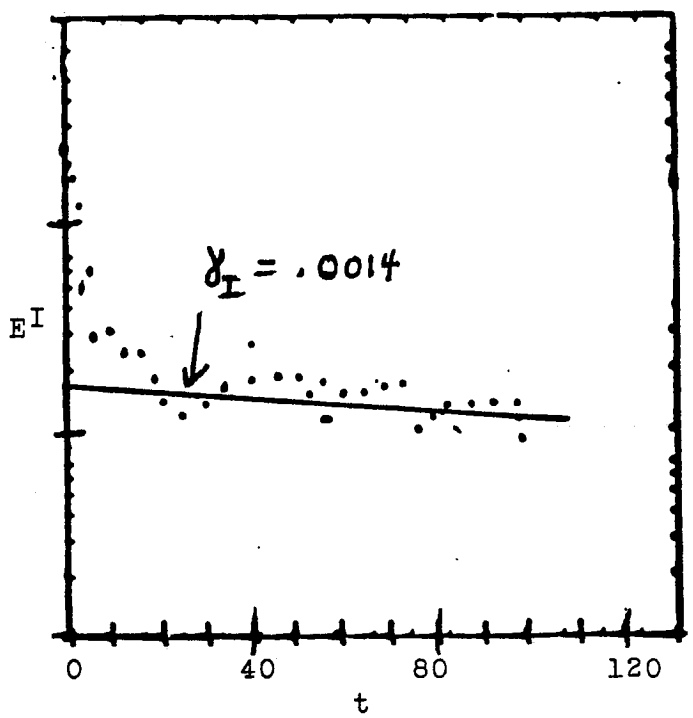

FIGURE 3.45. Time history of closure internal energy (E^I). Damping rate is $\gamma_I = .0014$.

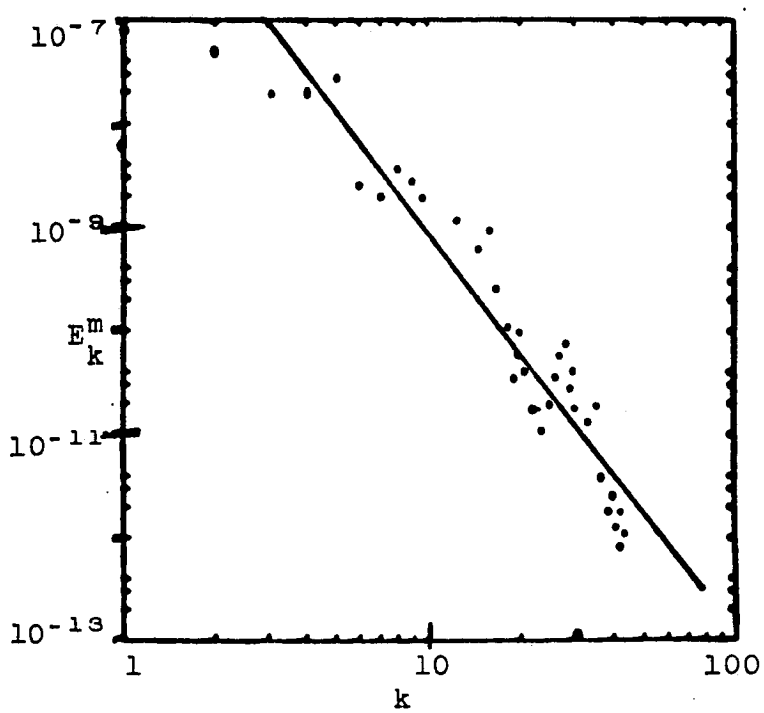

FIGURE 3.46. Spectrum of magnetic energy (E^m) in closure code. Line is $k^{-3.9}$ at t = 118.

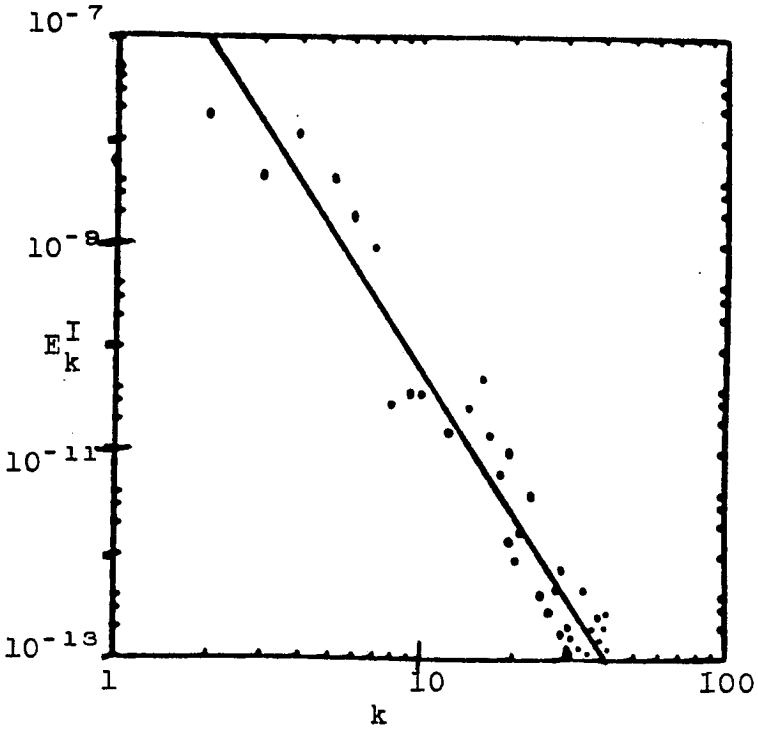

FIGURE 3.47. Spectrum of internal energy (E_k^I) in closure code. Line is $k^{-4.6}$ at t = 118.

3.7 Conclusion

In this section, we discuss the numerical results found in Sections 3.3 through 3.6 and conclude Chapter III. As discussed in Section 3.1, McWilliams has found similar intermittent behavior in 2-D Navier-Stokes flows. His "vorticity filaments" or vortices were long-lived and isolated, similar to the current filaments in our runs. Unlike McWilliams, we do not have a dynamical interpretation for the separation of the current flow into cascading and stationary elements, i.e., from the sign of $-2\ \mathrm{trace}(\nabla \underline{B})^2$. We also do not see any steepening of spectra (we could just need higher resolution runs). The lack of steepening is not critical, in that (as discussed earlier) spectra do not contain necessary phase information for the characterization of coherent structures.

In Moffatt's[46] paper, he postulates that the final state of constrained relaxation of 3-D MHD will be force free with a lower bound on the magnetic energy. Our code results have not confirmed this bound, although Figures 3.3 and 3.4 indicate that we are near equilibrium. Moffatt also says that the final state

will be broken into force free ergodic and current sheet regions (although he does not define ergodic). Our code results indicate that the filaments are force free, but the surrounding fluctuating current field is not. Further, Moffatt characterizes the two regions (ergodic and current sheet) by α, where $\underset{\sim}{B} \sim \alpha \underset{\sim}{J} \cdot \alpha$ is constant in the ergodic regions, but nonconstant on the sheets. Our α is nonconstant in the regions occupied by the current filaments, indicating that the current filaments might be related to current sheets.

Finally, the comparison of the intermittent direct numerical simulation with the closure[68] indicates minor differences between the energy damping rates. Both spectra are approximately k^{-4}, indicating that they agree (to within scatter of the data points). This result is readily seen by comparing Figures 3.40 and 3.41 with 3.46 and 3.47. The damping rates differ slightly (see Figures 3.42-3.45), with the closure code magnetic energy damping being greater than DNS, while the DNS internal energy damping being greater than the closure. We do not make conclusions at this point, since more extensive study over a wide variety of parameters is needed.

We summarize this chapter by presenting the principal facts derived from the computational study. The principal results are:

(i) For the viscosity dominated system (resistivity negligible), current filaments are found to appear out of initially random conditions, analogous to the vortices of McWilliams.[45]

(ii) Large values of kurtosis of current indicate a special kind of "spatial intermittency."

(iii) The filaments are long lived and force free such that $J = \alpha\psi$. α is nonconstant in the region of a long-lived filament.

(iv) Filaments of like sign tend to attract (current rods attracting) and merge, similar to vortex interaction in McWilliams.

(v) The quantity $Q = -2\text{Trace}((\underset{\sim}{\nabla B})^2)$ (current squared minus the magnitude of the "shear stress" on the magnetic field) is correlated with long-lived current filaments. No theoretical interpretation is proposed, though.

(vi) An accumulation of mean square flux at large scales is tied to the appearance of the current filaments.

(vii) Assuming that the current field is composed of cylindrical current rods, we find that the magnetic energy goes as k^{-4}. This result is compared with the simulation spectra. No evidence of steepening is found.

(ix) Preliminary comparisons[68] with a quasi-gaussian closure theory are made.

The constrained relaxation of microtearing is not a finished problem. Additional diagnostics need to be run, such as temporal and spatial correlations. Longer and higher resolution runs need to be run on the computer (go to a CRAY2). Spinoff problems of this computational chapter are immense. The constrained relaxation of 2-D MHD needs to be run (preliminary runs have indicated current filaments do appear, even at low resolution). Additional fields, such as a temperature/magnetic system, could be checked for intermittent behavior. Could the addition of diamagnetic drifts "break apart" the current filaments? How does shear (3-D) affect the intermittent behavior? How will current filaments affect a numerical saturation of the self-filamentation mode? Last, the closure comparison needs to be finished, with more extensive computer

runs. In the physics sense, this is the most far reaching project, because it chips away at the foundations of turbulence analytic theory.

C H A P T E R I V

CONCLUSION

In this dissertation, we have investigated two aspects of magnetic turbulence. Microtearing turbulence has been analytically studied and applied to the tokamak edge. Results seem to agree reasonably with experiment. The second study considered the constrained relaxation of the two dimensional, undriven limit of the microtearing problem. The numerical simulation exhibited spatial intermittency of current (possibly outside the limits of approximation of the analytic turbulence theory used in the first study).

In Chapter II, we studied microtearing turbulence using renormalized one and two point equations derived from a quasi-gaussian statistical closure theory. The saturated spectrum is applied to edge magnetic transport in Ohmically and beam heated tokamaks, with favorable comparison to experiment in the latter.

Although little change in the final results is expected, the theory can be used to treat electrostatic and temperature fluctuations in microtearing turbulence. Another interesting extension would be the effect of trapped particles on microtearing turbulence. Both of these projects seem to be worthwhile for future study.

In Chapter III, we numerically solved the two-dimensional, unforced microtearing equations under the constraint of mean square flux conservation. Out of the random initial distribution of current, current filaments appeared. These filaments were isolated, long-lived, and force free. Their appearance was tied to an accumulation of mean square flux at large scales and represented a special kind of "spatial intermittency." This nongaussian behavior was discussed in terms of a quasi-gaussian closure approximation.

The constrained relaxation problem is by no means finished. The search for isolated current filaments should be extended to 2-D MHD and a coupling to temperature fluctuations. Diagnostics of time and spatial correlations are needed. Analytically, a dynamical interpretation of the trace of the "magnetic stress" or the gaussian curvature of flux is needed. Finally, the addition of diamagnetic drifts and forcing (self-filamentation mode) would be an interesting numerical study. Their inclusion could have profound effects on the existence of the intermittent current filaments.

A P P E N D I X

A P P E N D I X

The exact solution of the driven equations, Eqs. 2-66, 2.67, 2-68, is found in this Appendix. Dropping subscripts and superscripts for convenience, we have:

$$- i\left(\omega - i\omega_*^T\left(1 + \alpha + i\alpha\frac{\alpha'\omega}{\nu_e}\right)\right)\psi$$

$$- \eta J\, ik_\parallel(\rho_s/a)^2 n = R, \tag{A-1}$$

$$- i\omega n = - ik_\parallel J + U, \tag{A-2}$$

and

$$J = \nabla_\perp^2\psi. \tag{A-3}$$

We assume R and U are constant[12] and $\left|\frac{\partial^2}{\partial x^2}\right| >> k_y^2$ ($k_y w_k < 1$). The equations to solve are:

$$\frac{\partial^2\psi}{\partial x^2} + i\epsilon\omega\left(\frac{\psi - \frac{iR}{\epsilon\omega} + \frac{ik_\parallel(\rho_s/a)^2 U}{\epsilon\omega^2}}{(1 + (x/w)^2)}\right) = 0 \tag{A-4}$$

where

$$\epsilon = \frac{1}{\Phi}\left(\omega - \omega_*^T\left(1 + \alpha + \frac{\alpha\alpha' i\omega}{\nu_e}\right)\right), \tag{A-5}$$

$$w^2 = \frac{\eta\omega a^2}{i(k_\parallel')^2\rho_s^2} \quad , \text{ and } k_\parallel = k_\parallel' x.$$

The following definitions are useful:

$$x_R^2 = \frac{-\eta}{i\epsilon\omega} \qquad \text{and} \qquad \sigma = \frac{1}{x_R^2\,(1 + (x/w)^2)}$$

Here, x_R is the resistive skin depth, σ is the linear conductivity, and w is the conductivity layer width (mode width). Eq. (A-4) has the general solution:[1]

$$\psi = \bar{a}(zP_\nu(z) - P_{\nu-1}(z)) + \bar{b}(zQ_\nu(z) - Q_{\nu-1}(z)) + \frac{iR}{\epsilon\omega} - \frac{ik_\parallel(\rho_s/a)^2 U}{\epsilon\omega^2} \qquad \text{(A-6)}$$

where $\bar{a}$ and $\bar{b}$ are constants, $\nu(\nu+1) = (w/x_R)^2$, P_ν and Q_ν are associated Legendre functions in the complex plane, and $z = (ix/w)$.

To determine $\bar{a}$ and $\bar{b}$, we impose the tearing mode boundary condition:[19]

$$\Delta' = \left.\frac{\partial\psi}{\partial x}\right|_{-\infty}^{+\infty} \Big/ \psi \quad |x| \to \infty \;, \quad (x=0) \qquad \text{(A-7)}$$

which matches onto an outer MHD solution.

Eq. A-7 is equivalent to the condition

$$\Delta'\psi_0 = \int_{-\infty}^{+\infty} dx\ J(x) \tag{A-8}$$

where $\psi_0 = \lim_{z\to\pm\infty} \psi \Big|_{x=0}$.

As a check of our solution, the condition

$$\lim_{w\to\pm\infty} J = \Delta'\psi_0 \delta(x) \tag{A-9}$$

should be satisfied (corresponding to the sparsely packed turbulence result).[12] Further, for R = U = 0, the linear dispersion relation should be recovered. Defining $\delta = (w/x_R)^2$, we see that $\delta = 0$ implies $\nu = 0$. The $\nu \to 0$ limit, along with $|x| \to \infty$ corresponds to the outer layer. solution.

Taking this limit of Eq. A-6 and making sure we analytically continue, then

$$\bar{a} = \frac{-\Delta'\psi_0 w}{\pi\delta}\,(1 + \delta) \tag{A-10}$$

and

$$\bar{b} = 0. \tag{A-11}$$

Solving for J, we find

$$J = \frac{\bar{a}(zP_\nu(z) - P_{\nu-1}(z))}{x_R^2(1 + x/w)2)} \quad . \tag{A-12}$$

When $w \to 0$,

$$J \to \frac{\delta\bar{a}(z - 1)}{w^2 + x^2} \to \Delta'\psi_0\delta(x).$$

The constant ψ solution[19] corresponds to

$$\left|\sigma \Big/ \frac{\partial\sigma}{\partial x}\right|^2 \gg \sigma \ ,$$

i.e., $w^2 \ll x_R^2$.

Thus, the "constant ψ" solution is:

$$\psi = \frac{\Delta'\psi_0 w}{\pi\delta} + \frac{Ri}{\epsilon\omega} - \frac{ik_\parallel(\rho_s/a)^2 U}{\epsilon\omega^2} \tag{A-1 }$$

When R and U are zero, we have

$$\psi = \psi_0 = \frac{\psi_0\Delta' w}{\pi\delta} \quad , \tag{A-14}$$

which is the linear dispersion relation for the

microtearing mode with constant ψ.[19] Taking the $x \to 0$ limit of ψ, we find that

$$\psi_0 = \frac{R}{-i\epsilon\omega - \frac{\Delta'\eta}{\pi w}}$$

where $\Delta'\eta/\pi w$ is the linear dissipation (when $\Delta' < 0$). Summarizing, the constant ψ solution is:

$$\psi = \frac{iR}{\epsilon\omega - \frac{i\Delta'\eta}{\pi w}} - \frac{ik_{\parallel}(\rho_s/a)^2 U}{\epsilon\omega^2} \qquad \text{(A-15)}$$

$$J = \frac{\Delta'}{\pi(1 \div (x/w)^2)} \frac{iR}{(\epsilon\omega - (i\Delta'\eta/\pi w))} \qquad \text{(A-16)}$$

and

$$n = \frac{iU}{\omega} + \frac{k_{\parallel} J}{\omega} \quad . \qquad \text{(A-17)}$$

R E F E R E N C E S

R E F E R E N C E S

1. Abramowitz, M., and Stegun, I. Handbook of Mathematical Functions with Formulas, Graphs, and Mathematical Tables. New York: Dover Publications, 1965.

2. Ames, W. F. Nonlinear Partial Differential Equations in Engineering, vol. 1, p. 346.

3. Armi, L., and Flament, P. J. Geophys. Res. 90, 11, 779 (1985).

4. Batchelor, G. K., and Townsend, A. A. Proc. Roy Soc. London A 199, 238 (1949).

5. Biskamp, D. Nucl. Fusion 19, 777 (1979).

6. Boozer, A. J. Plasma Phys. 35, 133 (1986).

7. Brachet, M. E. et al. Phys. Rev. Lett. 57, 683 (1986).

8. Braginski, S. I. "Transport Processes in a Plasma." In Reviews of Plasma Physics, vol. 1, p. 205. Edited by M. A. Leontovich. New York: Consultants Bureau, 1965.

9. Carnevale, G. J. Phys. A. Math Gen. 14, 1701 (1981).

10. Coppi, B. Comments Plasma Physics Cont. Fusion 5, 261 (1980).

11. Dahlburg, J. et al. J. Plasma Phys. 34 part 1, 1 (1985).

12. Diamond, P. H. et al. Phys. Fluids 27, 1449 (1984).

13. D'Ippolito, D. A. et al. Phys. Fluids 23, 771 (1980).

14. Drake, J. F. et al. Phys. Rev. Lett. 44, 994 (1980).

15. Drake, J. F., and Lee, Y. C. Phys. Fluids 18, 1778 (1977).

16. Dupree, Thomas H., and Tetreault, David J. Phys. Fluids 21, 425 (1978).

17. Frish, U. in Les Houches, Session 36, 1981 Chaotic Behavior of Dynamical Systems. North Holland.

18. Frisch, U. et al. Journel de Mecanique theorique et appliquee, Numero Special, 191 (1983).

19. Furth, H. P. et al. Phys. Fluids 6, 459 (1963).

20. _____. Phys. Fluids 16, 1054 (1973).

21. Fyfe, D. et al. J. Plasma Phys. 17, 317 (1977).

22. Fyfe, D., and Montgomery, D. J. Plasma Phys. 16 part 2, 181 (1976).

23. Gladd, N. T. et al. Phys. Fluids 23, 1182 (1980).

24. Hasegawa, A., and Mima, K. Phys. Fluids 21, 87 (1978).

25. Hassam, A. B. Phys. Fluids 23, 1182 (1980).

26. _____. Phys. Fluids 23, 2493 (1980).

27. Hazeltine, R. D. Phys. Fluids 26, 3242 (1983).

28. Hazeltine, R. D. et al. Phys. Fluids 18, 1778 (1975).

29. Hazeltine, R. D., and Strauss, H. R. Phys. Rev. Lett. 37, 102 (1976).

30. Herring, J. R., and McWilliams, James. J. Fluid Mech. 153, 229 (1985).

31. Kadomtsev, B. B., and Pogutse, O. P. In Plasma Physics and Controlled Nuclear Fusion Research (Proc. 7th Int. Conf. Vienna, 1978), vol. 1 IAEA, Vienna, 649 (1979).

32. Kaye, S. M. et al. J. Nucl. Matter 121, 115 (1984).

33. Kolmogorov, A. N. C. r. Acad. Sci. URSS 30, 301 (1941).

34. Kraichnan, R. H. J. Fluid Mech. 5, 497 (1959).

35. _____. Phys. Fluids 8, 1385 (1965).

36. _____. Phys. Fluids 10, 1417 (1967).

37. _____. Phys. Fluids 10, 2081 (1967).

38. _____. J. Fluid Mech. 47, 513 (1971).

39. _____. Phys. Fluids 16, 1903 (1973).

40. _____. J. Fluid Mech. 67 part 1, 155 (1975).

41. Kraichnan, R. H., and Montgomery, D. Rep. Prog. Phys. 43, 547 (1980).

42. Lee, T. D. Quart. Appl. Math 10, 69 (1952).

43. Lilly, D. K. Phys. Fluids, Suppl 12, 240 (1969).

44. Malacarne, M. et al. "Fluctuations during JET Discharges with H-mode." Submitted to Plasma Physics and Controlled Fusion (1987).

45. McWilliams, J. J. Fluid Mech. 146, 21 (1984).

46. Moffatt, H. K. J. Fluid Mech. 159, 359 (1985).

47. Ohyabu, N. et al. Nucl. Fusion 25, 49 (1985).

48. _____. Phys. Rev. Lett. 58 120 (1957).

49. Orszag, Steven A. Studies in Applied Mathematics 50, 293 (1971).

50. _____. Fluid Dynamics: Les Houches, pp. 235-374. Edited by R. Balin and J-L Peube. New York: Gordon and Breach, 1973.

51. Orszag, S. A., and Tang, C. M. J. Fluid Mech. 90, 129 (1979).

52. Patterson, G. S., and Orszag, Steven A. Phys. Fluids 14, 253 (1971).

53. Perkins, F. W. In Heating in Torroidal Plasmas. Proc. of the 4th Symposium, Rome, 1984 (ENEA, Frascati, 1984), vol. 2, p. 977.

54. Phillips, N. A. The Atmosphere and the Sea in Motion, p. 501 (1959).

55. Potter, D. Computational Physics. New York: John Wiley and Sons, 1973.

56. Pouquet, A. J. Fluid Mech. 88 part 1, 1 (1978).

57. Pouquet, A. J. et al. J. Fluid Mech. 77, 321 (1976).

58. Rebut, P. A., and Brasati, M. Plasma Phys. Controlled Fusion 28, 113 (1986).

59. Rechester, A. B., and Rosenbluth, M. N. Phys. Rev. Lett. 40, 38 (1978).

60. Rutherford, P. H. Phys. Fluids 16, 1903 (1973).

61. Saffman, R. G. Stud. Appl. Math. 50, 377 (1971).

62. Samain, A. Plasma Phys. Controlled Fusion 26, 731 (1984).

63. Scott, B. et al. Phys. Fluids 28, 275 (1985).

64. Strauss, H. R. Phys. Fluids 29, 3668 (1986).

65. Takamura, S. et al. Phys. Rev. Lett. 56, 2044 (1986).

66. Taylor, G. I., and Green, A. F. Proc. Roy Soc. London A. 294, 499 (1937).

67. Tennekes, H., and Lumley, J. L. A First Course in Turbulence. Cambridge, Mass.: MIT Press, 1972.

68. Thayer, D., Craddock, G., and Diamond, P. 1987 Sherwood Theory Meeting Poster 3B19. "Gaussian Closure Code and Direct Spectral Code Comparison of 2D, 2-Field Turbulent Relaxation."

69. Tolman, R. C. Principles of Statistical Mechanics. Oxford: Oxford University Press, 1938.

70. Von Neuman, J. "Recent Theories of Turbulence." (A Report to the Office of Naval Research). Collected Works 6, 437 (1949-1963).

71. Wagner, F. et al. Phys. Rev. Lett. 49, 1408 (1982).

72. Weiss, J. "The Dynamics of Enstrophy Transfer in Two Dimensional Hydrodynamics." La Jolla Institute Report (unpublished), 1981.

V I T A

Gerald G. Craddock, Jr., was born in Pensacola, Florida, on July 9, 1957, the son of Carole T. Craddock and Gerald G. Craddock. He entered Texas A&M University in September of 1975, majoring in Physics. In May of 1979, he received the degree of Bachelor of Science from the same university. In September of 1979, he entered the Graduate School of The University of Texas at Austin, majoring in Physics. He has been employed as a research assistant in the Institute for Fusion Studies since January, 1981.

Permanent address: 3610 Lynnwood Drive
Arlington, Texas